Journal of Energy Storage 154 (2026) 121157

Contents lists available at ScienceDirect

Journal of Energy Storage

journal homepage: www.elsevier.com/locate/est

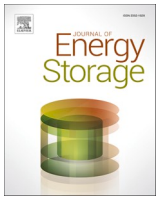

Review article

Conjugated microporous polymers as efficient electrode materials for supercapacitors: Recent progress and challenges

Ahmed F. Saber [a], Mohamed Gamal Mohamed [b], Mohamed Hammad Elsayed [a], Shiao-Wei Kuo [b], Mahmoud M. Abdelnaby [a,*]

[a] *Interdisciplinary Research Center for Hydrogen Technologies and Carbon Management (IRC-HTCM), King Fahd University of Petroleum & Minerals, Dhahran, 31261, Saudi Arabia*

[b] *Department of Materials and Optoelectronic Science, National Sun Yat-Sen University, Kaohsiung, 804, Taiwan*

A R T I C L E I N F O

Keywords:
Conjugated microporous polymers
Synthetic process
Chemical reactions
Energy storage
Supercapacitors

A B S T R A C T

Driven by increasing global energy demands and the escalating impact of climate change, the development of renewable, cost-effective, and sustainable energy storage technologies has become an urgent priority. Electrochemical supercapacitors (SCs) have emerged as attractive energy storage devices owing to their rapid charge–discharge capability, long operational lifetime, high power density, and environmentally benign characteristics. In this context, conjugated microporous polymers (CMPs) are rapidly gaining attention as outstanding polymeric materials with broad applicability, particularly in energy storage, where their intrinsic porosity, π-conjugated frameworks, and structural tunability offer unique advantages. Recent advances further demonstrate that CMPs can function not only as electrode materials but also as multifunctional electrolytes or electrolyte components in SCs, where their ion-conducting pathways, redox activity, and confinement effects enhance capacitance, rate performance, cycling stability, and operational voltage windows. In this review, we comprehensively summarize recent progress in CMP-based energy storage materials, with a particular focus on their applications in SCs. Key design strategies—including synthetic approaches, post-synthetic functionalization, reaction mechanisms, and structure–property–performance relationships—are systematically discussed to provide a framework for rational material optimization. A comparative analysis between CMPs and linear conjugated polymers is also presented to elucidate the advantages and limitations of porous conjugated architectures. Furthermore, the critical challenges associated with CMP-based SCs, such as conductivity, active-site utilization, volumetric performance, and pore accessibility, are examined alongside emerging strategies to overcome these limitations. This review aims to serve as a comprehensive and insightful reference for researchers and to inspire the future development of advanced CMP-based materials for high-performance energy storage technologies.

List of abbreviations

AG	Activated Graphene
AQ	Anthraquinone
BDT	Benzo[1,2-b:4,5-b']dithiophene
BET	Brunauer-Emmett-Teller
B–H	Buchwald–Hartwig
CMPs	Conjugated Microporous Polymers
CNFs	Carbon Nanotube Fibers
CNTs	Carbon Nanotubes
COFs	Covalent Organic Frameworks
CTFs	Covalent Triazine Frameworks
CV	Cyclic Voltammetry
2D	Two Dimension
3D	Three Dimension
DAQ	Diaminoanthraquinone
DTDO	Benzo[1,2-b:4,5-b']dithiophene-4,8-dione
ED	Energy Density
EDLCs	Electrochemical Double-Layer Capacitors
EIS	Electrochemical Impedance Spectroscopy
EQCM	Electrochemical Quartz Crystal Microbalance
ESR	Equivalent Series Resistance

* Corresponding author.
E-mail address: mahmoudm@kfupm.edu.sa (M.M. Abdelnaby).

https://doi.org/10.1016/j.est.2026.121157
Received 25 September 2025; Received in revised form 26 January 2026; Accepted 16 February 2026
Available online 24 February 2026

FSCs	Fiber-Shaped Supercapacitors
FTIR	Fourier Transform Infrared Spectroscopy
GCD	Galvanostatic Charge/Discharge
G-CMP	Graphene-based Conjugated Microporous Polymers
GMPs	Graphene–Microporous Polymer Sandwich Structures
HATN	Hexaazatrinaphthylene
HCPs	Hypercrosslinked Polymers
IUPAC	International Union of Pure and Applied Chemistry
MPcs	Metal Phthalocyanines
MOFs	Metal–Organic Frameworks
MO-CMPs	Metal–Organic Conjugated Microporous Polymers
MWNTs	Multiwalled Nanotubes
NCMPs	Nitrogen-Rich Conjugated Microporous Polymers
NMP	*N*-methyl Pyrrolidone
OXD	Oxadiazole
PAFs	Porous Aromatic Frameworks
PAQs	Polyaminoanthraquinone Frameworks
PDI	Perylene Diimide
PEDOT/PSS	Poly(3,4-ethylenedioxythiophene)–Poly (styrenesulfonate)
POPs	Porous Organic Polymers
PSM	Post-Synthetic Modification
PTFE	polytetrafluoroethylene
PTO	Pyrene-4,5,9,10-tetraone
PTPA	Polytriphenyl Amine
PVDF	poly(vinylidene fluoride)
PW	Potential Window
Py	Pyrene
rGO	Reduced Graphene Oxide
Rs	Ohmic Resistance
SCs	Supercapacitors
SEM	Scanning Electron Microscopy
TEM	Transmission Electron Microscopy
T_{d10}	Decomposition Temperature at 10% Weight Loss
TPBA	Triphenyl Bromo
TzTz	Thiazolo[5,4-*d*]thiazole
WH	Watt-Hour
XAS	X-ray Absorption Spectroscopy
XPS	X-ray Photoelectron Spectroscopy

1. Introduction

Porous materials have attracted considerable attention due to their unique structural features and wide-ranging applications in energy storage, catalysis, separation, and sensing [1–5] According to the International Union of Pure and Applied Chemistry (IUPAC), porous materials are classified as microporous (pore size <2 nm), mesoporous (2–50 nm), or macroporous (> 50 nm) [6,7] Over the past two decades, there has been significant research activity focused on the discovery of new classes of porous organic materials. These materials include crystalline structures like covalent organic frameworks (COFs) [8] and various amorphous structures like covalent triazine frameworks (CTFs) [9] porous aromatic frameworks (PAFs), conjugated microporous polymers (CMPs) [10–20] and hypercrosslinked polymers (HCPs) [21–24]. Notably, amorphous polymers constitute a distinct class of porous materials, recognized for their remarkable features, such as high porosity, ultralight composition, and robust 2-dimensional (2D) or 3D frameworks constructed through strong covalent bonding [23,24]. Amorphous polymeric materials feature a strongly networked structure, characterized by dense cross-linking and an extended π-conjugated framework. This architecture imparts enhanced structural stability, a rich porous morphology, and a high surface area, making it highly suitable for a wide range of applications [25,26].

Porous organic polymers (POPs) have emerged as promising electrode materials because they combine structural tunability with chemical diversity. Compared with inorganic electrodes, organic electrodes offer several advantages, including lower cost, molecular-level design flexibility, and versatile electrochemical behavior [27]. Nevertheless, conventional redox-active polymers often suffer from limited ion accessibility, low intrinsic conductivity, and structural instability during long-term cycling, which restrict their practical electrochemical performance [28]. In recent years, CMPs have gained increasing attention as advanced electrode materials capable of overcoming many of these limitations. CMPs integrate permanent microporosity with extended π-conjugated frameworks, enabling efficient ion diffusion, enhanced charge transport, and improved utilization of redox-active sites [29,30]. Comparative studies employing identical redox-active building blocks have demonstrated that CMPs consistently outperform linear polymer analogues in terms of specific capacitance, rate capability, and cycling stability. For example, incorporating DAQ into a porous conjugated framework resulted in markedly enhanced electrochemical performance compared with its linear polymer counterpart, primarily due to reduced solubility, enhanced microporosity, and a more robust structural architecture [31]. Similarly, porous conjugated polymers containing benzene or ethynylbenzene linkers exhibit superior electrochemical behavior relative to linear analogues, highlighting the decisive role of porosity and conjugation in facilitating rapid ion diffusion, improved electrolyte accessibility, and efficient charge transfer [32].

Despite these advantages, organic electrode materials still face challenges related to insufficient conductivity and limited active-site utilization [33,34]. To address these issues, strategies such as polymerization, composite formation, and binder-free electrode design have been widely adopted [35,36]. In this context, conductive polymer composites and nanocomposites—such as poly(o-aminophenol)-based systems—have provided valuable insights, demonstrating that morphology engineering, polymer–inorganic synergy, and conductive network construction can significantly enhance charge transport, ion diffusion, and long-term cycling stability [37–40]. These findings establish broadly applicable design principles that are directly relevant to the optimization of CMP-based electrodes. Recent comprehensive reviews have highlighted persistent challenges in supercapacitor (SC) development, including the trade-off between energy and power density, limited intrinsic conductivity of organic electrodes, and long-term cycling stability, providing important benchmarks for evaluating emerging materials [41–44].

Conjugated microporous polymers (CMPs) have recently gained prominence as a crucial and highly versatile class of porous materials. Composed entirely of organic components linked by covalent bonds, these polymers feature a π-conjugated framework. Their pore sizes, typically 2 nm or smaller, make them well-suited for a wide range of applications. As a result, CMPs hold great promise for advancing energy technologies. Their exceptional combination of conjugated frameworks, intrinsic microporosity, and robust chemical stability paves the way for various innovative applications [11,14–16,18]. Beyond their inherent properties, CMPs can be synthesized in a wide variety of structural forms, including 2D and 3D networks, dendrimers, and branched polymers [45].

Although molecular tunability in CMPs can guide porosity, redox functionality, and pore chemistry, the fundamental performance of SC remains constrained by inherent energy density limits and the competing requirements of high porosity and efficient charge transport. Similarly, reviews on carbon-based electrodes have shown that despite very high surface area and conductivity optimization, porous carbon systems still face significant challenges in achieving energy densities comparable to batteries without considerable structural modification or hybridization strategies [46,47].

This review provides a comprehensive and critical assessment of CMPs as electrode materials for SCs, with a particular focus on recent progress achieved over the past five years. It systematically summarizes advances in CMP frameworks and CMP-based hybrid materials, highlighting how molecular design, porosity control, conjugation, and composite engineering influence electrochemical performance. In

addition to showcasing significant achievements, this article critically examines the key challenges that currently limit the practical application of CMP-based electrodes, including issues related to conductivity, active-site utilization, rate capability, and long-term stability. By emphasizing structure–property–performance relationships, the review identifies emerging trends and outlines promising strategies to overcome these limitations. Furthermore, it highlights areas where deeper mechanistic understanding and continued innovation are required to fully unlock the potential of CMPs in SC applications. Overall, this work aims to serve as a valuable reference for researchers by providing clear insights into the design principles and future directions necessary for developing high-performance CMP-based SCs. Advances in this field have the potential to enable SCs with higher energy density, faster charging capability, and longer operational lifetimes, thereby contributing to more efficient, cost-effective, and sustainable energy storage technologies for a wide range of applications.

Fig. 1 outlines the review's structure, linking CMP design and synthesis to morphology control, charge-storage mechanisms, performance metrics, and key challenges, and highlighting future strategies for advancing CMP-based SCs toward practical applications.

2. Synthesis and functionalization of conjugated microporous polymers (CMPs)

2.1. Overview of CMPs

Within the spectrum of POPs, CMPs stand out as a unique category of nanocrystalline polymers that enable the connection of monomers through extended conjugation and exhibit network structures [48]. CMPs have found extensive applications in various fields, including photocatalysis [49], heterogeneous catalysis [50], adsorption [16,18,51], sensors [52–54], flame retardancy [55], storing energy [56–58], and numerous others. Given that CMPs exhibit characteristics such as a substantial surface area, a considerably extended conjugation, good hydrophilic characteristics, and modifiable active functional groups on their surfaces, they hold significant promise as innovative adsorbents in the field of sorption science. Since the initial synthesis of CMPs by Sonogashira through coupling condensation [59], there has been ongoing progress and advancement in the preparation of CMPs. Fig. 2 illustrates the CMPs that have been constructed and utilized across diverse applications [60].

2.2. Synthetic methods of CMPs

The creation of various CMPs has primarily been accomplished through many synthetic procedures, including solvothermal [61,62], iono-thermal [63,64], mechanochemical [65,66], microwave-assisted [67,68], and electro-polymerization methods [69,70] via chemical coupling reactions [71,72] the Friedel–Crafts reaction [73,74], the Buchwald reaction [75,76], and other synthetic reactions [77,78] These approaches are summarized as follows:

2.2.1. Solvothermal method

The solvothermal method stands out as the most frequently employed synthetic approach for CMPs. Researchers have harnessed this method extensively, leading to the successful synthesis of a significant array of CMPs that have found effective applications across various fields [79,80]. In 2018, Liao et al. utilized the solvothermal technique to create an anthraquinone-based CMP, which was named as a 3D polyaminoanthraquinone (PAQ) network [75]. Aside from 3D CMP, researchers have also synthesized and applied 2D sandwich-structured CMPs in various fields [81]. Lei and colleagues successfully fabricated a magnetic poly(phenylacetylene) composite material (CMP) through the solvothermal method, employing tribromobenzene, triacetylbenzene, and modified Fe_3O_4 nanoparticles. This innovative CMP was effectively utilized for the removal of various fungicides [82]. Wan and co-authors synthesized a CMP incorporating triazine units via the solvothermal technique. They harnessed this polymer as a material applied in solid-phase microextraction coatings [83] While the solvothermal method has gained popularity for CMP synthesis due to its simplicity and manageable control of the reaction, it does come with drawbacks like long reaction duration and challenges in real-time monitoring of the reaction progress.

2.2.2. Microwave-enhanced solvothermal technique

This approach offers the advantage of minimizing the duration of the reaction and enhancing the efficacy of synthesis. Zhang team [84] achieved a significant milestone by introducing a fluorescent building block into CMPs using the microwave-assisted technique. They employed a tetrafunctional monomer, which swiftly reacted with alkynyl monomers, presenting a rapid method for synthesizing CMPs. Lately in 2020, Cui and collaborators [68] innovatively incorporated three distinct functionalities into a copper porphyrin-containing polymer with the help of microwave technology. These introduced functional groups could fine-tune the electronic and porosity characteristics of the produced polymer. This, in turn, led to enhanced photocatalytic degradation performance, enabling the efficient removal of various dyes from wastewater. The incorporation of microwave heating into the solvothermal method indeed enhances its environmental friendliness and efficiency; however, it does face challenges when attempting large-scale synthesis.

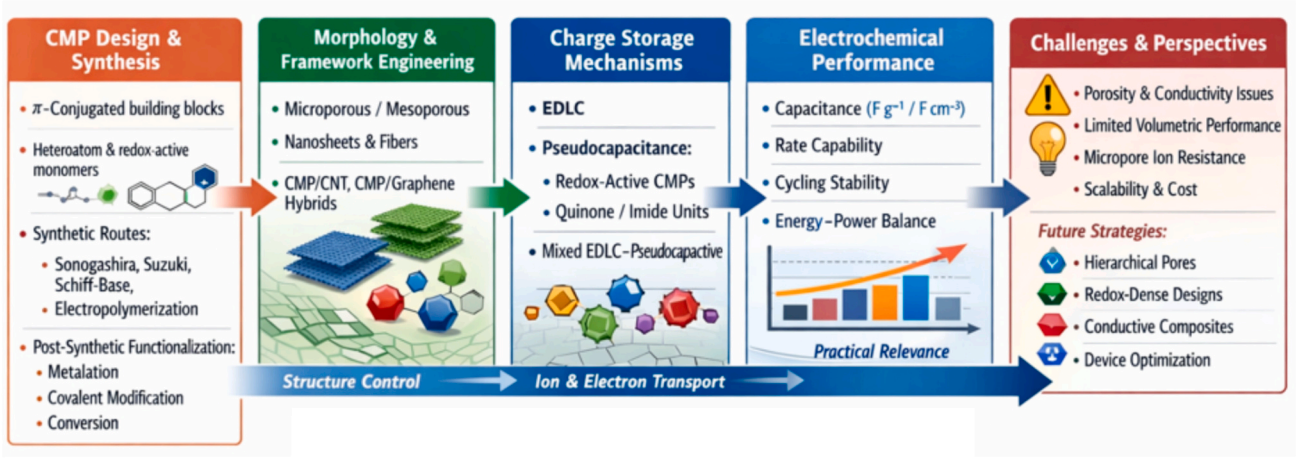

Fig. 1. Schematic illustration summarizing the scope and structure of this review.

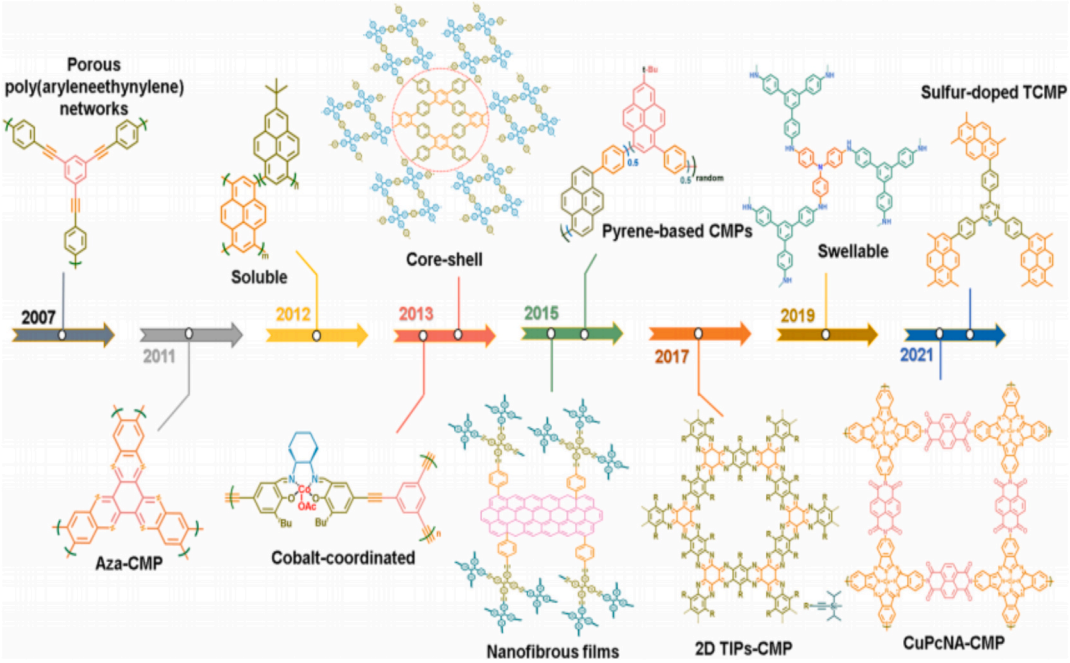

Fig. 2. Chronology of the CMP's advancement. Reproduced with permission from Ref. [60] Copyright 2022, American Chemical Society.

2.2.3. *Ionothermal technique*

Ionothermal synthesis provides an alternative pathway for preparing CMPs, characterized by its resistance to interference from other ions and the absence of solvents. Kim group [85] successfully prepared a CMP by employing molten $ZnCl_2$ as a solvent and methyl ketone as a starting building block. This ionothermal synthesis strategy offers several advantages, including cheap catalysts cost and the absence of reaction solvents, making it a promising approach for achieving large-scale synthesis of CMPs.

2.2.4. *Mechanochemical grinding*

Troschke's research group was the pioneer in synthesizing porous CTFs using a mechanochemical grinding method, via Friedel–Crafts alkylation reaction [65]. This specific alkylation reaction was made possible through mechanical grinding, as carbazole demonstrated higher reactivity with the cyanuric acid present within the amorphous network of carbazole-coupled triazine (Fig. 3). This technique offers several merits, including its safety, absence of solvent consumption, and time-saving attributes.

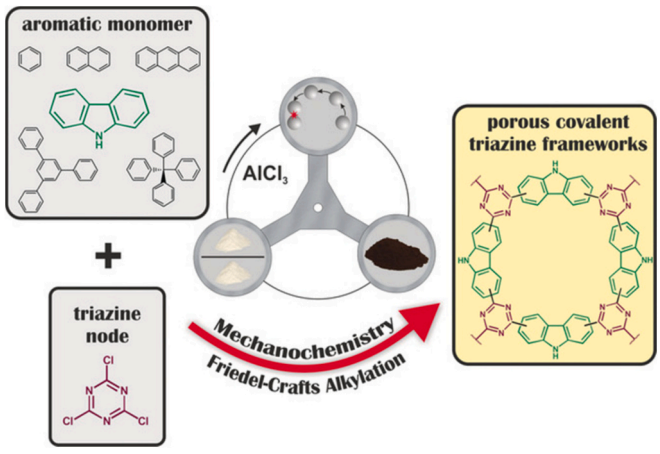

Fig. 3. Mechanochemical syntheses of porous CTFs by Friedel–Crafts alkylation of various aromatic monomers with cyanuric chloride. Reproduced with permission from Ref. [65] Copyright 2017, Wiley.

2.2.5. *Electropolymerization*

Electropolymerization has emerged as an effective technique for fabricating CMP films with excellent porosity [69]. Liu group utilized this method to fabricate dendrimer-based CMP films (TPETCz), employing dendritic macromolecule precursors. These films displayed remarkable adsorption capabilities for various organic compounds, owing to their microporosity (Fig. 4). Similarly, in 2021, Zhou et al. [86]. adopted the same electropolymerization strategy to prepare a polybenzazole CMP membrane, notable for its uniform and narrow pore sizes. This straightforward in situ electropolymerization approach offers a novel avenue for CMP preparation.

2.3. *Coupling and condensation strategies for CMP construction*

2.3.1. *Sonogashira-Hagihara reaction*

The initial synthetic procedure used for the construction of CMPs involves condensation polymerization. Since the construction of the poly(arylene) CMP using the Sonogashira reaction [59] this approach has become a prevalent technique for CMP preparation. The Sonogashira reactions find notable applications encompassing: the Zn-CMP microspheres with large diameters; the CMP nanotubes with great flame retardancy [55]; and a fluorescent CMP for the effective removal of uranyl ions [87].

2.3.2. *Suzuki-Miyaura reaction*

Two core–shell CMPs have been successfully prepared using the Suzuki polymerization. These CMPs were engineered to enable precise tuning of the emission of light across a broad range of wavelengths, showcasing their versatility in optical applications [88]. Additionally, in another research endeavor by Xu et al., they employed the Suzuki coupling to prepare ethyl phosphate-containing polymers (CMP-EP) that can adsorb the uranium ions generated during the treatment of nuclear fuel with high selectivity. This work underscores the potential of CMPs in addressing critical challenges related to nuclear waste disposal [89].

2.3.3. *Yamamoto coupling reaction*

Schmidt's research team [90] investigated the impact of varying the

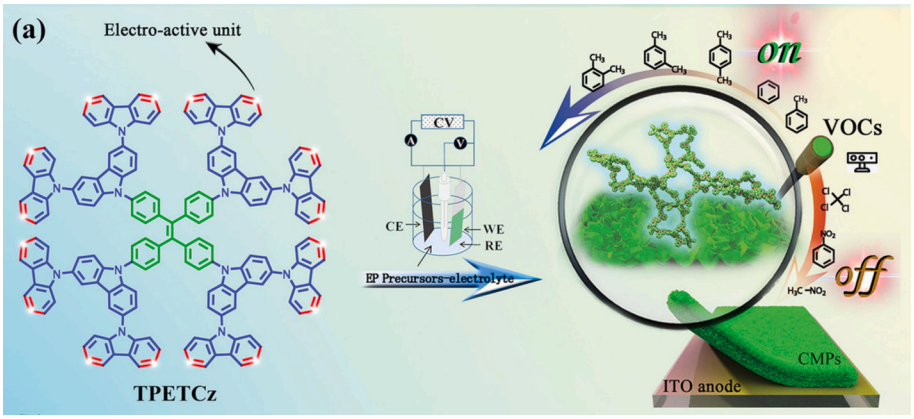

Fig. 4. Molecular structure of the dendritic monomer and schematic illustration of CMP film fabrication via electropolymerization. Reproduced with permission from Ref. [69] Copyright 2020, Wiley.

brominated monomer ratios on the resulting CMP when employing Yamamoto condensation. The group observed that various ratios caused alterations in the CMP characteristics, including changes in specific surface areas and pore volumes. Following this research, Yuan's research team [91] integrated the Yamamoto polymerization with the electrospinning technique to fabricate nanofiber thin film CMPs that were effectively employed as efficient sensors for phenoxy compounds and nitroaromatic hydrocarbons, demonstrating their potential in environmental sensing applications.

2.3.4. Heck coupling reaction

Sun and collaborators [92] have designed a novel luminescent CMP using a Heck reaction involving vinyl aromatic compounds with functional aromatic halides. This newly designed CMP was effectively employed as a sensor for the detection of explosives, primarily due to its luminescence that can be quenched using picric acid.

2.3.5. Cyclotrimerization reaction

Bohra team [93] employed a green cyclotrimerization reaction to synthesize a triazine-based CMP. The resulting CMPs were applied in the photocatalytic oxidation of benzylamine. Notably, the CMP with higher triazine unit content demonstrated exceptional catalytic performance, achieving a conversion rate up to 99% of benzylamine. Similarly, Kim et al. [85]. utilized the cyclotrimerization reaction to polymerize tetra-(4-acetylphenyl)methane and 1,3,5-triacetylbenzene, with fused $ZnCl_2$ serving as the solvent. The produced CMP exhibited significant potential for charge storage applications.

2.3.6. Glaser coupling reaction

Chen group [94] synthesized a 2D-PTNS CMP, employing a Glaser reaction using a triethynyltriptycene as the starting monomer. The research demonstrated that 2D-PTNS exhibits strong adsorption capabilities for gases. Also, a set of butenyl polymers has been produced from arylene building blocks with varying structures using the Glaser reaction [95]. The obtained CMPs exhibited an excellent CO_2 uptake, suggesting their potential utility in CO_2 capture and storage technologies.

2.3.7. Ullmann coupling reaction

In a study conducted by Liu et al. [96], they prepared donor-acceptor CMPs by employing pyrene (Py) donor and benzene, phenanthrene, and pyrazine acceptors, all through the Ullmann reaction. These polymers were found to possess outstanding photocatalytic efficiency and stability. Therefore, they were effectively utilized as photocatalysts for hydrogen evolution under visible light.

2.3.8. Scholl coupling reaction

The Scholl reaction is a chemical process that involves the condensation of benzene rings within aromatics, typically using $AlCl_3$ as a catalyst. Guo and colleagues [97] employed this reaction to synthesize a carbazole containing CMP (CZ-CMP), which was utilized as a solid-phase extraction adsorbent to capture herbicides, achieving a high level of extraction efficiency.

2.3.9. Oxidative coupling reactions

Recently, researchers have extended the use of oxidative coupling reactions to prepare CMPs. For example, the Qiao research group [77] synthesized five elastic chains with various longitudes and reacted with a rigid network to create a polycrazole framework. Nitrogen-rich CMPs (NCMPs) have also been synthesized using oxidative coupling reactions. The intermediate products formed by the reaction between various brominated monomers and aniline have been employed in the generation of nitrogen-rich CMPs via oxidative coupling reactions. These NCMPs have found successful applications in heterogeneous catalysis as well as gas storage [98].

2.3.10. Schiff base condensation reactions

In the work by the Ding group [99], they constructed a novel class of materials known as metallic phthalocyanine CMPs (MPc-CMPs) through the Schiff base reaction. These MPc-CMPs served as photosensitizers for singlet oxygen generation ($^1O_2$). These MPc-CMP had a rigid microporous structure, which helps overcome issues related to oxygen exposure that can be encountered with metallic phthalocyanine units. This structural feature of polymers enabled them to be utilized as photosensitizers for the sustainable production of singlet oxygen.

2.3.11. Knoevenagel condensation reaction

Zhuang and colleagues [100] achieved a significant milestone by synthesizing the first olefin-bridged CMP via Knoevenagel reaction. They utilized the major monomer 1,4-phenylenediacetonitrile with triformyl aromatic monomer. The resulting CMP exhibited crystalline structure with a layered morphology, which made it suitable as an electrode in supercapacitors and as an electrocatalyst for oxygen reduction reaction.

2.3.12. Aldol condensation reaction

Lyu team [101] successfully prepared an olefin-bridged CMP using the Aldol condensation. This CMP exhibited impressive characteristics, including a great surface area of 1715 $m^2\ g^{-1}$. Notably, it demonstrated remarkable chemical stability even under harsh conditions involving strong acids and alkalis. This exceptional stability makes it a valuable material in the field of catalysis.

2.3.13. Buchwald-Hartwig reaction

It is a widely utilized amination chemical reaction in synthetic

organic chemistry, facilitating the creation of polar C − N bonds through amine-aryl bromide coupling in the presence of a palladium catalyst [75,102]. This reaction not only serves as a source of intermediates for CMP synthesis but also enables the direct production of CMPs. For instance, researchers have leveraged the Buchwald−Hartwig reaction to create several 3D-PAQ frameworks by reacting 2,6-diaminoanthraquinone (DAQ) with various brominated aryl building units and utilizing these polymers as electrodes for SCs. To address the issue of the poor surface area of CMPs obtained from the Buchwald coupling, researchers have introduced inorganic salts into the reaction medium [102]. The research outcomes indicated a substantial enhancement in the surface area of the produced CMPs when inorganic salts like NaCl, NaF, and $LiNO_3$ were introduced, all while preserving their structural integrity. This indicates the possibility of precisely adjusting the porosity of the CMPs by integrating these salts into the synthesis procedure. Subsequently, Pan and coworkers [103] expanded on this approach by preparing a set of CMPs using inorganic salts, specifically $NaNO_3$, in the Buchwald coupling. The newly synthesized CMPs were employed in extracting nitroaromatics and eliminating poisonous organics.

2.3.14. Friedel-crafts coupling reaction

It is a valuable method for the preparation of certain CMPs, particularly for the synthesis of triazine-based polymers. This coupling reaction offers several merits, including its speed, simplicity, lack of metal catalyst, and cheapness. Geng et al. have harnessed this reaction to create various polymers with diverse structures [104]. Furthermore, they introduced stable cobalt nanoparticles into the process to synthesize a modified CMP. This network was subsequently calcinated and employed as a porous carbon for the oxygen reduction catalysis, demonstrating excellent efficiency [105].

2.3.15. Other synthetic reactions

Besides the coupling reactions discussed earlier, researchers have explored various other types of reactions for the construction of CMPs. For instance, the Dawson team [106] used the Gilch reaction to synthesize a polystyrene framework. This reaction involved the self-polymerization of 1,2,4,5-tetrabromomethylbenzene in purified THF solvent to result material that exhibited a permanent pore structure and demonstrated chemical stability. Additionally, researchers have developed three olefin-based CMPs using cationic cyclization condensation. These CMPs were synthesized from monomers with numerous acetylene groups and demonstrated efficiency in adsorbing carbon dioxide and iodine gases [78]. Cationic cyclization polymerization offers notable advantages, including cheapness and high yield, as it does not necessitate the use of metals and does not yield byproducts.

Furthermore, the efficient synthesis of 2D-CMPs with fused phenyl rings was achieved by fusing phenazine rings [107]. He and colleagues employed the Chichbabin reaction to produce CMPs holding pyridine rings (PCMPs) [108]. Subsequently, these PCMPs were carbonized and found to be applicable candidates for storing energy. The Chichbabin chemical reaction is considered a synthetic route, representing an environmentally friendly approach to prepare CMPs. Furthermore, Baig and co-authors [109] constructed several CMPs via the [4 + 2] cyclobenzannulation reaction in the presence of a copper catalyst. These CMPs exhibited a remarkable iodine adsorption capacity, with rates reaching up to 166 wt%. Additionally, these CMPs demonstrated selectivity as dye adsorbents, effectively removing 100% of methylene blue from a solution containing methyl orange.

2.4. Post-synthetic functionalization of CMPs

In contrast to de novo synthesis, which follows a bottom-up strategy and enables a high degree of molecular-level functionalization, post-synthetic modification (PSM) involves the chemical alteration of CMP networks after framework formation. However, owing to the facile functionalization of benzene rings present in most polymers, a high degree of grafting can still be achieved through PSM of CMPs. Hoskins and Robson were the first to suggest the concept of PSM [110]. This approach was later applied by Wang and Cohen in 2007 to functionalize MOFs [111]. Since then, PSM has been successfully extended to other porous organic materials such as CMPs [112], POPs [113], and COFs [114], owing to its versatility and practicality.

2.4.1. Post-synthetic metalation

Incorporating active metal sites into CMP networks introduces valuable chemical functionalities within their pores. Early studies reported the construction of metal–organic CMPs (MO-CMPs) by integrating metalloporphyrin cores into CMP frameworks, thereby significantly broadening their applications through the synergistic coupling of chemical and physical features within their porous structure [115] Cooper and his team [116] stated two versatile strategies for the synthesis of MO-CMPs without relying on porphyrin-derived monomers. In contrast to the widely studied MOFs, where metals or metal clusters act as linking nodes to bridge inorganic and organic components in an open framework, MO-CMPs achieve integration through alternative design strategies. In the resulting MO-CMPs, the metal sites no longer serve as connectors between organic monomers but are instead anchored onto the CMP skeleton surface, thereby enabling the incorporation of active metal centers and diverse functional groups without disrupting the framework integrity.

Moreover, modification of metal sites following CMP formation preserves the extended π-conjugation of CMPs. For instance, CMP-$(Bpy)_x$ was synthesized via Sonogashira coupling of 1,3,5-triethynylbenzene with 5,5`-dibromo-2,2`-bipyridine and 1,4-dibromobenzene, using different proportions of bipyridines and aromatic groups to control the content of active metal sites within the CMP framework. The synthesized CMP-$(Bpy)_x$ was reacted with $[Re(CO)_5Cl]$ to anchor Re metal sites, and successful coordination of Re within the polymer frameworks was confirmed by FTIR spectroscopy compared to the pristine CMP-$(Bpy)_x$. In this regard, Canivet's research team reported a series of bipyridine-based CMPs with varying Ni loadings, which were investigated for their catalytic efficiency in C—H arylation. The obtained analyses demonstrated that the Ni-doped CMPs, enriched with multiple active sites, exhibited great catalytic performance and a broad substrate field [117]. Evidently, PSM enables precise tuning of metal incorporation within CMP networks and control of chemically active functionalities as required, without disrupting the extended π-conjugation. As a result, the excellent porosity of CMPs is preserved, ensuring efficient molecular transport after functionalization.

2.4.2. Covalent post-synthetic modification

Beyond the incorporation of diverse metal sites into CMP networks to produce functional materials, covalent PSM offers a powerful approach to modify the chemical and physical characteristics of CMPs relative to their pristine forms. In recent years, extensive research on PSM of porous materials has employed so-called 'click' chemistry, including azide–alkyne cycloaddition [118,119] and thiol–yne reactions [120] which were broadly applied to attach functionalities onto the pore surfaces of porous materials. Weber team synthesized CMP-1 as a template to interact with different amounts of thioethanol (C_2SH) or 6-mercaptohexanol (C_6SH), yielding CMP derivatives with aliphatic alcohol functionalities [121]. The radical thiol–yne reaction, a form of 'click' chemistry between thiol groups and the CMPs ethynylene units, altered the network morphology and modulated the optical characteristics depending on the degree of thiol grafting. To explore the synergetic applications of modified CMPs, Chen and coworkers prepared a series of CMPs in which the pristine CMP was reacted with many thiol-containing groups [122]. Specifically, they constructed the BTT CMP via Sonogashira coupling of BTT and 1,3,5-triethynylbenzene, which subsequently reacted with cysteamine in the presence of AIBN in anhydrous DMF at 90 °C for 24 h (Fig. 5a). The resulting CMP BTT-SC_2NH_2 was investigated for photocatalytic hydrogen generation, exhibiting 27.2-fold

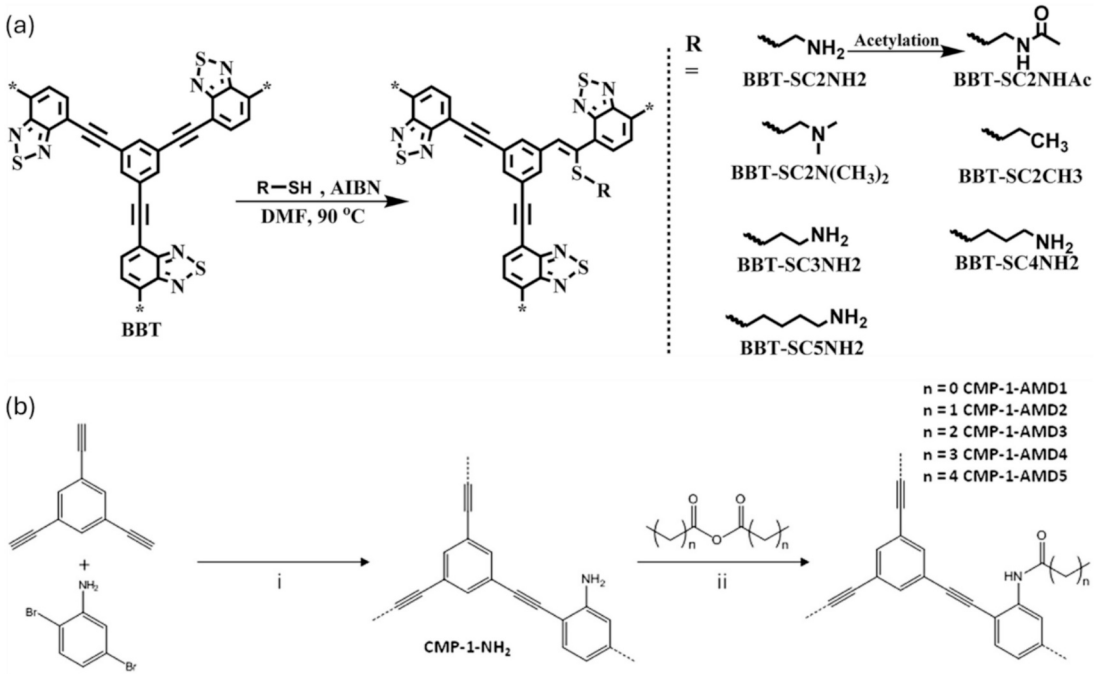

Fig. 5. (a) Preparation of functionalized BBT via thiol–yne click reaction and its possible structures. Reproduced with permission from Ref. [122] Copyright 2019, Royal Society of Chemistry, (b) Synthesis of CMP-1-NH_2 and its post-synthetic modification using anhydrides. Reproduced with permission from Ref. [123] Copyright 2014, Elsevier.

higher activity compared with BTT. These results indicated that amino-group incorporation enhances CMP-SC_2NH_2 hydrophilicity, improves charge separation, and extends electron lifetime, leading to more efficient proton reduction.

Cooper's research group reported the preparation of an amino-functionalized CMP (CMP-1-NH_2) and its subsequent conversion into amide-based CMP (CMP-1-AMD) through reactions with various anhydrides (Fig. 5b) [123]. The amidation of CMPs enables control over porosity and surface area through the length and geometry of alkyl chains, while also allowing engineering of the pore environment through the insertion of diverse functionalities. In summary, integrating pore size control with pore surface engineering paves the way for functionalized CMPs.

The structural tunability and tailored composition of CMPs enable improved gas uptake capacity and selectivity. To enhance CO_2 adsorption, Xu and his team developed metalloporphyrin-based CMPs functionalized with fluorine through PSM using alkyne–azide coupling [124] By varying the composition of azide-based monomers, CMPs with different fluoride loadings were obtained, revealing that higher fluorine incorporation strengthens CO_2 binding but simultaneously reduces porosity, limiting uptake. These findings highlight that balancing high surface areas with enhanced surface electronegativity is a promising strategy for designing effective CO_2 adsorbents, offering valuable guidance for porous organic material development.

2.4.3. Post-synthetic conversion

Given the challenges of synthesizing monomers with pre-installed functionalities, post-synthetic conversion provides an effective route to tailor the pore environment of CMPs for targeted applications. In 2020, a functionalized CMP adsorbent was reported for effective uranium removal [125]. A CMP synthesized from 1,3,5-triethynylbenzene was first functionalized with bis-CN groups (HCMP-CN) via malononitrile treatment and subsequently converted to amidoxime-functionalized networks (HCMP-AO) with high affinity toward uranyl ions. Adsorption studies in aqueous solutions showed that HCMP-AO exhibited markedly higher uranium uptake than HCMP or HCMP-CN, attributed to the unique coordination of bis-amidoxime ligands with uranyl species. This strategy highlights post-synthetic modification as a powerful approach for designing CMP-based adsorbents with superior performance for uranium and other ionic contaminants.

In summary, CMPs represent a versatile subclass of POPs distinguished by permanently porous, π-conjugated networks that enable broad functionality across catalysis, adsorption, sensing, and energy-related applications. A wide toolbox of synthetic routes—including solvothermal, microwave-assisted, ionothermal, mechanochemical, and electropolymerization methods—has enabled access to diverse CMP architectures with tunable porosity and framework chemistry. In parallel, CMP construction relies on multiple coupling/condensation strategies (e.g., Sonogashira, Suzuki, Yamamoto, Glaser, Schiff base, and Friedel–Crafts reactions), offering flexibility in monomer selection and structural design. Beyond framework formation, post-synthetic functionalization (metalation, covalent modification via “click” reactions, and post-synthetic conversion) provides an efficient pathway to tailor pore environments and introduce active sites while preserving porosity and conjugation, thereby expanding the performance and applicability of CMP in targeted advanced functions.

3. Supercapacitors (SCs)

SCs are characterized by their rapid charge and discharge capabilities, making them highly promising for electrochemical energy storage. Unlike conventional systems, they operate without chemical processes and mechanical dynamics like high-speed rotation, resulting in zero pollution and noise. Their simple structure, compact size, and efficient performance make them excellent candidates for advanced energy storage devices [126,127]. Notable features of SCs include ultra-fast charging, capable of reaching over 95% of their rated capacity within just 10 s to 10 min, as well as exceptionally long cycle life. They can endure deep charge–discharge cycles ranging from 1 to 500 k cycles [128–130]. SCs are manufactured, operated, stored, and recycled in an environmentally friendly way, making them an excellent option for sustainable energy solutions [131]. They offer a high level of safety and require little to no maintenance, even during long-term use. Furthermore, the low internal resistance of SCs enables outstanding

charge–discharge efficiency, often exceeding 90%. They also operate reliably across a wide temperature range of −40 °C to 70 °C, with minimal influence of temperature on the reaction kinetics of their electrode materials [132,133]. In addition, they offer ease of monitoring and control, further enhancing their practicality. The residual electrical energy in SCs can be precisely evaluated through the equation $E = CV^2/2$, where the stored energy is easily determined through measurement of the terminal voltage alone. This determines the state of charge simply and precisely. As a result, SCs greatly simplify energy management and control [134–137]. Therefore, designing SCs with both increased power density and great energy density is highly significant from both scientific and practical perspectives. Fig. 6 presents the Ragone curve, demonstrating the trade-off between energy and power densities, an essential parameter in energy storage technologies. The Ragone plot also helps identify the optimal operating range of various energy storage devices [138–140].

3.1. Structure of SCs

Fig. 7 shows the structural configuration of a typical SC, which mainly consists of porous materials with high surface area, current collectors, porous separators, and electrolytes [141]. Ensuring tight integration between the electrode materials and current collectors is essential to minimizing contact impedance. On the other hand, the separator should be optimized for maximum ionic conductivity while maintaining minimal electronic conductivity. This effect is generally realized through the use of fibrous electron-insulators, for example, polypropylene membranes [142,143]. The choice of a suitable electrolyte is determined by the properties of the electrode materials. When an external potential is applied across the two conductive electrodes, the capacitor charges, with one electrode storing positive charges and the other storing negative charges. Once the applied potential is removed, the charges remain stored on their corresponding electrodes [144].

3.2. Types of SCs

SCs are generally divided into two main categories based on their charge storage mechanisms: (i) electrochemical double-layer capacitors (EDLCs) and (ii) pseudocapacitors. In EDLCs, charge storage takes place through the reversible adsorption of ions at the electrode–electrolyte interface. When the electrode is charged, the polarized surface attracts oppositely charged ions from the surrounding electrolyte, which adhere to the electrode surface. This process forms a dual-layered charge arrangement, giving rise to double-layer capacitance. The minute spacing of the charge layers, generally less than 0.5 nm, combined with

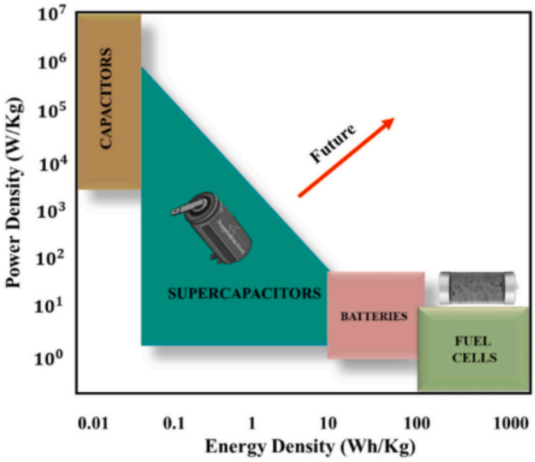

Fig. 6. Ragone diagram. Reproduced with permission from Ref. [138] Copyright 2021, Royal Society of Chemistry.

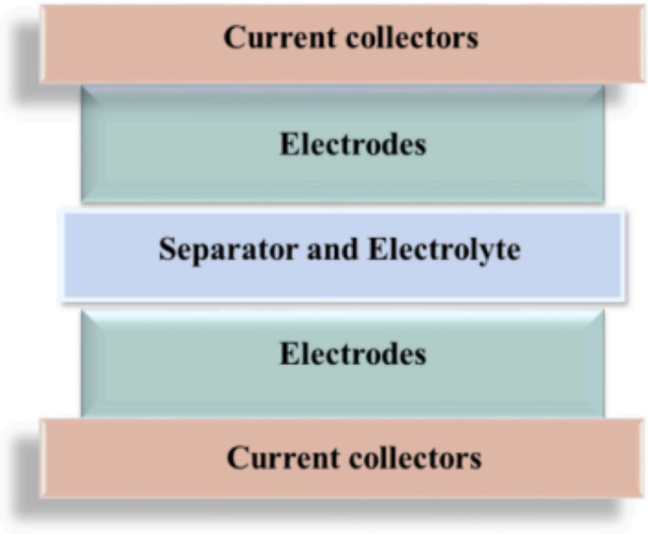

Fig. 7. Internal structure of supercapacitors. Reproduced with permission from Ref. [141] Copyright 2021, Elsevier.

specially designed electrode structures that greatly increase the electrode surface area, leads to a significantly enhanced capacitance [145]. Pseudocapacitance arises from the deposition of electroactive species either on the electrode surface or within its bulk phase. It involves highly reversible processes such as chemical adsorption, desorption, oxidation, and reduction, leading to a capacitance that varies with the electrode's charge potential. Pseudocapacitance can occur both at the electrode surface and throughout the bulk of the electrode material, enabling it to achieve greater electrochemical capacitance and higher energy density compared to double-layer capacitance [146,147].

In terms of electrochemical behavior, pseudocapacitors fall into three categories (Fig. 8): (1) underpotential deposition, (2) redox processes, and (3) intercalation mechanisms. Underpotential deposition refers to the adsorption of metal ions from solution onto the surface of a different metal at potentials more positive than the equilibrium redox potential, leading to the formation of a single atomic layer. This phenomenon occurs between two different metals; a well-known example is the formation of a lead monolayer on a gold electrode via underpotential deposition [148,149]. Redox pseudocapacitors function through the electrochemical ion adsorption from the electrolyte to the surface or near-surface regions of the active material. This process is accompanied by redox reactions mediated by electron transfer, which convert the adsorbed species into stored charges. Intercalation pseudocapacitors represent a newer type of pseudocapacitor designed for layered or tunnel-structured materials. In this mechanism, electrolyte ions migrate into the porous framework or interlayer gaps of the material, where redox reactions with neighboring atoms occur via electron transfer [150–152]. Fig. 9 depicts the mechanisms of charge storage in EDLCs and pseudocapacitors. In EDLCs, charge is stored through non-Faradaic processes and electrostatic interactions, typically utilizing carbon-based materials.

Improving conductivity and specific surface area is essential to maximize capacitance in these systems. A fundamental limitation in CMP-based SC electrodes arises from the intrinsic trade-off between high surface area and electronic conductivity. While ultrahigh BET surface areas (>1000 m^2 g^{-1}) and dominant microporosity enhance ion-accessible interfaces and EDLC, excessive pore confinement and disrupted π–π stacking often impede charge carrier transport through the polymer backbone. As a result, CMPs with the highest surface areas often exhibit inferior rate capability and lower power density than more conductive porous carbons [154,155].

Quantitative studies reveal that CMPs with moderate surface areas

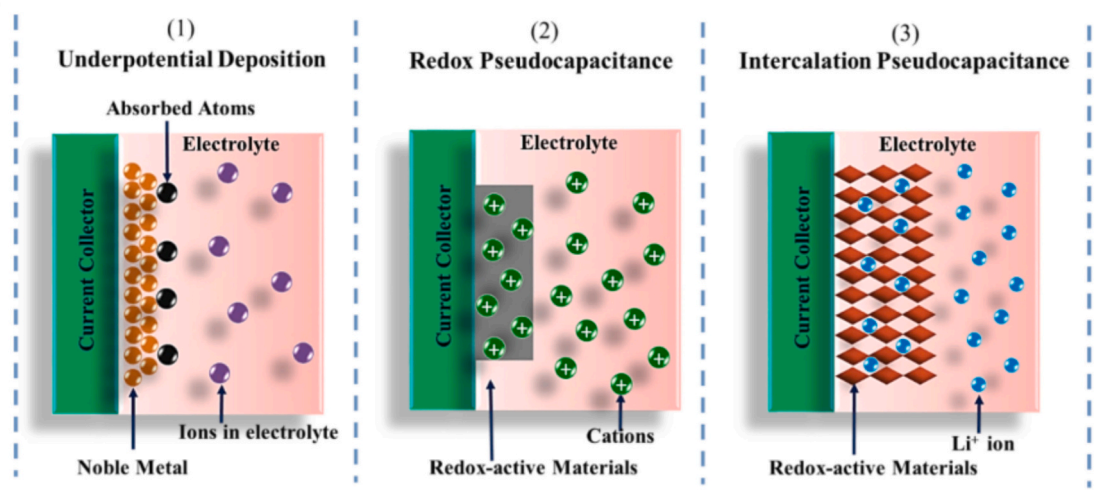

Fig. 8. Types of pseudocapacitors. Reproduced with permission from Ref. [153] Copyright 2023, MDPI.

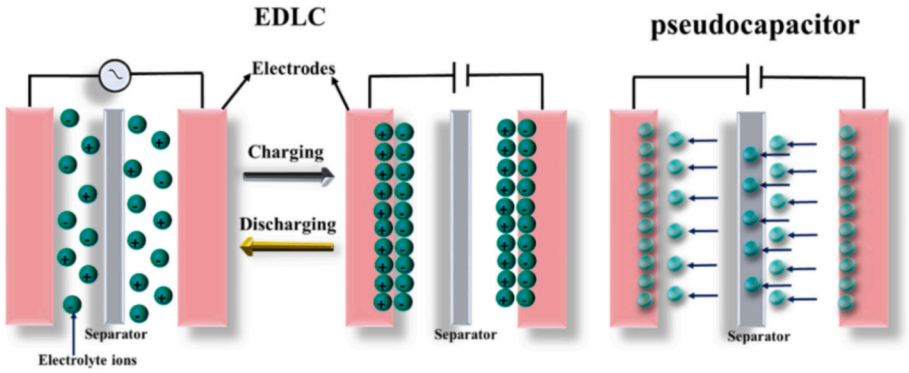

Fig. 9. Schematic diagram of the charge and discharge energy storage mechanism of EDLC and pseudocapacitors. Reproduced with permission from Ref. [153] Copyright 2023, MDPI.

(500–900 m^2 g^{-1}) but improved backbone planarity or extended conjugation often outperform highly porous analogues at high current densities, highlighting that conductivity and charge transport are more critical than surface area alone [156,157]. Strategies such as heteroatom incorporation, π-conjugation extension, and hybridization with conductive carbon additives have been proposed to mitigate this trade-off. However, these approaches frequently introduce secondary compromises, including pore blockage, reduced accessible surface area, or increased synthesis complexity. Therefore, optimizing CMP performance requires balancing porosity with intrinsic conductivity rather than maximizing surface area alone. Fig. 10 outlines the key factors that influence the overall performance of supercapacitors [153,158].

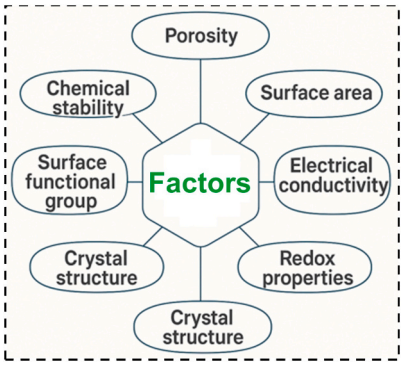

Fig. 10. The main factors affect the performance of supercapacitors.

3.3. Electrochemical measurements

To assess the electrochemical efficiency of a material for electrode application, several key parameters must be studied, including specific capacity, current, voltage, energy, and power densities. These parameters can typically be obtained through electrochemical investigations such as cyclic voltammetry and galvanostatic charge/discharge tests. These tests provide valuable insights into how the material behaves in terms of its energy storage capabilities [159,160].

3.3.1. Cyclic voltammetry (CV)

CV is a widely utilized technique in electrochemical measurements due to its simple operation. In this technique, the electrode potential is scanned forward and backward within a defined potential range at a constant sweep rate. To perform a CV measurement, the terminal voltages (E1 and E2) and the scan rate (ν) must be determined initially. Then, the corresponding voltage is applied to evaluate the electrochemical system, as shown in Fig. 11a. In electrochemical devices, such as SCs and batteries, the typical relationship between current and potential is represented by a CV graph, as shown in Fig. 11b. This graph allows us to determine peak current (ip) and peak potential (Ep). To determine the reversibility of an electrochemical system, you need to evaluate the ratio of peak currents (ipa and ipc) and the difference in peak potential (ΔEp) between the anodic and cathodic segments. When CV curves are converted to voltage versus capacity profiles, the charge

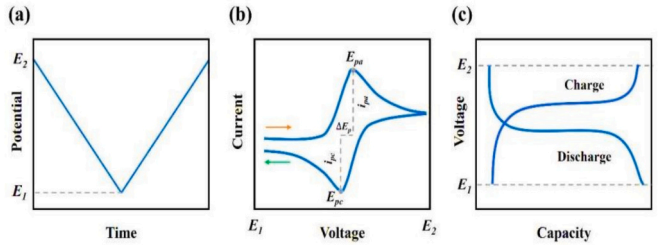

Fig. 11. Model of CV measurements: (a) potential plot applied in a CV test, (b) current response vs. voltage curves, and (c) voltage vs. integral current curves. Reproduced with permission from Ref. [159] Copyright 2019, Wiley.

and discharge curves will correspond to the anodic and cathodic peak potentials, as illustrated in Fig. 11c.

For a standard SC, capacitance (C) can be determined using the following relation:

$$C = I/S \quad (1)$$

In the equation, I represent the applied current, and S stands for the potential sweep rate. In the context of a standard SC, the current obtained is graphically presented in Fig. 12. Specifically, during the negative scan voltage, the current should consistently be negative, while it should be positive during the positive sweep. Ideally, for a perfect supercapacitor, the current-versus-potential plot (CV profile) should exhibit symmetrical, rectangular characteristics, as depicted in Fig. 12b. This symmetrical behavior aligns with Eq. (1).

In reality, SCs often deviate from this ideal behavior due to various non-idealities that arise in real-world scenarios. For instance, at high scan rates, the CV profile can take on a leaf-like shape, as depicted in Fig. 13a. To elaborate, in many SCs, increasing the scan rate results in the 'rounding off' of the CV corners. This phenomenon is attributed to rate-limiting factors like electrical transport constraints within the electrode or ionic transport restrictions within the electrolyte. Consequently, at higher sweep rates, the formation of the interfacial double layer is hindered due to these transport limitations. Another non-ideality phenomenon in SCs is electrolyte degradation, which occurs in most cases. Each type of electrolyte has its own limited voltage stability window, and exceeding this window leads to faradaic reactions within the electrolyte. For instance, aqueous electrolytes typically have a limited potential range of around 1.0 V, if the potential goes too low or too high, water may undergo reduction or oxidation, resulting in the formation of hydrogen and oxygen, respectively. These reactions result in an increase in current higher than the applied double-layer charging current because they require ion movement at the electrode-electrolyte interface. This additional current is referred to as I_{excess}, as shown in Fig. 13b. It involves electrolyte interactions but does not contribute to charge storage and should not be used to determine capacitance using eq. (1). Ultimately, electrolyte degradation reduces the performance and lifetime cycling of SCs.

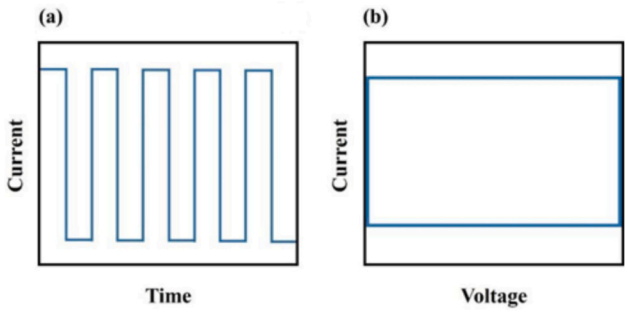

Fig. 12. Typical CV profiles: (a) the measured current of a typical supercapacitor plotted against time; (b) the CV profile, representing the current plotted against voltage. Reproduced with permission from Ref. [160].

Certainly, pseudocapacitive current can significantly contribute to the energy storage capacity of SCs instead of the current resulting from the degradation of the electrolyte. Reversible faradaic interactions at the electrode surface can result in capacitive currents, effectively increasing the capacitance arising from double-layer charge. This extra capacitive current is denoted as I_{Φ}, as illustrated in Fig. 13c, which depicts a typical CV graph for a pseudocapacitance.

3.3.2. Galvanostatic charge/discharge (GCD)

In addition to CV measurements, galvanostatic charge/discharge (GCD) analyses are also commonly utilized to investigate the electrode capacitance, and they are often preferred for this purpose. GCD tests involve the application of a fixed charging current until the higher potential is attained, followed by the setting of an equal discharge current until a lower potential is attained. The maximum potential applied during GCD tests depends on the nature of the electrodes and electrolytes. For instance, in aqueous electrolytes, the highest voltage typically ranges from 0.0 to 1.0 V, while in organic electrolytes, they range from 0.0 to 2.5-2.7 V. Therefore, GCD measurements can provide more accurate assessments of capacitance compared to CV tests, reflecting the actual efficacy of the electrode materials. Fig. 14 provides some examples of GCD curves.

In fact, for a typical SC, the graphical curve of charge and discharge should be symmetric, and the slope should remain fixed throughout, as shown in Fig. 13a. The capacitance (C) can be determined by applying the following relationship:

$$C = I/(\Delta V/\Delta t) \quad (2)$$

While "I" represents the applied current magnitude, "$\Delta V/\Delta t$" is calculated from the slope of the discharge GCD curve. It's clear that there is a similarity in specific capacitance calculation when using CV and GCD measurements, but there's a difference in what remains constant: the denominator (potential) is constant in CV, whereas the numerator (current) is fixed in GCD measurements.

Real SCs don't always produce linear plots, and nonlinear curves are sometimes obtained, indicating various non-idealities in SC operation. For instance, Fig. 14b illustrates an example of surpassing the electrolyte stability window, which is a type of non-ideal behavior. To explain, there is a charge transfer that takes place at the electrode-electrolyte interface, leading to a decrease in the slope of the charge or discharge curves. This charge transfer is a result of reactions occurring in the electrode, the electrolyte, or both. Moreover, if these processes take place in the electrolyte, it can lead to electrolyte degeneration, resulting in a reduced potential window within the electrochemical stability limits of the electrolyte. Furthermore, when these reactions occur on the surface of the electrode, they can lead to pseudocapacitive charge storage, which may or may not be reversible. If the behavior is irreversible, it can cause electrode decay, which is unfavorable. Additionally, Fig. 14c illustrates another type of non-ideal behavior that occurs in all SCs at sufficiently high currents, similar to the leaf-shaped profile shown in CV Fig. 13a. The initial portion of the discharge curve is generated by an instantaneous voltage drop when transitioning from charge to discharge. This potential drop is referred to as the IR drop and is produced from the internal total impedance of the system, including electrolyte resistance, electrode resistance, and any other contact resistances [159–162].

3.3.3. Cycle life-time

Indeed, charge storage in SCs primarily relies on electrostatic mechanisms rather than electrochemical processes, which are distinct from batteries. This characteristic makes SCs potentially capable of having a relatively long cycle life, especially when double-layer capacitance dominates the charge storage mechanism. However, if pseudocapacitive redox interactions occur, irreversibility may decrease the overall lifetime performance. To assess the cycle life of an electrode

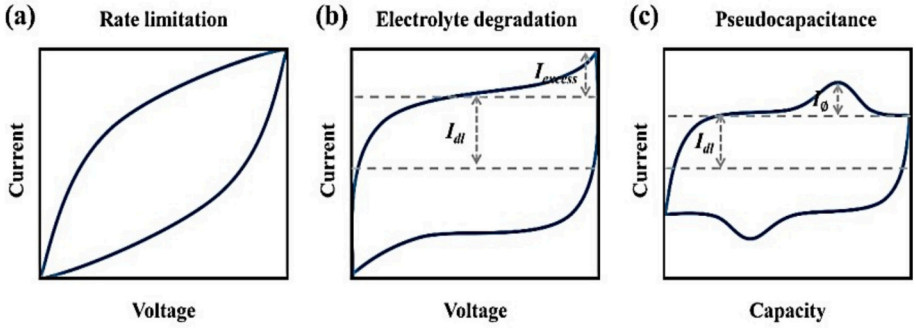

Fig. 13. Supercapacitor CV non-idealities: (a) sweep rate limitations, (b) potential window that exceeds electrolyte stability window, and (c) pseudocapacitive charge storage. Reproduced with permission from Ref. [160]

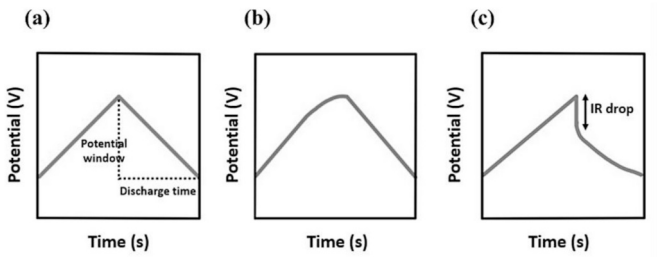

Fig. 14. GCD profiles. (a) A typical charge-discharge cycle includes the slope, (b) a charging plot which surpasses the electrolyte stability window, resulting in extra charge transfer, and (c) a discharge plot which is preceded by an IR potential drop. Reproduced with permission from Ref. [160]

material or a device, it's essential to subject it to repeated charge and discharge cycles using techniques like CV or GCD. The parameters, including the applied current, potential window, and potential scan rate, should be carefully chosen to mimic real-world operating situations. For instance, very slow sweeping rates ($< 10\ mVs^{-1}$) or very high sweeping rates ($> 10\ Vs^{-1}$) in CV cycles are not representative of typical device operation and can yield deceptive results. These parameters, along with other factors like electrolyte composition and sample size, should be considered when determining cycle life. In practice, SCs are often tested for a significant number of cycles, ranging from at least 104 to 106 cycles. This extended cycle life is one of the significant advantages of SCs compared to batteries [163,164].

3.3.4. Energy and power density

Energy and power densities are considered crucial factors for investigating the efficiency of supercapacitor materials and devices. The energy density (E) of a device can be estimated from the following relation:

$$E = 1/2\ CV^2 \tag{3}$$

In which C represents the capacitance calculated from CV or GCD, and V is the ultimate reached potential range. E is usually given in units of Wh cm^{-2} or Wh cm^{-3}; hence, a factor of (1/3600) is inserted into the previous equation. In addition, the power density can be determined by using one of the following two equations:

$$P = E/\Delta t \tag{4}$$

$$P_{max} = V^2/4ESR \tag{5}$$

Here, Δt is the time of discharge, and the ESR is calculated from GCD. Eq. (5) determines the highest available power, while Eq. (4) gives the total output power within the discharge. Every CV sweep rate or discharge current could be utilized to calculate E and *P* values. These previous values of E and P could be plotted on a Ragone figure to evaluate the working potential window of the device [162,165].

3.4. Electrolytes for SCs

The electrolyte is a critical component of SCs, much like the electrodes. It must meet specific criteria related to electrochemical stability and ionic conductivity to ensure the efficient operation of the supercapacitor. Currently, many SCs employ liquid electrolytes, including ionic liquids, aqueous salt solutions, and organic salt solutions. Moreover, there is a growing research focus on solid-state electrolytes, which show promise for applications in high-temperature environments and integrated on-chip devices. The choice of electrolyte depends on the specific requirements of the SC application, with liquid electrolytes being suitable for many commercial SCs due to their high ionic conductivity, while solid-state electrolytes are preferred in situations where safety, elevated-temperature performance, or miniaturization are critical factors.

3.5. Electrode materials for SCs

Certainly, the choice of material for a SC electrode is crucial and hinges on two primary properties. Firstly, the material must exhibit electrical conductivity to facilitate the transfer of charge carriers to the electrode-electrolyte interface. Secondly, it should possess electrochemical stability to endure long-term electrochemical cycling, unless it is specifically designed for pseudocapacitive charge storage. Additionally, a great surface area of the electrode material is essential to achieve higher energy and power densities, while considering factors such as safety, cost, and environmental impact is also critical during material selection. In this context, CMPs emerge as promising candidates for SC electrodes due to their favorable properties and tunability, which can contribute to improved performance and sustainability in energy storage applications [166,167].

Although CMP-based electrodes are frequently described as combining EDLC and pseudocapacitive storage, the literature often lacks quantitative reporting of the relative contributions and the robustness of the underlying analysis. In principle, CV-based kinetic metrics—such as the power-law relationship ($i = av^b$) and Dunn's capacitive–diffusion separation—can estimate the fraction of surface-controlled (capacitive) versus diffusion-limited charge storage as a function of scan rate. However, these methods can be sensitive to the selected potential window, scan-rate range, IR-drop compensation, and assumptions about linear separability, which may lead to overestimation of "capacitive" contributions, especially in porous polymers with distributed resistances. Complementary analyses (e.g., Trasatti method, GCD-based separation, and impedance-derived time constants) and, critically, operando techniques—such as in situ Raman/FTIR, XPS/XAS, EQCM, or gas analysis—are increasingly necessary to validate whether the Faradaic component arises from reversible redox of defined functional

groups, ion intercalation/confinement effects, or parasitic reactions. A more standardized, multi-technique workflow would therefore improve mechanistic confidence and enable more meaningful cross-comparison of CMP-based SC performance [168–170].

In summary, SCs are high-power energy-storage devices characterized by their rapid charge–discharge capability, long life cycle, high efficiency, and safe operation over a wide temperature range. Their basic structure consists of porous electrodes, current collectors, separators, and an electrolyte, and their performance is governed by the charge-storage mechanism, either non-faradaic ion adsorption in EDLCs or faradaic processes in pseudocapacitors. Key electrochemical metrics such as capacitance, rate capability, cycling stability, energy density, and power density are typically quantified using CV and GCD measurements, while Ragone plots highlight the inherent trade-off between energy and power. Finally, electrolyte choice and electrode material properties (conductivity, stability, accessible surface area) jointly determine device-level performance, motivating the development of tunable porous electrodes such as CMP-based materials for next-generation SCs.

4. CMP as electrode materials for SCs

Compared to batteries, SCs are considered a sustainable energy storage technology, offering higher power density but relatively lower energy density. Each of these traits carries its own advantages and limitations. Ongoing research is focused on creating technologies that combine the high-power density of SCs with the high energy density of batteries [171]. CMPs are proposed as a potential solution for achieving this objective through careful structural optimization of the materials (Fig. 15).

4.1. Nitrogen-rich CMPs

Notably, the redox-active CMPs (TAT/CMP-1 and TAT/CMP-2) have been utilized as highly effective electrode materials for SCs [172]. The integrated design strategies of TAT/CMP-1 and TAT/CMP-2 offer exceptional permeability, complemented by nitrogen-rich frameworks (Fig. 16a). Owing to their advantageous porosity and higher nitrogen content, TAT-CMP-1 and TAT-CMP-2 deliver notable electrochemical capacitances of 141 F g^{-1} and 183 F g^{-1}, respectively, at 1 A g^{-1} in a three-electrode system. Notably, they achieve an exceptionally great electrochemical capacitance per unit surface area, exceeding 160 mF cm^{-2} (Figs. 16b and c). Additionally, TAT-CMP displays outstanding reversibility, maintaining cycling performance of 95% and 83% at 10 A g^{-1} over 10 k cycles (Fig. 16d). These findings demonstrate that precisely tuning the content of nitrogen through chemical doping is an efficient strategy for enhancing electrochemical performance.

According to Yuan et al., nitrogen-rich graphene CMP sandwich structures (GMPs) are synthesized by first pyrolyzing CMPs into 2D porous carbon nanofilms using a 4-iodophenyl substituted graphene (RGO—I) matrix. These GMP sandwiches are then pyrolyzed to produce visibly plastic-doped porous carbon/graphene nanofilms [173]. The microporous polymer frameworks form simultaneously on both sides of the 2D graphene matrix, ensuring structural stability of the graphene-based layers even through subsequent high-temperature calcination. Moreover, three individual GMP-based SCs, when connected in series, demonstrate enhanced capacitance compared to single-cell SCs. Under similar charge density and nearly the same charge–discharge times, the GCD performance of multiple GMP-based SCs connected in series shows a remarkable increase. Both the type of dopants and the appropriate pore distribution play crucial roles in optimizing the performance of porous carbon nanocomposites.

The Berton group [174] reported a series of electrodeposited CMPs derived from bis-thiophene-carbazole bis-adduct monomers with different aromatic spacers for SCs. Extended phenyl and biphenyl cores (PBBTC-Ph and PBBTC-BPh) lower the oxidation potential, broaden the electroactive window, and enhance porosity, resulting in high areal capacitances of 235 mF cm^{-2} and 271 mF cm^{-2}, respectively, among the best reported for polymeric SCs. The films also exhibit excellent coulombic efficiency (>99.8% after 1 k cycles) and can withstand high current densities up to 10 mA cm^{-2}, highlighting the advantages of extended conjugation and optimized core linkers in improving charge storage, ion transport, and electrochemical robustness in electrodeposited CMP systems.

Nitrogen-rich doping and extensive specific surface area are key factors in enhancing Faradaic pseudocapacitive storage. In this respect, a conductive CMP synthesized from tetracyanoquinodimethane (TCNQ) was reported, featuring a nitrogen content exceeding 8% and an exceptionally great surface area of 3600 m^2 g^{-1} [175]. In a three-electrode system, this material delivered a great capacitance of 383 F g^{-1} and demonstrated outstanding cyclic stability, maintaining performance over 10 k GCD cycles. To address the lower electronic conductivity of CMPs, a composite of graphene hydrogel-based CMP was developed in earlier work [176]. The resulting material exhibited a hierarchical porous structure—comprising micro-, meso-, and macropores—with a surface area of 219 m^2 g^{-1}. Upon evaluation as electrodes for SCs, the composite demonstrated a notable capacitance of 206 F g^{-1}. Electrochemical impedance spectroscopy (EIS) further revealed that the composite displayed the lowest charge transfer impedance compared to the pristine CMPs, although no direct conductivity measurements were reported by the authors. This set of studies illustrates the diverse ways CMPs are used as capacitive energy-storage materials across various device configurations and charge-storage mechanisms. The compiled results indicate that nitrogen-doped CMPs, in particular, show strong promise for narrowing the performance gap between batteries and SCs (Table 1).

4.2. Quinone- and anthraquinone-based CMPs

Thomas et al. reported the synthesis of CMP networks via Buchwald–Hartwig (B—H) polymerizations for SCs (Fig. 17a) [75]. The resulting PAQs exhibited a unique integration of large surface area, redox activity, and excellent dispersibility—an uncommon property for CMPs. When utilized as SC electrodes, PAQs achieved a capacitance of

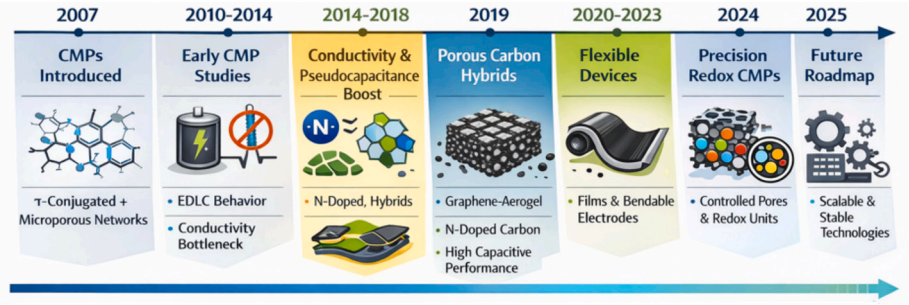

Fig. 15. Key milestones in the development of CMP-based supercapacitor electrodes.

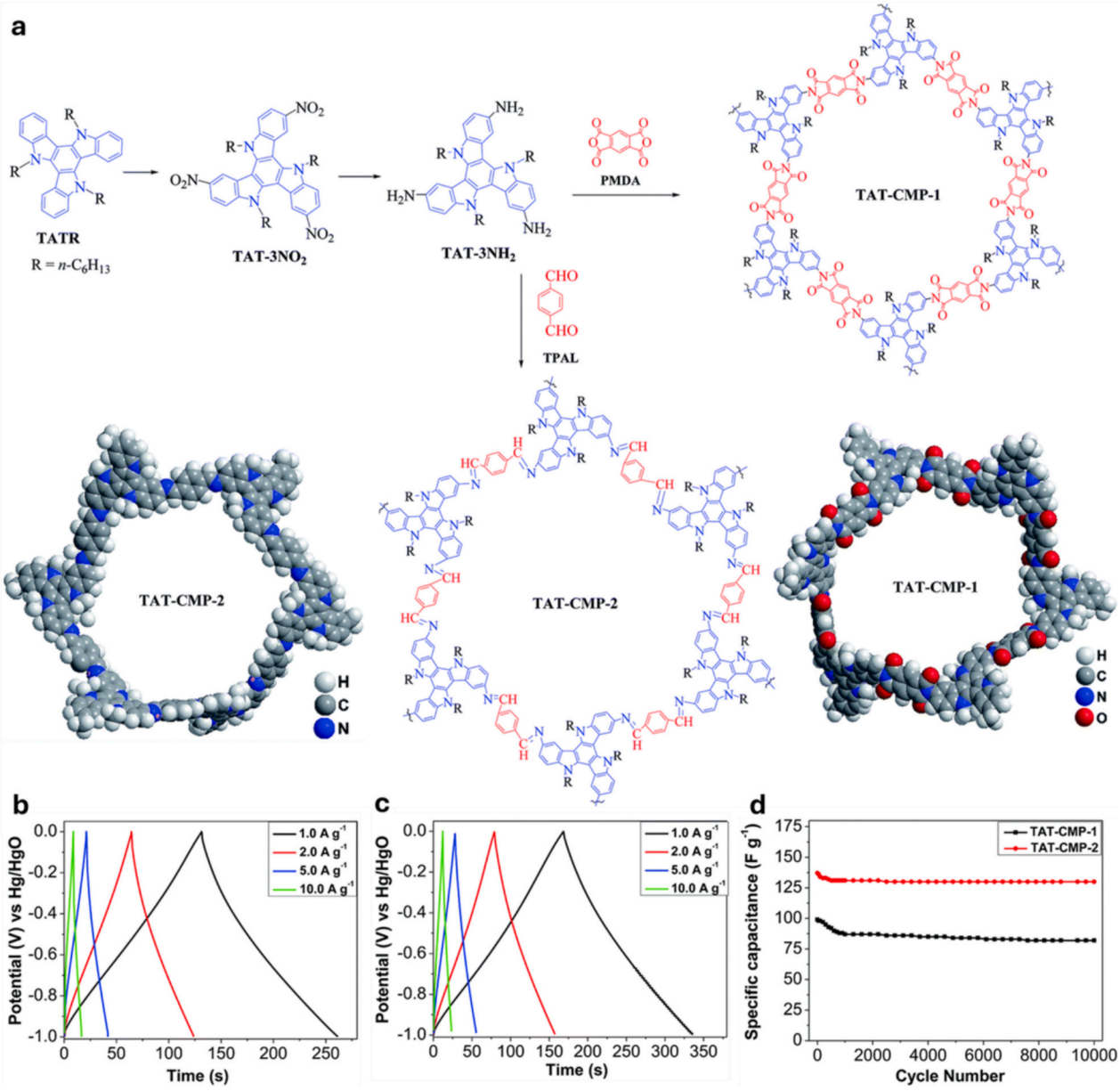

Fig. 16. (a) Chemical structure of TAT-CMP-1 and TAT-CMP-2. GCD curves of (b,c) GCD curves of TAT-CMP-1 and TAT-CMP-2, respectively, recorded at various current densities. (d) Cycling stability profiles showing the variation of specific capacitance for TAT-CMP-1 and TAT-CMP-2 over 10 k GCD cycles at a current density of 10 A g^{-1}. Reproduced with permission from Ref. [172] Copyright 2017, Royal Society of Chemistry.

570 F g^{-1} and maintained 80–85% of their electrochemical capacitance after GCD 600 cycles, with nearly 100% coulombic efficiency. The electrochemical applications were investigated in both symmetric and asymmetric SC configurations, as well as in a flexible device designed to demonstrate their potential for use in flexible electronics (Fig. 17b). It was further observed that the device's specific capacitance arose from a combined contribution of EDLC and pseudocapacitance.

A CMP framework incorporating a nitrogen-rich aza-fused linker was developed for application in SCs (Fig. 17d) [195]. The fused aza structure was found to enhance electrical conductivity, while its high surface area offered abundant active sites. Additionally, the microporous architecture facilitated rapid ion diffusion during charge–discharge cycles, thereby improving overall efficiency. Leveraging the above-mentioned benefits, aza-based CMPs accomplished an excellent electrochemical capacitance of 946 F g^{-1} in a three-electrode configuration, markedly greater than other polymers reported during that period (Fig. 17c). At a high current density of 10 A g^{-1}, they maintained a capacitance of 378 F g^{-1}, with no noticeable degradation after 10 k GCD cycles.

In insightful research, the Chandra group examined the influence of hydrogen bonding and the significance of redox-active functionalities on the performance of energy storage of the two COFs, namely: TpPa-$(OH)_2$ and TpBD-$(OH)_2$ [196]. Their findings revealed that the supreme specific capacitance of the synthesized COFs primarily stemmed from proton-coupled electron transfer processes based on hydroquinone/benzoquinone (H_2Q/Q) redox couples. When the H_2Q/Q units were substituted with phenolic or methoxy groups, no redox peaks were detected, resulting in a significantly reduced specific capacitance. The study also demonstrated that pseudocapacitance is the dominant contributor to the overall capacitance, regardless of the material's surface area. Hydrogen bonding between HQ groups and adjacent amine functionalities enhanced the structural stability, thereby ensuring excellent reversibility of the redox processes—an effect not previously reported.

A new porous polymer, TPDA-1, has been prepared via Schiff base

Table 1
Representative examples of CMPs for SCs in recent years.

CMPs	Electrolyte	SC	CD	CR/CN	PW	ED	PD	Ref
TPA-QP	1 M KOH	356	1.0	97/2000	-1.0–0.0	50.42	500	[177]
PAQs	1 M H_2SO_4	576	1.0	95.5/2000	0.0–1.6	60	1300	[75]
NCMs	0.5 M H_2SO_4	324	0.1	>97/10000	0.0–1.0	—	—	[108]
TBN-TPA	1 M KOH	251	0.5	94/5000	-1.0–0.0	5.0	500	[178]
PyPH-HATN-1.5	1 M KOH	1790	1.0	97/5000	-1.0–0.0	—	—	[179]
PYBDA	2 M H_2SO_4	476	0.5	130/5000	-0.2–0.6	40	3095	[180]
TPP-DBTh	3 M KOH	222	0.5	87.86/10000	-0.7–0.0	—	—	[181]
DBTh-TPT	1 M KOH	1823	0.5	81.75/10000	-1.0–0.0	—	—	[182]
Fe—P800	1 M H_2SO_4	183	1.0	100/5000	0.0–0.9	—	—	[183]
Py-Ph-BDT	1 M KOH	712	0.5	72.87/5000	-0.7–0.0	48.7	175	[156]
CuTAPP/CNTs-3	—	207.8	1.0	100/3700	-0.15–1.35	—	—	[184]
CMAP@AG	1 M H_2SO_4	751	1.0	95/20000	0.0–1.0	—	—	[185]
GH-CMP	1 M H_2SO_4	208	0.02	92.6/3000	0.0–1.0	12.55	252.5	[186]
N-GA/CMPs	6 M KOH	325	0.5	95/10000	-1.0–0.0	12.95	—	[187]
MWNT/CMP	6 M KOH	248	—	100/1000	-0.8–0.2	—	—	[188]
BHSM-CMP-3	1 M H_2SO_4	774	1.0	87/6000	0.0–0.8	—	—	[189]
CC-DAQ-CMP	6 M KOH	184	1.0	48/500	0.5–1.2	10.39	500	[190]
Fl-TPA	1 M KOH	276	0.5	95.23/5000	-1.0–0.0	38.33	250	[11]
BC-PT	1 M KOH	373	0.5	94.37/5000	-1.0–0.0	51.81	500	[191]
H-CMP-BPPB	1 M H_2SO_4	189	1.0	90/10000	-0.5–0.5	—	—	[192]
Fc-CMPs/rGO	1 M H_2SO_4	470	0.5	95/8000	0.0–1.0	8.0	124	[75]
PAQTA	0.5 M H_2SO_4	576	1.0	85/6000	0.0–1.6	60	1300	[75] [193]
CAP-2	2 M KCl	240	1.0	80/10000	0.0–1.0	—	—	[194]
PYT-TABQ/rGO	1 M Na_2SO_4	312	1.0	94.5/10000	-0.8–0.0	12.6	258.6	[76]
PTPA-25	1 M H_2SO_4	335	0.5	65/5000	0.1–0.9	—	—	

SC: specific capacitance in three electrode system (F g^{-1}); CD: current density (A g^{-1}); CR: cycling retention (%); CN: cycles number; PW: potential window; ED: energy density; PD: power density.

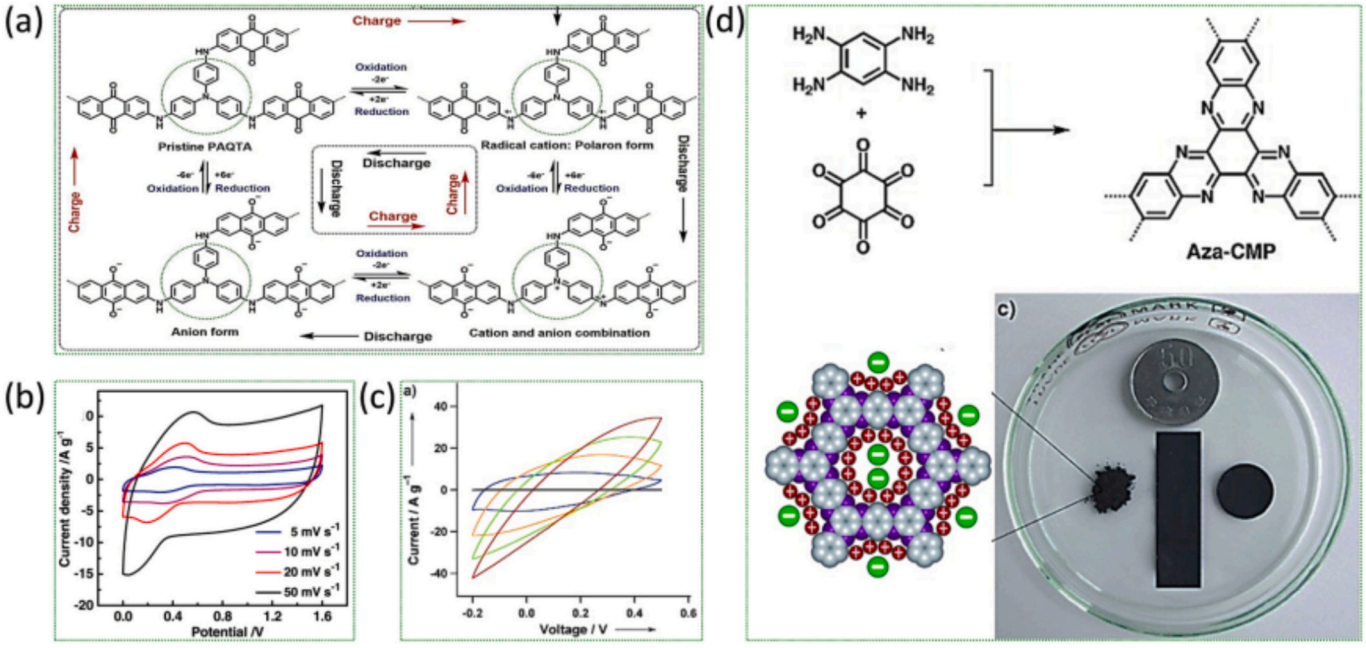

Fig. 17. (a) Schematic illustration of the proposed charge–discharge mechanism for PAQTA-based SCs. (b) Electrochemical performance of the PAQTA//activated carbon asymmetric SC device. (c) CV profiles of a SC device based on aza-fused CMPs. (d) Synthetic route for the preparation of aza-fused CMPs. (a) and (b) Reproduced with permission from Ref. [75] Copyright 2018, Wiley; (c) and (d) Reproduced with permission from Ref. [195] Copyright 2011, Wiley.

polymerization of two organic building units: 2,4,6-trihydroxyisophthalaldehyde and 1,3,5-tris(4-aminophenyl)triazine [197]. The resulting material featured a high surface area and an extended conjugated framework. In a three-electrode system, TPDA-1 delivered a remarkable specific capacitance of 469.4 F g^{-1} at 2 mV s^{-1} and retained 95% of its electrochemical capacity over 1 k GCD cycles. The study attributed this performance primarily to ion diffusion channels formed by the microporous framework in combination with the large surface area.

A 3D PAQ framework was introduced by the Liao research team [75] as a novel CMP framework for SC applications. This polymer was synthesized through B—H polymerization between DAQ and various aryl bromides, resulting in different derivatives (PAQTA, PAQTB, PAQCB, PAQSF, and PAQTM) (Fig. 18a). The PAQ network features a high surface area and shows outstanding dispersibility in polar solvents, rendering it well-suited for flexible electrode fabrication. Among the derivatives, PAQTA achieved an electrochemical capacitance of 576 F g^{-1} in a three-electrode system, when tested in 0.5 M H_2SO_4 at 1 A g^{-1}. Furthermore, it retained 80–85% of its capacitance over 6 k GCD cycles

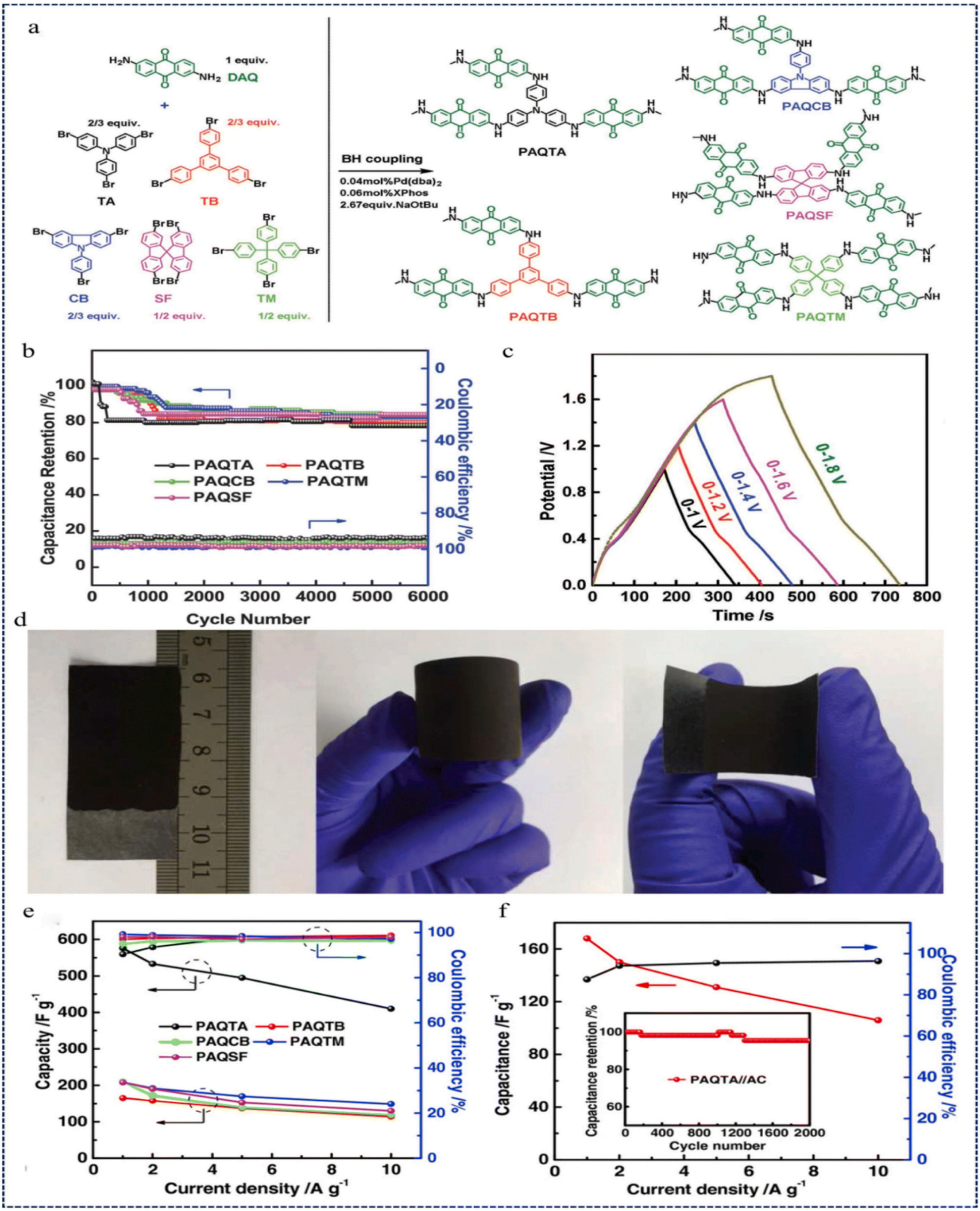

Fig. 18. (a) Synthesis of PAQTA, PAQTB, PAQCB, PAQSF, and PAQTM. (b) Cycling stability and coulombic efficiency of PAQ-based electrodes. (c) GCD curves recorded at a current density of 1.0 A g^{-1}. (d) Photographs of flexible PAQTA electrodes and electrochemical performance of PAQs measured in 0.5 M H_2SO_4. (e) Specific capacitance and coulombic efficiency of PAQs at various current densities. (f) Specific capacitance and its retention as well as the coulombic efficiency based on the total mass of both electrodes, as a function of current density, with the inset showing the device cycling durability 2.0 A g^{-1}. Reproduced with permission from Ref. [75] Copyright 2018, Wiley.

at 2 A g^{-1}, with a coulombic efficiency of 95–98% (Figs. 18b–e). The PAQ-based asymmetric two-electrode SCs delivered a capacitance of 168 F g^{-1}, achieving an energy density of 60 Wh kg^{-1} at a power density of 1300 W kg^{-1} within a broad operating potential window of 0.0–1.6 V. The device exhibited an excellent coulombic efficacy of 97% and retained 95.5% of its capacitance after 2 k GCD cycles (Fig. 18f). This study introduces novel CMP networks with strong potential for charge storage applications. Fiber-based SCs have also emerged as promising energy storage devices, particularly suited to the increasing need for miniaturization, flexibility, and integration in wearable electronics [198,199]. However, their relatively lower energy density compared to batteries continues to pose a significant challenge for Real-world deployment [200,201].

In 2023, Gaber and *co*-workers [156] developed novel redox-active polymers, namely Py-BDT and Py-Ph-BDT CMPs. These materials, constructed from Py and BDT building blocks, function as high-performing and robust electrode materials for SC applications. CMPs demonstrated outstanding thermal stability ($T_{d10} \approx 564$ °C) and a high surface area (427 m^2 g^{-1}). The Py-BDT and Py-Ph-BDT polymers achieved impressive capacitances of 636 F g^{-1} and 712 F g^{-1} at 0.5 A g^{-1}, respectively—significantly surpassing the reported electrochemical capacitances of other polymers. Symmetric SCs assembled with Py-Ph-BDT CMP delivered a great capacitance of 429 F g^{-1} with an energy density of 38.21 Wh kg^{-1}. They also demonstrated good durability, with cycling stability of 80% over 4 k cycles (Figs. 19a–c). Consequently, integrating Py and BDT building blocks within the CMP frameworks enables rapid charge transfer, outstanding Faradaic energy storage, and excellent conductivity (Fig. 19d). These results introduce a novel approach for designing high-performance SCs by utilizing reducible polymers as electrode materials.

Recently, in May 2025, El-Mahdy et al. [32] carried out an in-depth study on the influence of porosity and linker design on the electrochemical behavior of four polymeric materials incorporating redox-active DTDO unit. They synthesized two porous CMPs (pH-DTDO porous and TEPh-DTDO porous) and two linear polymers (pH-DTDO linear and DEPh-DTDO linear) using Suzuki and Sonogashira polymerizations, respectively. Among them, the Ph-DTDO CMP exhibited the best efficiency, achieving a GCD capacitance of 842.4 F g^{-1} at 0.5 A g^{-1} and outstanding stability with 98.78% retention after 6 k cycles in a three-electrode setup. In a symmetric SC, it delivered an electrochemical capacitance of 428.21 F g^{-1} and an energy density of 59.4 Wh kg^{-1}. The comparative analysis revealed that the porous framework and phenyl-bridged linker significantly improved electrochemical properties by enabling faster ion diffusion, greater capacitive contribution, reduced charge-transfer impedance, and stronger π–π stacking interactions. This work highlights the pivotal role of structural engineering in conjugated polymers and provides valuable design strategies for the design of next-generation efficient energy storage materials.

Redox-active CMPs with precisely controlled pore sizes were synthesized via a Suzuki coupling reaction to elucidate the role of pore confinement in SC performance. Two 9,9-bifluorenylidene-based CMPs (BF-Ph-DTDO and BF-DTDO) exhibited high surface area (~336.2 m^2 g^{-1}) and well-defined pore sizes of 2.14 and 1.8 nm, respectively. The larger-pore BF-Ph-DTDO delivered a high specific capacitance of 288.8 F g^{-1} at 0.5 A g^{-1} and retained ~76.6% capacitance after 10 k cycles. In a symmetric device, it achieved 272.7 F g^{-1} at 0.4 A g^{-1}, with an energy density of 37.88 Wh kg^{-1} and a power density of 462 W kg^{-1} at 1.0 V, highlighting the importance of pore-size engineering for high-performance SCs [157].

In 2024, Hu's group reported a quinone-enriched polymer (PDAQ) synthesized from DAQ and 1,3,5-benzenetricarboxaldehyde, which was integrated with reduced graphene oxide (rGO) to form an efficient organic electrode [202]. Owing to its extended π-conjugation, high carbonyl density, and strong π–π interactions with rGO, the PDAQ/rGO-0.3 electrode delivered a high specific capacitance of 622 F g^{-1} at 5 mV s^{-1} and retained 87.8% of its capacitance at 100 mV s^{-1}, together with excellent cycling stability. An asymmetric SC assembled with DAQ/rGO achieved an energy density of 32.97 Wh kg^{-1} at 605.57 W kg^{-1} and maintained 88% capacitance after 10 k cycles, demonstrating strong potential for high-energy SC applications.

4.3. Imide-based CMPs

Lai's research team [203] introduced a series of PDI-based CMPs—CMP-1, CMP-2, and CMP-3—developed as electrodes for SCs. Morphology investigation revealed that these CMPs possess highly cross-linked, irregularly stacked structures, along with combined micro- and mesoporous architectures (Figs. 20a–c). Owing to their redox-active electron-withdrawing centers, hierarchical porosity, and amide-linked framework, these CMPs exhibit n-type pseudocapacitive behavior.

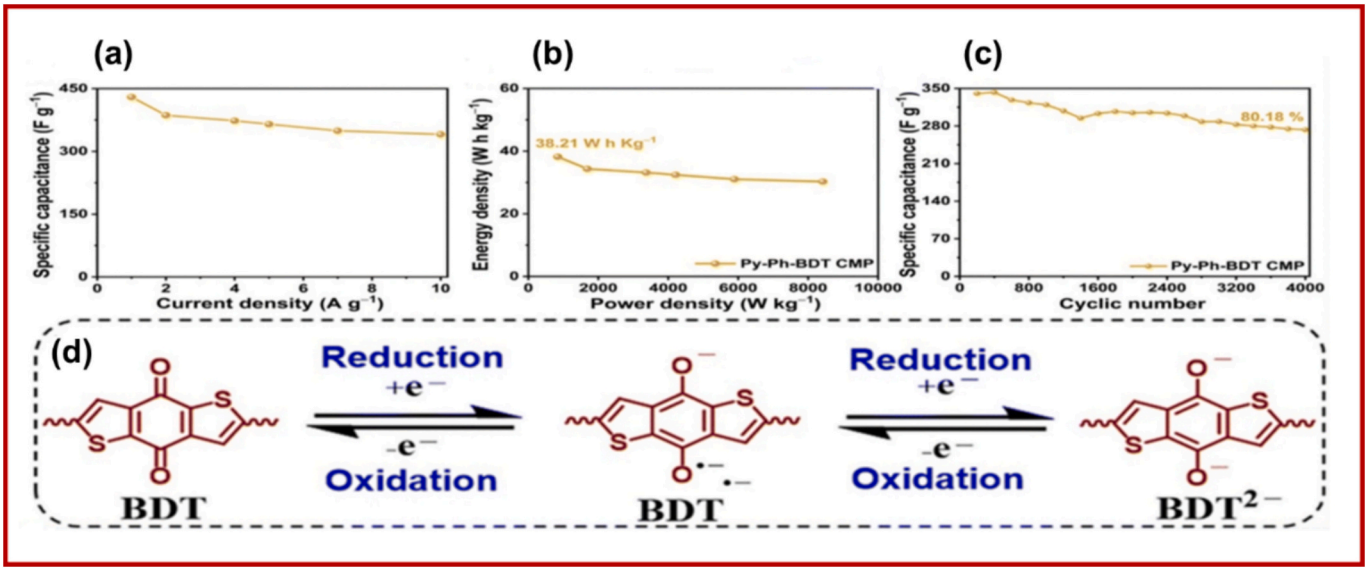

Fig. 19. (a) Calculated electrochemical capacitances of the Py-Ph-BDT electrode. (b) Ragone plot illustrating the relationship between energy density and power density for the Py-Ph-BDT CMP-based SC. (c) Cycling stability of the Py-PhBDT CMP-based SC evaluated at a current density of 5 A g^{-1}. (d) Schematic representation of the Redox mechanism associated with the BDT unit. Reproduced with permission from Ref. [156] Copyright 2023, Royal Society of Chemistry.

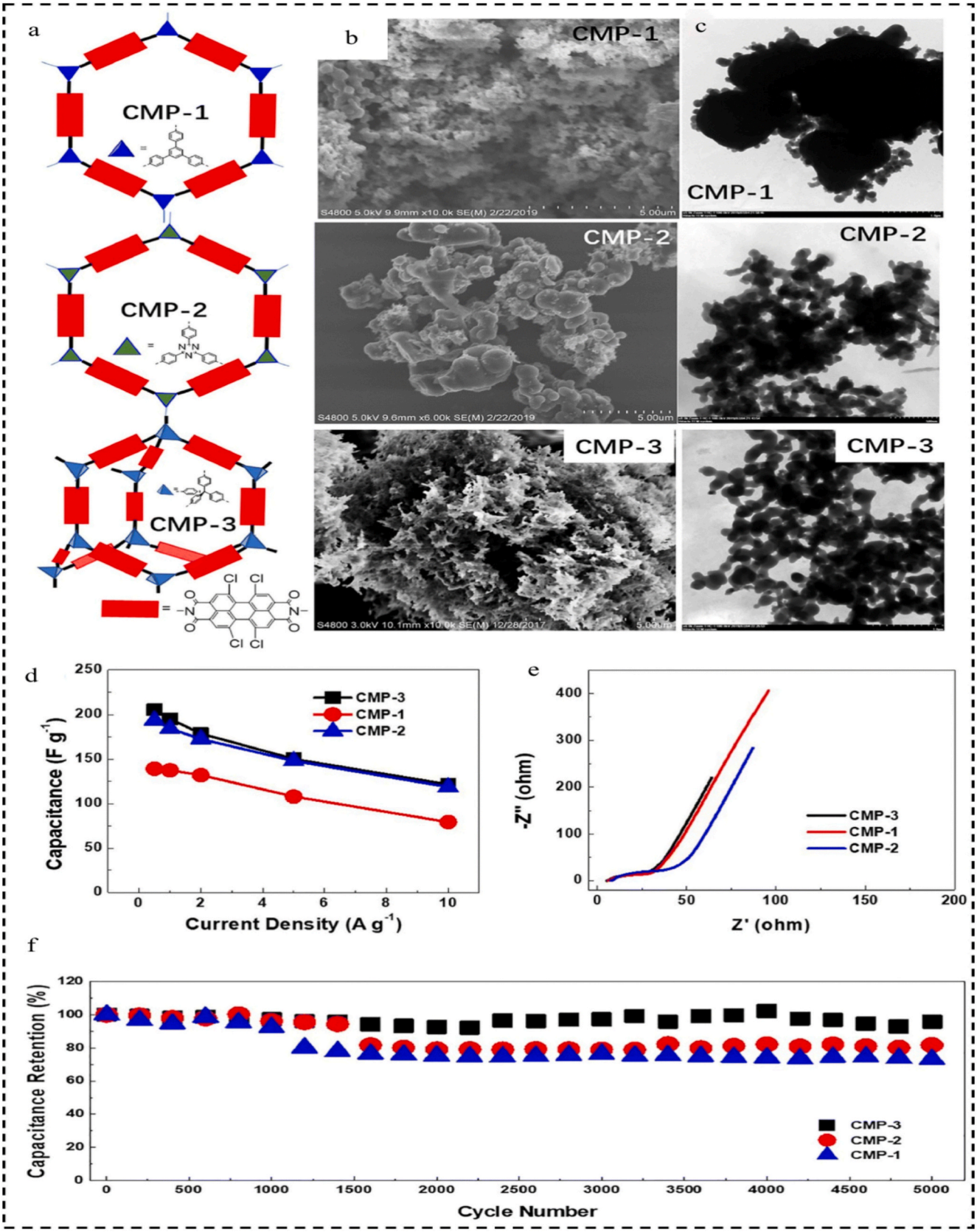

Fig. 20. (a) Schematic representation; (b) SEM photos; (c) TEM photos; (d) Specific capacitance as a function of current density; (e) Nyquist plot; and (f) Cycling stability at a current density of 10 A g^{-1} for CMP-1, CMP-2, and CMP-3. Reproduced with permission from Ref. [203] Copyright 2022, Springer.

They deliver high capacitances of 139–205 F g^{-1} at 0.5 A g^{-1}, operate over a wide negative potential window (−1.0 to 0.0 V), and demonstrate excellent stability (Figs. 20d and e). In contrast to CMP-1, CMP-3 incorporates a robust backbone composed of tetraphenylmethane 3D units combined with PDI moieties. This structural design facilitates ion transport, strengthens ionic interactions, and improves surface accessibility, resulting in excellent electrochemical capacitance, resistance to thermal degradation, and outstanding reversibility. Significantly, CMP-3 maintains a stability performance of 96% over 5 k cycles at 10 A g^{-1} (Fig. 20f). The superior ion diffusion kinetics of CMP-3 and CMP-2 relative to CMP-1 are ascribed to the 3D robust framework of CMP-3 and the bent molecular configuration of CMP-2. CMP-3-based asymmetric SCs coupled with poly(3,4-ethylenedioxythiophene)-poly (styrenesulfonate) (PEDOT/PSS) achieved a broader operating voltage range of 1.8 V and a higher capacitance of 17.4 mF cm^{-2}, outperforming symmetric SCs constructed solely with PEDOT/PSS electrodes. This study provides fundamental insights into the key structural variables governing the electrochemical and transport behavior of these materials. Such understanding highlights the rational development of stable, high-performance n-type organic electrodes tailored for flexible energy storage.

A series of imide-based CMPs with different core units were synthesized via a condensation strategy to investigate their structure, morphology, and electrochemical energy storage performance [204]. The authors prepared three distinct CMPs (pNTCDA-TAPB, pNTCDA-TAPM, and pNTCDA-TPAT) and further fabricated composites with CNTs through in-situ growth to improve electronic conductivity and ion transport. Electrochemical testing demonstrated that among the polymers, pNTCDA-TPAT exhibited the highest specific capacitance of 217.4 F g^{-1} at 0.5 A g^{-1} in neutral electrolyte, representing a high value for CMP-based energy storage materials. Notably, the corresponding CNT composites, especially pNTCDA-TAPB@CNT, showed significantly enhanced energy storage performance compared to the pristine polymers, attributed to improved electrical conductivity and effective ion diffusion pathways provided by the CNT network.

4.4. CMP/carbon and CMP/CNT hybrid electrodes

Liao's research group [205] employed different amine monomers together with 1,3,5-tris(3-bromo)benzene. Polymerization was carried out on the surface of CNFs via a B—H coupling reaction. This approach produced a composite (CNF@CMP) featuring a tunable porous architecture and reversible redox behavior (Fig. 21a), which delivered excellent capacitive performance. The flexibility and excellent electrical conductivity of the CNFs, combined with the porosity and enhanced redox activity of the PTPA polymer, and the efficient interaction between the CNF and PTPA, enabled the fabrication of superb wearable SCs, achieving 671.9 mF cm^{-2} at 1 mA cm^{-2}. All-solid-state symmetrically twisted CNF@PTPA FSCs, fabricated using PVA/H_3PO_4 as the gel electrolyte, demonstrated a high areal capacitance of 398 mF cm^{-2} at 0.28 mA cm^{-2} (Figs. 21b and c). They also achieved an operating voltage of 1.4 V and an impressive energy density of 18.33 mWh cm^{-2} (Fig. 21d). Additionally, these devices show outstanding mechanical flexibility, cycling stability of 84.5% over 10 k cycles (Fig. 21e). These materials open up a promising pathway for the development of efficient wearable SCs, offering broad potential for wearable electronics applications. CMPs containing redox-active functionalities have also attracted growing interest in energy conversion systems [206,207]. Nevertheless, their inherently poor conductivity often leads to reduced capacitance, posing a challenge for their practical application [208,209].

In 2021, Duan and co-workers [210] synthesized CMPs constructed from trityl aldehydes connected to metal phthalocyanines (MNC, Co, and Fe). To enhance conductivity, composite membranes were fabricated by incorporating these CMPs with CNTs in varying stoichiometric ratios (MNC: CNT = 1:1, 1:2, 1:3, and 1:5), employing a microwave-assisted approach followed by filtration under vacuum. The obtained composites were designated as MNCCs-x (where x = 1, 2, 3, 5) (Fig. 22a). Owing to the great metallic characteristics of CoNC, it can be combined with CNTs via strong π–π interactions, forming CoNCCs without the need for covalent bonding. The prepared CoNCCs-3 materials delivered a great electrochemical capacitance of 213.4 F g^{-1} at 0.5 A g^{-1} (Fig. 22b). Moreover, they retained 85.3% of their capacitance after 1750 cycles (Fig. 22c). The excellent performance is primarily assigned to the integrated effects and robust biphasic interactions between the MNC units and CNTs. These results highlight the potential for developing efficient organic SC electrodes while maintaining reduced ecological consequences. Metal phthalocyanines (MPcs) are important π-conjugated structural units, consisting of 2D aromatic macrocycles with a central metal atom embedded in the inner core. The strong interaction between the phthalocyanine ring and the metal center imparts excellent electron-transfer capabilities [211–214]. Consequently, the incorporation of MPcs into CMPs endows them with substantial potential for energy storage applications [215].

In 2020, Duan and his team [216] synthesized three MPc-based CMPs (M = Co, Fe, and H_2) via a fast microwave-assisted technique. These polymers were then combined with CNTs via non-covalent interactions to form free-standing, flexible composite membranes. The resulting membranes functioned as binder-free, additive-free flexible electrodes for SCs (Fig. 22d). The flexible electrodes CoPc-CMP/CNTs-2, HPc-CMP/CNTs-2, and FePc-CMP/CNTs-2 delivered electrochemical capacitances of 289.1 F g^{-1}, 53.6 F g^{-1}, and 100.7 F g^{-1} at 1 A g^{-1}, respectively (Fig. 22e). Remarkably, the CoPc-CMP/CNTs-2 maintained an outstanding capacitance (107.2 F g^{-1}) with a cycling retention (89.2%) after 1350 cycles (Fig. 22f). This research demonstrates that the synergistic interactions and enhanced functionalities of MPcs-based CMPs combined with exceptionally conductive CNTs create promising opportunities for the engineering of highly efficient SCs.

Porphyrin-based CMPs hold significant promise for energy storage applications; however, their inherently low conductivity hinders practical use [217,218]. To overcome this challenge, Duan et al. [184] in 2021 designed and synthesized copper porphyrin-CMPs (CuTAPP-CMPs) as a potential solution. They also developed CuTAPP-CMP/CNTs-3 by combining CuTAPP-CMPs with CNTs using a simple vacuum filtration technique (Fig. 23a). The resulting composites function as binder-free, self-supporting flexible electrodes for SCs. Without requiring covalent bonding, the active CuTAPP-CMP associates with conductive CNTs through strong π–π interactions. The CuTAPP-CMP/CNTs-3 electrode achieved an electrochemical capacitance of 207.8 F g^{-1} at 1 A g^{-1} (Fig. 23b) and demonstrated excellent durability, maintaining stable performance for over 3700 cycles (Fig. 23c). The remarkable electrochemical efficiency can be ascribed to the effective combination of CNTs' excellent conductivity with the great pseudocapacitance of CuTAPP-CMP. The discussions thus open new avenues for the development of efficient organic active electrodes for SCs.

Mohamed and his research group [219] synthesized three oxadiazole-based CMPs (OXD-CMPs: TPA-OXD-CMP, Py-OXD-CMP, and TPE-OXD-CMP) via a straightforward Sonogashira polymerization reaction. These OXD-CMPs were then integrated with CNTs through π–π interactions, resulting in OXD-CMP/CNT hybrid materials (Fig. 23d). When applied as SC electrodes, the OXD-CMP/CNT composites demonstrated significantly improved capacitance and cycling stability. In particular, the Py-OXD-CMP/CNT hybrid delivered an excellent electrochemical capacitance of 504 F g^{-1} at 0.5 A g^{-1}, far surpassing the performance of the other OXD-CMP-based samples. It also showed excellent durability, retaining 91.1% of its capacitance over 2 k cycles, as confirmed by GCD measurements (Figs. 23e and f). These findings highlight OXD-CMP/CNT nanocomposites as highly promising materials for high-performance SCs.

A conjugated microporous PTPA was synthesized via a CNT template-assisted strategy to enhance pore structure and conductivity for SCs. By incorporating amino-multiwalled nanotubes (NH_2-MWNTs) during in-situ polymerization, the specific surface area of the resulting

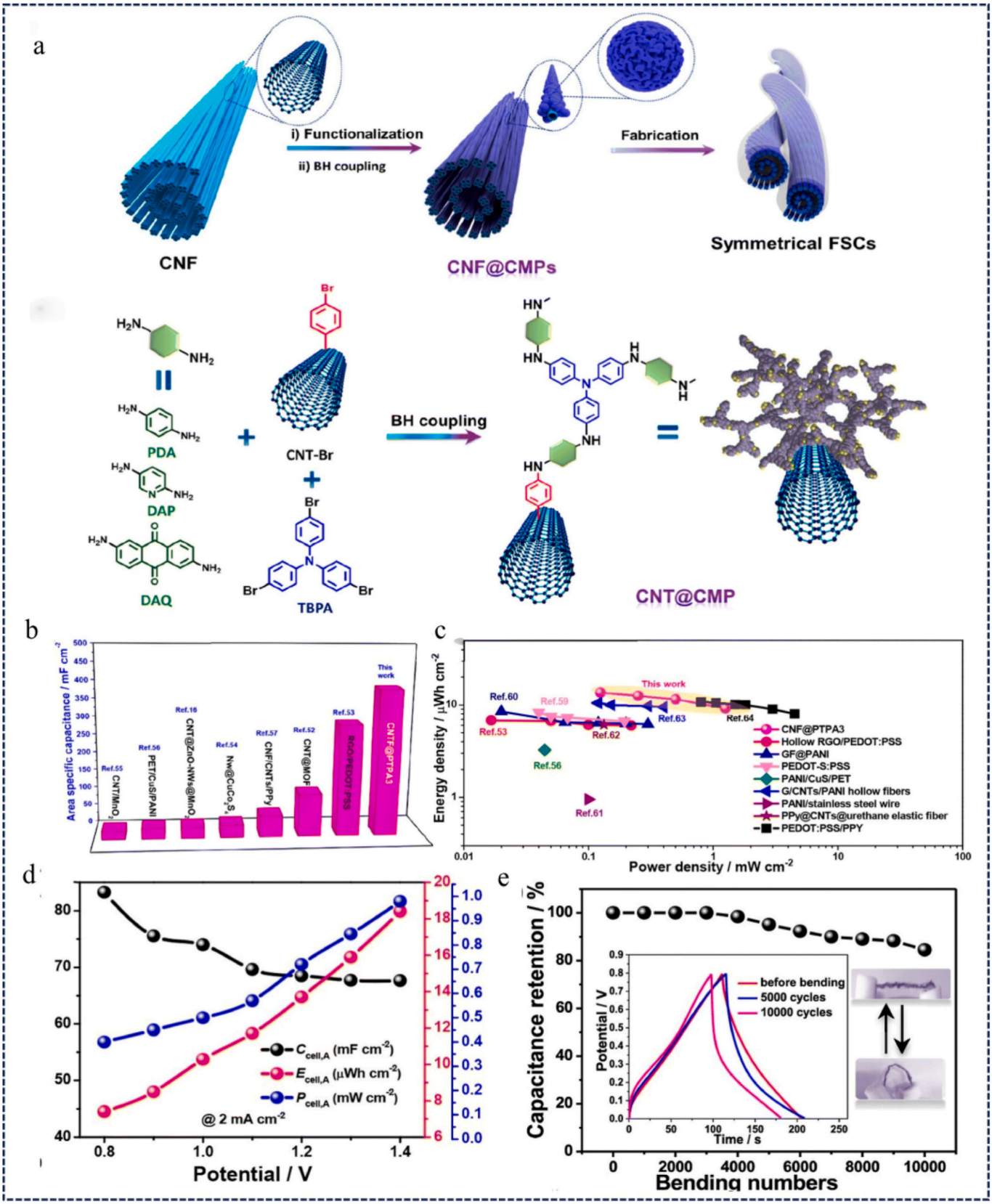

Fig. 21. (a) The fabrication process for symmetrical FSCs. (b) Areal Ragone plots of the CNF@PTPA-based FSCs. (c) Comparison of the electrochemical performance of CNF@PTPA FSCs with other FSCs in terms of specific capacitance. (d) GCD curves of CNF@CMP fibers. (e) Relationship between capacitance retention and bending times. Reproduced with permission from Ref. [205] Copyright 2020, American Chemical Society.

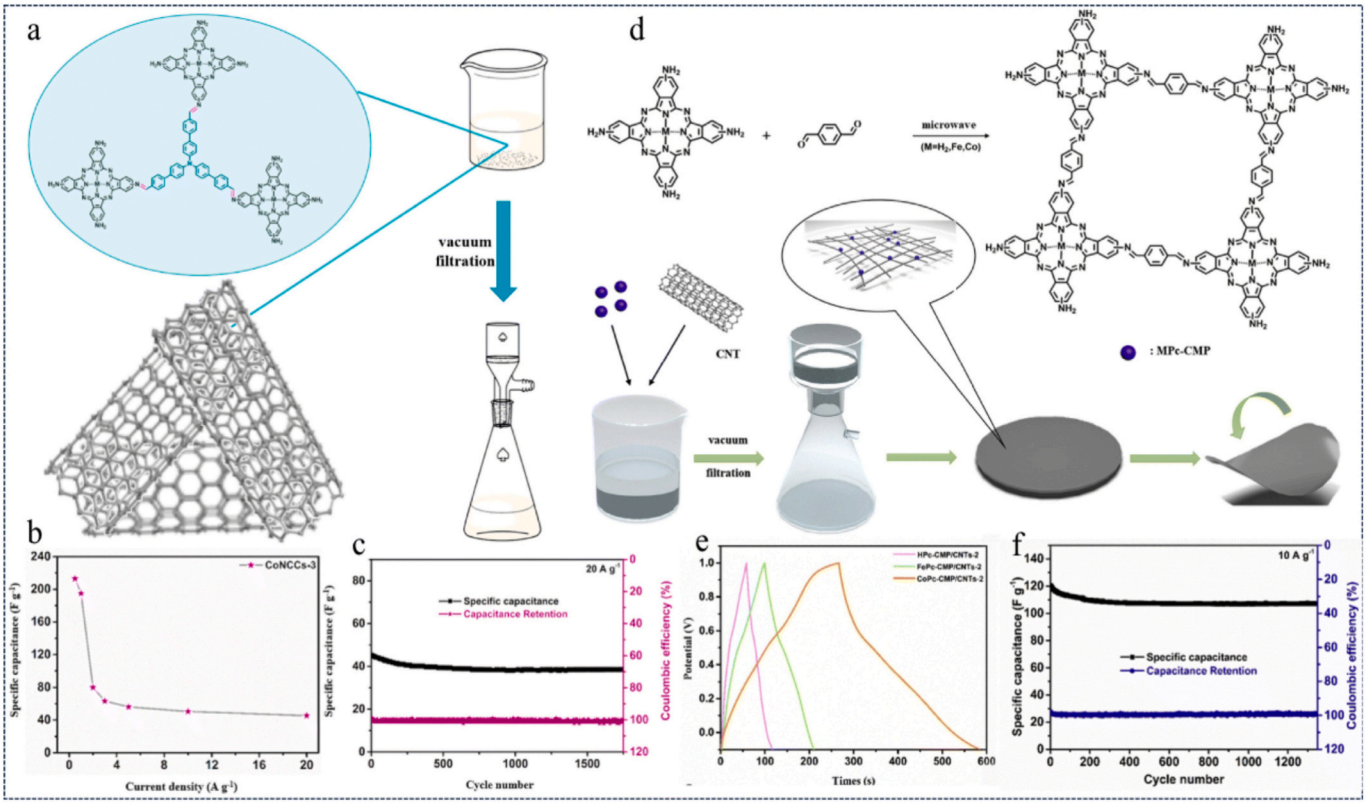

Fig. 22. (a) The preparation process for MNCCs (M = Co, Fe). (b) Electrochemical capacitances of CoNCCs-3 at various current densities. (c) Cycling stability and coulombic efficiency of CoNCCs-3 at 20 A g^{-1}. Reproduced with permission from Ref. [210] Copyright 2021, Elsevier. (d) The synthetic process of MPc-CMP/CNTs. (e) GCD curves of MPc-CMP/CNTs-2 (M = H_2, Co, Fe) evaluated at 1 A g^{-1}. (f) Cycling stability and coulombic efficiency of CoPc-CMP/ CNTs-2 at 10 A g^{-1}. Reproduced with permission from Ref. [216] Copyright 2020, Elsevier.

PTPA@MWNT composite increased dramatically from 32 to 484 m^2 g^{-1}, creating hierarchical *meso*–micro pores that facilitate ion transport. The optimized PTPA@MWNT-4 electrode exhibited a high specific capacitance of 410 F g^{-1} at 10 A g^{-1} in 0.5 M H_2SO_4, attributed to improved redox activity and electronic conductivity. In a symmetric SC device, the composite maintained a total capacitance of 216 F g^{-1} and retained ~71% of its initial capacitance after 6 k cycles, demonstrating good cycling stability [220].

4.5. CMP-derived and pyrolyzed carbon materials

In 2022, the Jang group [185] synthesized an anthraquinone-based amide-linked CMP (CMAP@AG) with electron-conducting characteristics. The polymerization was carried out using anthraquinone amide and tris-aniline as the core building blocks, directly on an activated graphene (AG) support (Fig. 24a). By adjusting the etching time of the AG substrate, the structural features of the CMAP@AG hybrids were tailored to enhance their functionality (Fig. 24b). The optimized material delivered a high capacitance of 751 F g^{-1} at a current density of 1.0 A g^{-1} (Fig. 24c) and exhibited excellent cycling stability (97%) over 20 k cycles when tested at an elevated current density of 10 A g^{-1} (Fig. 24d). Furthermore, asymmetric SCs assembled with CMAP@A4G achieved an excellent energy density (76.6 Wh kg^{-1}) and an impressive power density (27,634 W kg^{-1}). In addition, the CMP composites demonstrated flexibility and mechanical robustness, making them a superior candidate for flexible CMP-based energy storage materials. Through extensive experimental evaluation, this study confirmed that CMAP@A4G possesses strong redox efficiency, excellent electrochemical performance, and great cycling behavior, with a surface area reaching 498 m^2 g^{-1}. These findings offer valuable guidance for the design and precise tuning of CMP-based AG hybrids for advanced energy storage applications.

CMPs are typically produced as amorphous or semi-crystalline solids. Considering this, electrospinning has emerged as a well-established and versatile method for fabricating nanofibers with diameters ranging from tens of nanometers to several micrometers. These nanofibers generally exhibit high flexibility and possess a large surface area-to-volume ratio, making them particularly optimized for developing chemosensor devices with rapid response times and high sensitivity [221–223]. Chen group [91] synthesized CMPs via a Sonogashira coupling using a tetraaryl ethylene building unit. By blending these CMPs with PLA through electrospinning, they fabricated a highly flexible and porous sensor with a large surface area-to-volume ratio. The resulting device exhibited high sensitivity and was suitable for detecting nitroaromatic compounds, benzoquinone vapors, and oxidizing metal ions (Fig. 24e). In addition, graphene-based CMP (G-CMP) sandwich structures offer a large surface area. These were prepared via pyrolysis at high temperature (800 °C), resulting in hierarchical, carbon-rich 2D porous nanosheets. Outstanding SC performance was observed for these carbon nanosheets, with a 48% increase in electrochemical capacitance compared to porous carbon prepared in the absence of graphene templates. Graphene scaffold incorporation provides efficient pathways for inter- and intralayer electron transfer, improving ion injection and extraction at the electrodes and substantially boosting energy storage capacitance.

A porous sandwich-like CMP–graphene composite film (PTPAH@rGO) was developed for high-performance flexible solid-state SCs [224]. The hierarchical CMP–rGO architecture enhances charge transport and exposes abundant redox-active sites, enabling a high specific capacitance of 545 F g^{-1} at 1 A g^{-1} and 450 F g^{-1} at 10 A g^{-1}. Flexible devices assembled with a PVA/H_2SO_4 gel electrolyte exhibit a specific capacitance of 220 F g^{-1} and a high-power density of 3345 W kg^{-1}, demonstrating excellent rate capability and mechanical stability. These results highlight the effectiveness of CMP–graphene hybridization

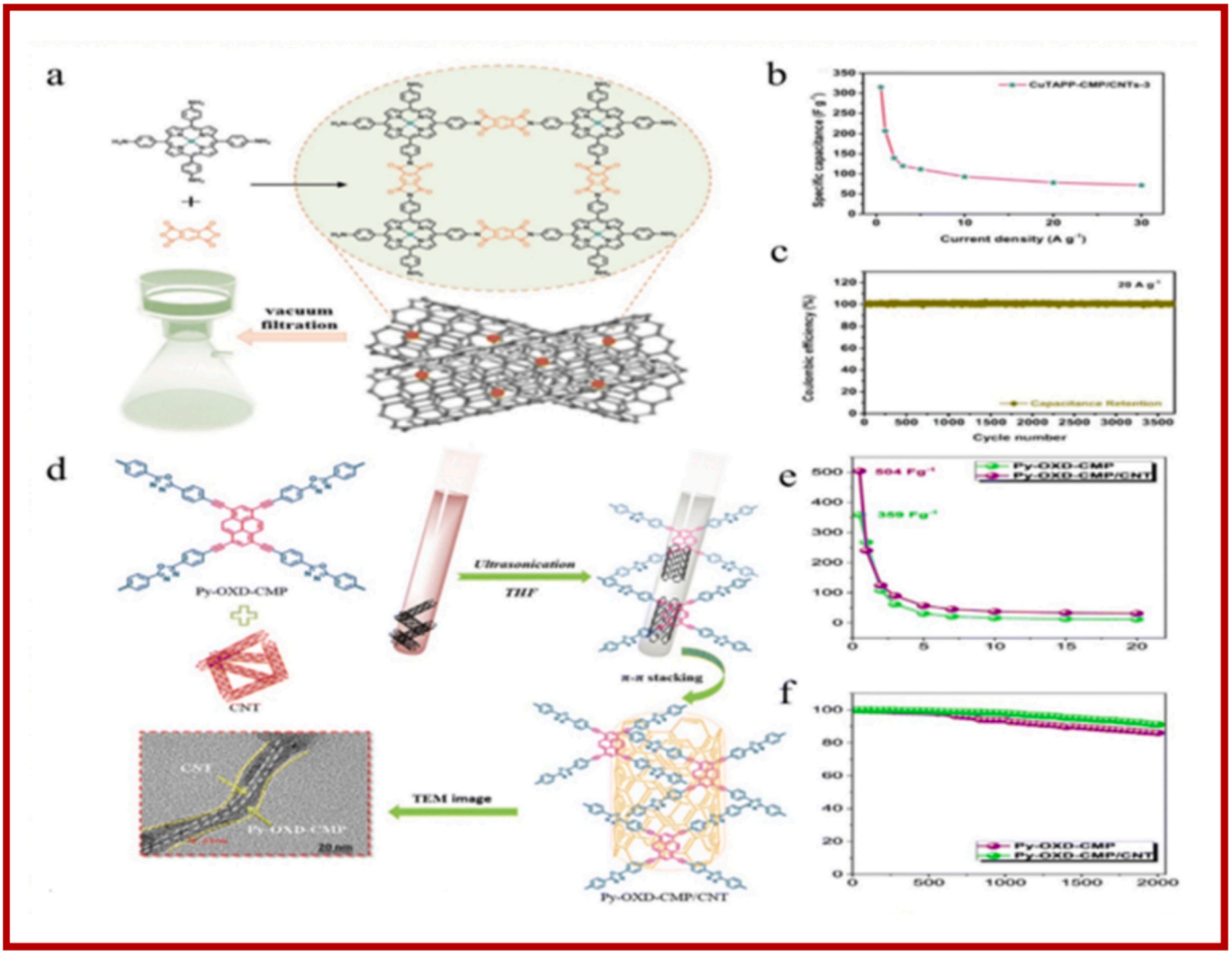

Fig. 23. (a) The preparation process for MTAPP-CMP/CNTs (M = Cu and H_2). (b) Electrochemical capacitances of CuTAPP-CMP/CNTs-3 at various current densities. (c) Coulombic efficiency of CuTAPPCMP/CNTs-3 at 20 A g^{-1}. Reproduced with permission from Ref. [184] Copyright 2021, Springer. (d) The synthesis of the Py-OXD-CMP/CNT nanocomposite. (e) Electrochemical capacitances of the Py-OXD-CMP and Py-OXD-CMP/CNT nanocomposites. (f) Cycling stability of the Py-OXD-CMP and Py-OXD-CMP/CNT nanocomposites. Reproduced with permission from Ref. [219] Copyright 2022, American Chemical Society.

and sandwich-like morphology in addressing conductivity and processability limitations, making such composites highly promising for flexible energy-storage applications.

4.6. Other CMP-based electrodes

Mohamed and his team [225] synthesized two CMPs—Py-Ph-TzTz and Py-Th-TzTz—through a Schiff-base reaction between dithiooxamide and Py aldehydes. Thermal stability studies revealed T_{d10} values of 502 °C for Py-Ph-TzTz and 352 °C for Py-Th-TzTz, with substantial carbon residues of 67 wt% and 63 wt%, respectively, at 800 °C. In a three-electrode configuration, Py-Th-TzTz and Py-Ph-TzTz CMPs delivered specific capacitances of 652 F g^{-1} and 464 F g^{-1} at 1 A g^{-1}, respectively. Symmetric devices were also fabricated for practical evaluation, showing capacitances of 226 F g^{-1} for Py-Th-TzTz and 108 F g^{-1} for Py-Ph-TzTz CMPs, as determined from GCD curves. Both materials demonstrated excellent cycling stability, retaining 96% (Py-Th-TzTz) and 95% (Py-Ph-TzTz) of their capacitance after 5 k charge–discharge cycles at 10 A g^{-1}. The impressive capacitance values of these TzTz-CMPs, comparable to other porous CMPs, are assigned to the presence of electronegative TzTz units, which enhance electron distribution, boost conductivity, and strengthen electrostatic interactions. These results show that employing a thiophene linker and integrating TzTz units into CMPs offers an efficient strategy for high-performance SCs. This strategy underscores the importance of molecular-level design and tailoring organic materials to attain superior performance in next-generation energy storage technologies.

In 2025, the same research group [179] synthesized two CMP variants, PyPH-HATN CMP-0.75 and PyPH-HATN CMP-1.5, via a Suzuki coupling by adjusting the monomer ratio of Py-4Br and 2,8,14-tribromodiquinoxalino[2,3-a:2′,3′-c]phenazine (HATN-3Br). Among them, PyPH-HATN CMP-1.5 displayed a distinct rod-like morphology, underscoring the effectiveness of monomer ratio tuning in tailoring polymer structure. Electrochemical studies revealed the outstanding performance of the PyPH-HATN CMP-1.5 electrode, which achieved an outstanding electrochemical capacitance of 1790 F g^{-1} at 1 A g^{-1}, owing to its enhanced porosity, heteroatom-enriched composition, and structural optimization. Even at a high current density of 20 A g^{-1}, it maintained a capacitance of 640 F g^{-1}. The charge storage mechanism was dominated by a diffusive contribution (75%), with a capacitive contribution of 25% at 1 mV s^{-1}, and a diffusion coefficient of 1.27 × 10^{-10} cm^2 s^{-1}. Additionally, the PyPH-HATN CMP-1.5 demonstrated excellent rate capability and remarkable cycling retention (97%) over 5 k GCD cycles at 20 A g^{-1}. These findings clearly establish PyPH-HATN CMP-1.5 as a

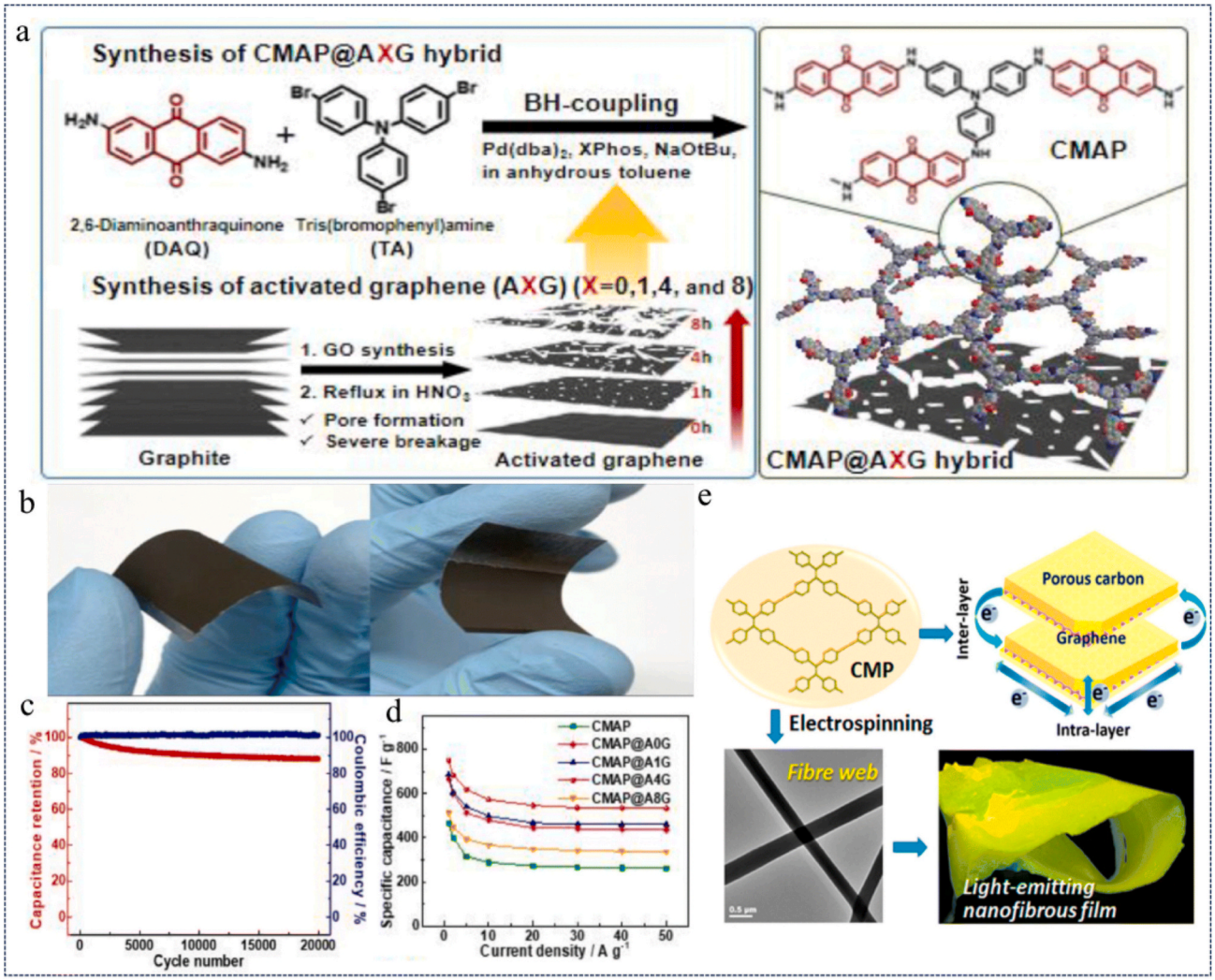

Fig. 24. (a) The preparation of the CMAP@XG hybrid. (b) Photographs of flexible CMAP@A4G electrodes. (c) electrochemical capacitance at various sweep rates. (d) Cyclic stability and coulombic efficiency at a current density of 10 A g^{-1}. Reproduced with permission from Ref. [185] Copyright 2022, Elsevier. (e) Schematic representation of electron transfer in graphene templated CMPs. Reproduced with permission from Ref. [91] Copyright 2015, American Chemical Society.

promising organic electrode material for efficient SCs, owing to the straightforward synthetic route, HATN-enriched units, and tailorable morphology, highlighting its potential for integration into advanced energy storage platforms.

Ho et al. reported a metal-free 2D-CMP that integrates three-state electrochromism with efficient faradaic energy storage. Owing to its planar π-conjugated network and highly accessible redox-active sites, the 2D-CMP delivers a specific capacitance of approximately 192.9 F g^{-1} and a charge storage capacity of about 37.5 mAh g^{-1} at a current density of 5 A g^{-1}. The combination of high capacitance, good rate capability at elevated current density, and stable faradaic behavior highlights the effectiveness of 2D conjugation and porosity in enabling multifunctional CMP-based electrodes for SCs and electrochromic energy-storage applications [226].

Conjugated tetraphenylethene-based polymers were developed as electrode materials for SCs, demonstrating effective faradaic charge storage. Two polymers (P1 and P2) exhibited specific capacitances of ~274.8 F g^{-1} and ~ 207.9 F g^{-1}, respectively, at a scan rate of 1 mV s^{-1}, attributed to their extended π-conjugated backbones and redox-active units. Both materials showed good electrochemical stability, retaining over 90% of their capacitance after 5 k charge–discharge cycles, highlighting the potential of tetraphenylethene-based conjugated polymers for SC applications [227].

Fig. 25 presents a performance-landscape comparison of CMP-based electrodes with established porous carbon materials using volumetric capacitance and electronic conductivity as device-relevant metrics. The landscape reveals that pristine CMPs occupy a distinct low-conductivity, low-volumetric-capacitance region, reflecting their low packing density and limited intrinsic charge transport despite high gravimetric capacitance arising from redox activity [156,157]. In contrast, activated carbons, graphene-derived carbons, and carbide-derived carbons cluster at higher conductivities and volumetric capacitances, underscoring their superiority in compact device performance consistent with established benchmarks for compact devices [228–230]. CMP-derived carbon and CMP/carbon hybrids shift toward this carbon-dominated regime, indicating that conductivity enhancement and densification significantly improve performance but also reduce the influence of CMP molecular architecture [12,13]. Overall, this performance landscape clarifies that the principal value of CMPs does not lie in surpassing porous carbons in absolute volumetric or transport metrics, but rather in their molecular tunability, redox functionality, and multifunctionality, which may enable application-specific advantages beyond conventional carbon electrodes.

To summarize, CMPs have emerged as highly versatile organic electrode platforms for SCs because their permanent microporosity and π-conjugated networks can be engineered to improve ion accessibility

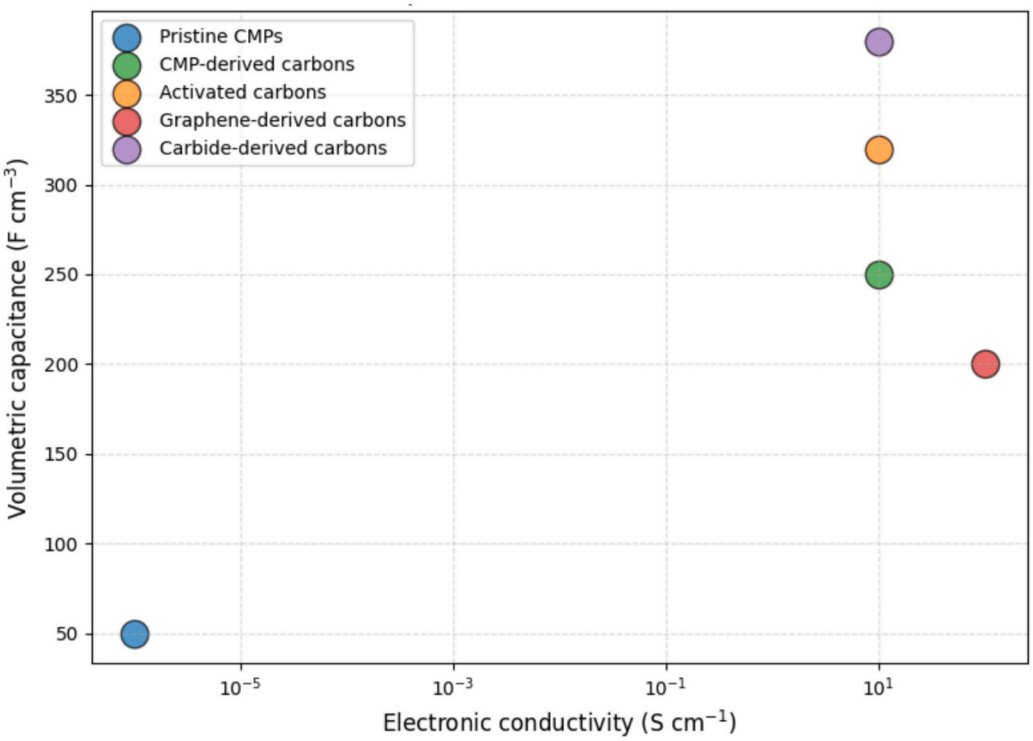

Fig. 25. Performance landscape comparing CMP-based electrodes with porous carbon materials.

and enable pseudocapacitive charge storage. Recent progress demonstrates multiple effective design routes, including (i) nitrogen-rich CMPs that enhance wettability, active-site density, and reversible faradaic behavior; (ii) quinone/anthraquinone and other redox-active CMPs that deliver high capacitance and improved energy density through fast redox couples; (iii) imide-based CMPs that provide stable n-type pseudocapacitance over wide negative potential windows; and (iv) CMP/carbon, CNT, and graphene hybrid electrodes that address conductivity limitations and enable flexible, binder-free devices. Collectively, these studies highlight that the best-performing CMP-based SC electrodes typically rely on synergistic structural engineering—balancing redox functionality, pore architecture, and conductive scaffolds—to simultaneously enhance capacitance, rate capability, and long-term cycling stability.

5. Role of morphology in charge storage mechanisms

Beyond molecular structure and chemical composition, the morphology of CMP-based materials plays a critical role in governing their charge-storage behavior and electrochemical performance. CMPs reported in the literature exhibit diverse morphologies, including irregular particulate aggregates, hierarchical porous networks, nanosheets, fibrous structures, and carbon-supported composite architectures. For example, nitrogen-rich CMPs such as TAT-CMP-1 and TAT-CMP-2 mainly consist of aggregated particulate morphologies, which provide high surface area but may partially limit ion accessibility at high current densities due to dense packing [172]. In contrast, graphene–CMP sandwich structures form 2D layered and hierarchical architectures, offering enhanced electrolyte penetration and improved charge transport pathways, thereby leading to superior capacitance and rate performance [173].

Redox-active CMPs, including PAQ-based frameworks, typically exhibit irregular yet porous morphologies that enable combined EDLC and pseudocapacitance contributions, where ion diffusion and redox accessibility are strongly morphology-dependent [75]. Notably, imide-based CMPs, such as PDI-based CMPs, display highly cross-linked and micro/mesoporous network morphologies, which facilitate efficient ion diffusion and stabilize n-type pseudocapacitive processes over wide negative potential windows [203]. Furthermore, CMP/carbon hybrid electrodes, including CMP/CNT composites grown on carbon nanotube fibers, possess interconnected fibrous or network-like morphologies that significantly enhance electrical conductivity, reduce charge-transfer resistance, and improve mechanical flexibility, making them particularly attractive for wearable and flexible SCs [205]. CMP-derived carbons obtained through high-temperature pyrolysis, especially graphene-templated CMP carbons, exhibit hierarchical porous nanosheet morphologies that further promote rapid ion transport and efficient electron conduction, resulting in markedly enhanced electrochemical performance [173].

While CMP-based electrodes are often described as benefiting from combined EDLC and pseudocapacitive charge storage, the relative contribution of each mechanism is strongly governed by framework conjugation, redox-site density, and nanopore characteristics. Quantitative analyses using power-law ($i = a\nu^b$) and capacitive–diffusive separation methods have demonstrated that increased π-conjugation enhances electronic delocalization and increases the capacitive contribution by facilitating rapid surface redox reactions, particularly in CMPs incorporating quinone, anthraquinone, or imide motifs. For example, polymer-based systems with extended conjugation and high redox-site density have been shown to exhibit capacitive contributions exceeding 60–75% at moderate scan rates, compared with less conjugated analogues where diffusion-controlled processes dominate [231,232].

The nanopore environment further plays a decisive role in determining accessible capacitance. CMPs with ultra micropores (<1 nm) often exhibit high BET surface areas but reduced electrochemical utilization due to ion desolvation barriers and increased ionic resistance, whereas frameworks with optimized micro–mesoporous distributions enable higher effective capacitance and superior rate capability. In addition, enhanced surface wettability arising from heteroatom-rich backbones improves electrolyte penetration and increases the fraction of electrochemically active surface area. Recent polymer studies further confirm that balancing redox density, conjugation length, and pore

accessibility, rather than maximizing surface area alone, is essential for achieving high and rate-stable capacitance. Collectively, these findings highlight that charge storage in CMP-based SCs is quantitatively controlled by the interplay between electronic structure and nanoscale ion-transport environments [233].

These studies demonstrate that morphological engineering—together with molecular design and electronic tuning—is a key determinant of charge-storage mechanisms in CMP-based electrodes, and future research should emphasize precise control over morphology to optimize ion diffusion, active-site utilization, and long-term cycling stability (Table 2).

In summary, the morphology of CMP-based electrodes plays a decisive role in dictating their charge-storage mechanisms and electrochemical performance. Dense particulate morphologies may limit ion accessibility at high rates, whereas hierarchical, layered, fibrous, and composite architectures promote efficient electrolyte penetration, faster ion diffusion, and improved charge transport. In particular, nanosheets, imide-based porous networks, and CMP/carbon hybrids effectively balance EDLC and pseudocapacitive contributions by enhancing electrochemically accessible surface area and stabilizing redox-active sites. These findings underscore that morphology control—complementing molecular and electronic design—is essential for optimizing ion transport, rate capability, and cycling stability in CMP-based SCs.

6. Challenges for CMPs in energy storage

While CMPs are recognized for their unique and promising properties in energy storage applications, they still face significant challenges that hinder their commercial deployment. The following sections discuss these challenges in detail, along with reported strategies and promising solutions.

6.1. Limited theoretical capacity

The foremost drawback associated with CMPs is the poor theoretical capacity. Their preparation typically involves two monomers; only one of these is generally redox-active, while the other mainly serves a structural role and is electrochemically inactive. Incorporating such non-redox-active components increases the molecular weight without enhancing charge storage, thereby reducing the electrochemical capacity of the polymer. Designing porous materials with great theoretical capacity is therefore a significant challenge. One possible strategy is to increase the number of redox-active functionalities within each repeating unit. Nevertheless, while this can enhance capacity, it may also compromise the overall stability or conductivity of the system. Several efforts have been made to increase the redox-active group content per repeating unit to boost theoretical capacity. For example, Li's research group developed a crystalline COF that delivered 800 mAh g^{-1} at 100 mA g^{-1} as a cathode material [234]. Another study incorporated fused azine with carbonyl groups, achieving a theoretical capacity of 773 mAh g^{-1}, though the practical capacity quickly dropped from ~500 mAh g^{-1} [235,236].

While high gravimetric capacitance (F g^{-1}) is often emphasized in academic studies, real-world SC performance also critically depends on volumetric metrics such as volumetric capacitance (F cm^{-3}) and volumetric energy density. Recent reviews highlight that increased electrode porosity can reduce packing density and thus degrade volumetric performance, and that strategies to improve overall device energy storage must balance gravimetric and volumetric considerations [237].

6.2. Redox potential tuning

Achieving high-energy-density batteries depends mainly on two parameters: electrochemical capacity and electrode voltage. Cathodic materials require a high redox voltage, with inorganic cathodes typically operating around 4 V vs. Li/Li^+, while organic cathodes generally show lower values near 2.5 V vs. Li/Li^+. For anodes, the optimal potential should be nearly 0 V vs. Li/Li^+, but organic anodes usually exhibit higher values, typically around 1 V vs. Li/Li^+. Given the low capacity of organic electrodes, it is crucial to develop structures with optimized redox potentials if they are compared with commercial electrodes. In a noteworthy study, Dichtel and co-workers incorporated a phenazine unit (10-dihydrophenazine) in place of an anthraquinone (AQ) unit within a 2D COF framework (Figs. 26a–c) [238], resulting in a rise of approximately 0.3 V in electrode potential compared to the DAAQ-based COF. In another report, triphenylamine-based CMPs displayed redox potentials around 3.7 V vs. Li/Li^+, nearly matching those of commercial inorganic materials [239].

6.3. Poor electrical conductivity

An additional major limitation with many CMPs is their inherently low electrical conductivity, as they are typically insulators with very limited electron transport. A common strategy to address this issue is the incorporation of conductive additives, usually carbon-based materials. However, since these additives are non-redox-active, their inclusion reduces the energy density of the battery, which is undesirable. One widely used strategy to enhance the electrical conductivity of organic polymeric electrodes involves the formation of hybrids with conductive additives such as graphene and CNTs [240] which have been shown to significantly improve their electrochemical performance. Another strategy, emphasized by the Meng research team [241] involves

Table 2
Relationship between CMP Type, Morphology, Charge-Storage Mechanism, and Electrochemical Performance.

CMP type	Representative Material	Dominant Morphology	Charge-storage Mechanism	Key Advantage of Morphology	Ref
Nitrogen-rich CMPs	TAT-CMP-1 TAT-CMP-2	Aggregated particulate networks	EDLC + minor pseudocapacitance	High surface area, dense packing may limit ion diffusion at high rates	[172]
Graphene-templated CMPs	GMP sandwich structures	2D layered / hierarchical nanosheets	EDLC-dominated	Improved electrolyte penetration and fast ion transport	[173]
Quinone-based CMPs	PAQ-based CMPs	Irregular porous aggregates	EDLC + strong pseudocapacitance	Accessible redox sites enable combined capacitive behavior	[75,195]
Aza-fused CMPs	Aza-fused CMPs	Microporous interconnected networks	Pseudocapacitance-dominated	Enhanced conductivity and rapid ion diffusion	[195]
Schiff's base CMPs	TPDA-1	Microporous particulate framework	EDLC + pseudocapacitance	Ion diffusion channels from porous framework	[197]
Imide-based CMPs	PDI-based CMP-1/2/3	Cross-linked micro/mesoporous networks	n-type pseudocapacitance	Stabilized redox activity and a wide negative potential window	[203]
CMP/CNT hybrids	CNF@CMP, CMP/CNT composites	Interconnected fibrous networks	EDLC + pseudocapacitance	Enhanced conductivity and reduced charge-transfer resistance	[205]
CMP-derived carbons	Graphene-templated CMP carbons	Hierarchical porous nanosheets	EDLC-dominated	Rapid ion transport and efficient electron Conduction	[173]

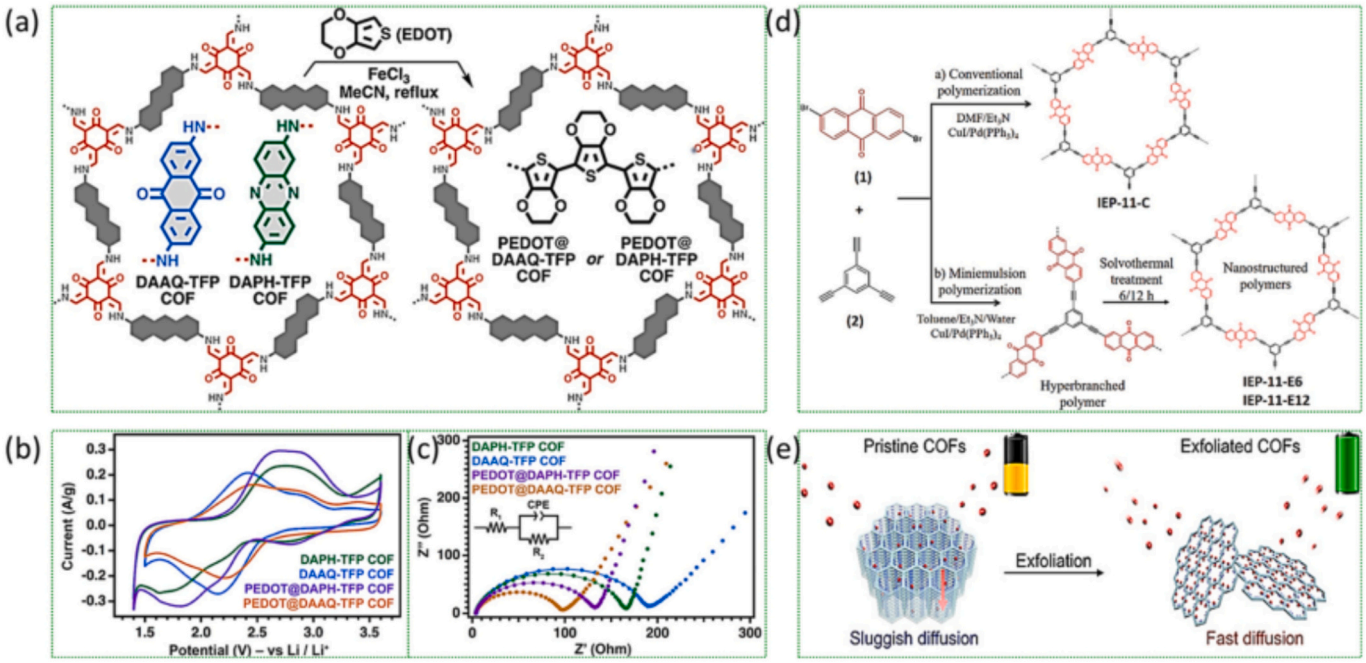

Fig. 26. (a) A COF in which the anthraquinone unit was replaced with a phenazine unit, combined with growth of PEDOT inside the pores, (b) the CV shows an increase in redox potential and (c) shows better conductivity for phenazine based COF, (d) A newly developed synthesis route which helps to obtain a nanostructured COF with improve solubility and (e) exfoliation of COF to improve the diffusion process. (a)–(c) Reproduced with permission from Ref. [238] Copyright 2019, American Chemical Society, (d) Reprinted with permission from Ref. [252] Copyright 2019, Wiley, (e) Reproduced with permission from Ref. [245] Copyright 2019, American Chemical Society.

designing materials with inherently high conductivity. They synthesized a nitrogen-enriched porous polymer featuring extended conjugation to boost electron transport. The material demonstrated good cycling retention and strong rate capability at higher current densities, largely due to the high density of nitrogen atoms integrated into the π-conjugated framework. Embedding heteroatoms into π-conjugated polymer frameworks has proven especially promising. For instance, π-conjugated quinoxaline-based molecules have demonstrated excellent rate capability and cycling stability [242].

The use of binders is another aspect that lowers the energy density of electrochemical systems. Despite this drawback, binders are often necessary to maintain the structural integrity and stability of composite electrodes. To overcome this limitation, a boroxine-based COF containing pyrene-4,5,9,10-tetraone (PTO) as the electroactive unit was combined with CNTs to construct a binder-free cathode for lithium-ion batteries [235,241]. In this design, the soft PTO units were expected to contribute flexibility and stretchability, while the rigid, porous structure provided mechanical stability and facilitated fast ion diffusion.

Conductivity in CMPs can be effectively improved through heteroatom doping and metal incorporation, and increasing the number of active positions for energy storage. Recently, researchers applied this approach to design metal-coordinated, highly crystalline M@C2N frameworks [243]. In these systems, adjacent C2N layers were interconnected by metal atoms, which extended π–π conjugation and significantly enhanced electrical conductivity.

Although CMPs offer high surface area and tunable porosity, increasing network porosity can interrupt effective π-electron delocalization and thereby limit intrinsic electronic conductivity—one of the recurring bottlenecks for electrochemical applications. Consequently, post-treatments such as carbonization/pyrolysis are frequently adopted to improve conductivity; however, this approach often yields heteroatom-doped porous carbons whose performance may increasingly reflect carbon microstructure and surface chemistry rather than the original CMP's molecularly encoded functionality. This trade-off motivates deeper discussion on when 'CMP-to-carbon' strategies preserve genuine structure–function advantages versus when they converge toward advanced activated-carbon-like behavior [154,244].

6.4. Utilization of active material

Another major obstacle for organic electrode materials, particularly CMPs, is their limited utilization of active material. This challenge is closely tied to conductivity, since poor electrical conductivity reduces the effective use of active sites, and in turn, low utilization limits overall conductivity. However, even in cases where conductivity is adequate, utilization can remain low if many active sites are inaccessible, for example, when they are buried within rigid, densely packed layered structures. Such architecture hinders electrolyte penetration and restricts electron diffusion, preventing full participation of the active material in the electrochemical process.

Recently, researchers applied exfoliation techniques to enhance active material utilization (Fig. 26e) [245,246]. For example, a straightforward ball-milling method has been utilized to exfoliate 2D-layered COFs into few-layer nanosheets [245]. While this approach improved accessibility of active sites, the poor yield of few-layer structures remains a significant obstacle, limiting scalability for commercial applications. Developing methods that increase yield or introducing new strategies for improved active material utilization continues to be a key challenge. An AQ-based COF grown on CNTs (AQ COF@CNTs) was employed to enhance conductivity. In addition to improved electron transport, this composite also boosted active material utilization, achieving 96% of the theoretical capacity [247].

6.5. Solubility

In general, low-solubility electrode materials in liquid electrolyte systems are favored to ensure improved stability, as discussed earlier. However, in certain situations, a moderate level of solubility is desirable for improved processability and performance. For instance, during electrode fabrication using solution-phase techniques, materials need to

disperse well with additives (generally in NMP), forming a suspension, which is then cast onto a current collector to prepare the working electrode. CMPs, however, typically exhibit poor solubility in the majority of solvents due to their conjugated, robust, and inflexible nature [248]. As a result, dispersing them in NMP or other solvents becomes difficult, making it more difficult to produce efficient electrodes with a homogeneous distribution of active materials. Early attempts were made to improve the solubility and processability of CMPs using techniques such as hyperbranching and alkylation [249–251]. However, introducing additional electrochemically inactive chains or groups reduces the theoretical capacity, which is undesirable. To address this, an AQ-linked CMP has been synthesized via a combination of mini-emulsion and solvothermal techniques (IEP-11-E12) (Fig. 26d) [252]. Unlike the conventionally prepared polymer (IEP-11-C), this material dispersed readily in acetone, enabling the preparation of a uniformly dispersed electrode with a smooth surface. This approach significantly enhanced electrochemical performance, attributed to improved electrode preparation, greater surface area, and rapid electrode kinetics from its micro- and mesoporous structure. In another study, a spatial confinement strategy was employed to grow polymeric nanoparticles through a Sonogashira coupling, which resulted in 5 nm conjugated polymer, allowing the straightforward preparation of thin films [251].

6.6. Accessible versus BET surface area

Although high BET surface area is frequently highlighted as a key advantage of CMPs, it does not necessarily correlate with improved SC performance. Numerous studies have shown that a significant fraction of the ultra-high surface area in highly microporous materials may be electrochemically inaccessible, particularly under practical charge–discharge conditions, due to limited ion penetration and slow transport within narrow micropores. Excessive microporosity can also introduce substantial ionic resistivity, which becomes increasingly detrimental at high current densities and leads to poor rate capability despite large surface areas. Moreover, surface area determined from gas adsorption measurements does not directly reflect the effective pore utilization for solvated electrolyte ions during electrochemical operation. As emphasized in recent reviews, hierarchical pore architectures, combining micropores for charge storage with meso- and macropores for efficient ion transport, are more effective in maximizing electrochemically accessible surface area and improving rate performance than simply increasing BET surface area alone. These considerations underscore the need to move beyond surface-area-centric metrics and instead focus on pore size distribution, ion transport resistance, and accessible active surface when evaluating CMP-based SCs [253].

6.7. Economic viability and cost-to-performance considerations

Beyond electrochemical performance, the economic feasibility of CMPs is a critical factor governing their practical adoption. Most CMPs are synthesized from functionalized aromatic monomers via cross-coupling reactions, such as Sonogashira, Suzuki, or Yamamoto polymerizations, which often require noble-metal catalysts, inert atmospheres, and multistep monomer preparation. These factors substantially increase production costs compared to activated carbons derived from abundant, inexpensive biomass or petrochemical precursors [254].

From a cost-to-performance perspective, although CMPs can rival or exceed activated carbon in gravimetric capacitance, their advantage diminishes when volumetric capacitance, conductivity, and processing cost are considered. Compared with emerging competitors such as MOFs, CMPs offer superior chemical stability but lack the cost maturity and scalability required for commercial deployment [48]. Consequently, future CMP research must prioritize low-cost monomer design, catalyst-free polymerization strategies, and scalable synthesis routes to improve economic competitiveness.

6.8. Failure mechanisms and stability under practical conditions

Beyond commonly reported cycling numbers, the long-term stability of CMP-based SC electrodes must be evaluated in a more mechanistic and application-relevant manner. Several potential degradation pathways have been identified or implied in the literature, including conjugated backbone degradation, loss of π–π stacking and pore collapse, and chemical instability of redox-active functional groups under repeated oxidation–reduction cycles. In particular, CMPs incorporating highly redox-active moieties (e.g., quinone, imide, or heteroaromatic units) may undergo gradual structural or chemical changes that are not fully captured by standard room-temperature cycling tests at moderate current densities. Moreover, most stability studies are conducted under mild operating conditions, whereas practical SC devices are often exposed to wide voltage windows, elevated temperatures, and fluctuating charge–discharge rates, which can accelerate degradation processes. As highlighted in recent reviews, the absence of standardized protocols for high-voltage, high-temperature, and long-term durability testing represents a critical gap between laboratory-scale demonstrations and commercial requirements. Addressing these gaps will demand standardized high-stress testing protocols, combined with post-mortem structural analysis (e.g., TEM, XPS) and operando electrochemical characterization to link specific chemical or structural changes with performance decay [255].

6.9. Reliability of electrochemical performance evaluation

A critical issue in evaluating CMP-based SC electrodes is the widespread reliance on three-electrode electrochemical measurements. While three-electrode configurations are valuable for probing intrinsic redox behavior and fundamental charge-storage mechanisms, they often lead to overestimates of capacitance, rate capability, and cycling stability compared with practical two-electrode full-cell devices. In such configurations, the working electrode benefits from an excess electrolyte reservoir and an idealized counter electrode, conditions that do not reflect realistic operating environments [181,182].

In contrast, two-electrode measurements impose stricter constraints on ion transport, electrode balancing, and internal resistance, providing a more accurate representation of device-level performance. Several CMP systems that demonstrate exceptionally high specific capacitance in three-electrode tests show markedly reduced capacitance, narrower voltage windows, and inferior rate capability when evaluated in symmetric or asymmetric full-cell configurations. This discrepancy underscores the risk of directly extrapolating laboratory-scale performance metrics to practical applications.

Moreover, literature often compares capacitance values derived from different electrochemical configurations without sufficient contextualization. Such comparisons can be misleading, particularly when variations in electrode mass loading, voltage window, electrolyte composition, and testing protocol are not standardized. To ensure meaningful benchmarking, capacitance, energy density, and power density values should be clearly reported with explicit reference to the testing configuration and normalized using consistent methodologies.

6.10. Electrode fabrication, device integration, and sustainability

While significant progress has been achieved at the material level, the practical deployment of CMPs in SC devices is strongly influenced by electrode fabrication strategies and cell-level integration. In contrast to conventional porous carbons, CMPs typically exhibit low intrinsic electronic conductivity, necessitating the incorporation of conductive additives such as carbon black, graphene, or CNTs. Although these additives improve charge transport, high additive contents (often 20–40 wt %) dilute the active CMP fraction, thereby diminishing the effective gravimetric and volumetric capacitance of the electrode and complicating fair performance assessment [205].

Binder selection and content further influence electrode integrity and electrochemical behavior. Common polymeric binders such as poly (vinylidene fluoride) (PVDF) or polytetrafluoroethylene (PTFE) enhance mechanical stability but may block micropores, reduce electrolyte accessibility, and introduce interfacial resistance. Water-based binders (e.g., carboxymethyl cellulose or styrene–butadiene rubber) offer improved environmental compatibility but may compromise chemical stability in certain electrolytes [256,257]. The lack of systematic studies evaluating binder–CMP interactions and their long-term effects on cycling performance remains a notable gap in the literature.

At the device level, most reported CMP-based SCs are evaluated in three-electrode configurations using low mass loadings (< 2 mg cm^{-2}), which do not reflect practical operating conditions. When transitioned to two-electrode full-cell configurations with higher areal loadings, CMP electrodes often exhibit reduced rate capability and energy density, highlighting the discrepancy between intrinsic material performance and device-level behavior. Addressing this gap requires optimization of electrode architecture, including thickness control, hierarchical porosity, and current collector integration.

From an environmental perspective, the sustainability of CMP production warrants critical scrutiny. The extensive use of solvents, catalyst residues, and energy-intensive synthesis steps contributes to a substantial environmental footprint. Moreover, catalyst recovery and solvent recycling are rarely addressed in CMP studies, despite their importance for green manufacturing. Developing alternative synthesis strategies—such as catalyst-free polymerizations, solvent-minimized reactions, and biomass-derived monomers—will be essential for improving the environmental compatibility of CMP-based electrodes.

Overall, while CMPs offer unique structural tunability and rich redox chemistry for SC applications, their translation from laboratory demonstrations to practical devices remains constrained by a series of interconnected challenges. These include limited theoretical capacity arising from inactive structural components, suboptimal redox potentials, poor intrinsic electrical conductivity, low utilization of active sites, solubility and processability issues, and the frequent mismatch between BET surface area and electrochemically accessible surface. At the device level, additional hurdles emerge from electrode fabrication, binder and additive dilution effects, unrealistic three-electrode testing protocols, and insufficient evaluation under high mass loading and full-cell conditions. Furthermore, economic and environmental considerations—such as the cost and sustainability of monomers, reliance on noble-metal-catalyzed coupling reactions, solvent intensity, and lack of scalable synthesis routes—pose significant barriers to commercialization. Addressing these challenges will require a holistic approach that integrates molecular design, electrode engineering, realistic performance benchmarking, scalable green synthesis, and mechanistic stability studies to unlock the true potential of CMPs in next-generation energy storage systems.

7. Conclusions and future perspectives

CMPs have emerged as a versatile and robust class of functional materials owing to their permanent porosity, high chemical and thermal stability, and rich structural tunability. Past efforts in CMP design, synthesis, and functional evaluation have clearly demonstrated their strong potential across a broad range of energy-related applications, particularly in SCs, where CMPs combine the advantages of organic molecular functionality with extended porous frameworks.

In the context of SCs, the rigid backbone of CMPs effectively suppresses the dissolution of redox-active units, thereby improving cycling stability, while their high surface area and interconnected porosity facilitate efficient electrolyte ion transport and exposure of active sites. Nevertheless, many CMP-based electrodes still face intrinsic challenges, most notably limited active-site utilization and poor intrinsic electrical conductivity, which restrict their rate capability and practical performance. To overcome these limitations, current research has converged on four major structural optimization strategies: (i) heteroatom doping to introduce additional redox-active sites and modulate electronic structure; (ii) metal incorporation through coordination or confinement to enhance pseudocapacitive behavior; (iii) hybridization with conductive carbon materials (e.g., CNTs, graphene) to improve charge transport; and (iv) combined or synergistic approaches that integrate multiple modification strategies to maximize electrochemical performance.

Looking forward, several key directions should be prioritized to further advance CMP-based electrode materials. While CMP research has grown rapidly, future progress must prioritize technological relevance over structural novelty. High-priority research directions include improving intrinsic electronic conductivity without sacrificing porosity, developing environmentally benign and scalable synthesis methods, and validating performance under realistic device conditions. In contrast, incremental structural modifications that yield marginal performance improvements under idealized laboratory conditions are unlikely to translate into commercial relevance. Emphasis should be placed on integrating CMPs into practical electrode architectures, advancing full-cell testing protocols, and understanding long-term degradation mechanisms. Such a shift from exploration material synthesis toward application-driven optimization is essential for advancing CMPs from academically promising materials to viable components of next-generation energy storage systems.

Beyond SCs, CMPs offer exciting opportunities in emerging technologies such as flexible electronics, wearable devices, and smart energy systems, where lightweight, mechanically robust, and multifunctional electrode materials are required. Moreover, the inherent modularity of CMPs makes them attractive for a wide range of applications extending beyond energy storage, including gas adsorption and separation, photocatalysis, water purification, sensing, and biomedical materials. With continued advances in molecular design, synthetic chemistry, and mechanistic insight, CMPs are expected to play an increasingly important role in both fundamental research and future industrial technologies.

CRediT authorship contribution statement

Ahmed F. Saber: Writing – original draft, Conceptualization. **Mohamed Gamal Mohamed:** Writing – review & editing, Software. **Mohamed Hammad Elsayed:** Writing – original draft. **Shiao-Wei Kuo:** Writing – review & editing, Supervision. **Mahmoud M. Abdelnaby:** Writing – review & editing, Supervision.

Declaration of competing interest

The authors declare that they have no known competing financial interests or personal relationships that could have appeared to influence the work reported in this paper.

Acknowledgment

The authors acknowledge the Interdisciplinary Research Center for Hydrogen Technologies and Carbon Management (IRC-HTCM) at King Fahd University of Petroleum and Minerals (KFUPM) for its support.

Data availability

Data will be made available on request.

References

[1] Z. Ajmal, M.K. Irshad, A. Qadeer, M.Z. Ul Haq, R. Ullah, M.A. Sarwar, T. Saeed, M. Abid, A. Hayat, A. Ali, A. Noman, R. Dong, Novel magnetite nano-rods-modified biochar: A promising strategy to control lead mobility and transfer in soil-rice system, Int. J. Environ. Sci. Technol. 20 (2023) 7543–7558, https://doi.org/10.1007/s13762-022-04452-w.

[2] H. Ali, R. Chen, B. Wu, T. Xie, L. Weng, J. Wen, Q. Yao, L. Su, Y. Zhao, P. Zhao, B. Sa, Y. Liu, C. Wang, H. Su, A. Hayat, The site preference and doping effect on mechanical properties of Ni_3Al-based γ' phase in superalloys by combing first-principles calculations and thermodynamic model, Arab. J. Chem. 15 (2022) 104278, https://doi.org/10.1016/j.arabjc.2022.104278.
[3] Z. Ajmal, Y. Naciri, M. Ahmad, A. Hsini, A. Bouziani, M. Laabd, W. Raza, A. Murtaza, A. Kumar, S. Ullah, A.G. Al-Sehemi, A.A. Al-Ghamdi, A. Qadeer, A. Hayat, R. Djellabi, Use of conductive polymer-supported oxide-based photocatalysts for efficient VOCs & SVOCs removal in gas/liquid phase, J. Environ. Chem. Eng. 11 (2023) 108935, https://doi.org/10.1016/j.jece.2022.108935.
[4] A. Hayat, M. Sohail, H. Ali, T.A. Taha, H.I.A. Qazi, N. Ur Rahman, Z. Ajmal, A. Kalam, A.G. Al-Sehemi, S. Wageh, M.A. Amin, A. Palamanit, W.I. Nawawi, E. F. Newair, Y. Orooji, Recent advances and future perspectives of metal-based Electrocatalysts for overall electrochemical water splitting, Chem. Rec. 23 (2023) e202200149, https://doi.org/10.1002/tcr.202200149.
[5] A. Hayat, M. Sohail, T.A. Taha, S.K.B. Mane, A.G. Al-Sehemi, A.A. Al-Ghamdi, W. I. Nawawi, A. Palamanit, M.A. Amin, A.M. Fallatah, Z. Ajmal, H. Ali, W.U. Khan, M.W. Shah, J. Khan, S. Wageh, Synergetic effect of bismuth vanadate over copolymerized carbon nitride composites for highly efficient photocatalytic H_2 and O_2 generation, J. Colloid Interface Sci. 627 (2022) 621–629, https://doi.org/10.1016/j.jcis.2022.07.012.
[6] A. Ur Rehman, T. Zhao, M.Z. Shah, Y. Khan, A. Hayat, C. Dang, M. Zheng, S. Yun, Nanoengineering of $MgSO_4$ nanohybrid on MXene substrate for efficient thermochemical heat storage material, Appl. Energy 332 (2023) 120549, https://doi.org/10.1016/j.apenergy.2022.120549.
[7] R. Shah, S. Ali, S. Ali, P. Xia, F. Raziq, F. Mabood Adnan, S. Shah, A. Zada, P. M. Ismail, A. Hayat, A.U. Rehman, X. Wu, H. Xiao, X. Zu, S. Li, L. Qiao, Amino functionalized metal-organic framework/rGO composite electrode for flexible Li-ion batteries, J. Alloys Compd. 936 (2023) 168183, https://doi.org/10.1016/j.jallcom.2022.168183.
[8] A. Giri, Y. Khakre, G. Shreeraj, T.K. Dutta, S. Kundu, A. Patra, The order–disorder conundrum: A trade-off between crystalline and amorphous porous organic polymers for task-specific applications, J. Mater. Chem. A 10 (2022) 17077–17121, https://doi.org/10.1039/d2ta01546c.
[9] X.M. Lu, H. Wang, Y. Sun, Y. Xu, W. Sun, Y. Wu, Y. Zhang, C. Yang, Y. Wang, Covalent Triazine-based frameworks with donor-donor-π-acceptor structures for dendrite-free Lithium metal batteries, Angew. Chem. 136 (2024) e202409436, https://doi.org/10.1002/ange.202409436.
[10] A.F. Saber, H.T. Liao, P.J. Li, Y.F. Chen, L. Mabuti, S.W. Kuo, J. Lüder, A.F.M. EL-Mahdy, Synergistic structural engineering of donor–acceptor–acceptor type conjugated microporous polymers as photocatalysts for boosting sunlight-driven hydrogen evolution, J. Colloid Interface Sci. 699 (2025) 138156, https://doi.org/10.1016/j.jcis.2025.138156.
[11] A.F. Saber, Y.F. Chen, L. Mabuti, S.V. Chaganti, S.U. Sharma, J. Lüder, J.T. Lee, S. W. Kuo, A.F.M. EL-Mahdy, Engineering carbonyl-rich conjugated microporous polymers with a pyrene-4,5,9,10-tetraone building block as highly efficient and stable electrodes for energy storage, Mater. Adv. 6 (2025) 607–616, https://doi.org/10.1039/d4ma00928b.
[12] A.F. Saber, M. Ahmed, S.W. Kuo, A.F.M. EL-Mahdy, Tetraphenylcyclopentadiene-based conjugated microporous polymers for high-performance energy storage carbons, Polym. Chem. 14 (2023) 4079–4088, https://doi.org/10.1039/d3py00671a.
[13] A.F. Saber, S.W. Kuo, A.F.M. EL-Mahdy, Microporous carbons derived from nitrogen-rich triazatruxene-based porous organic polymers for efficient cathodic supercapacitors, J. Mater. Chem. A 12 (2024) 15373–15385, https://doi.org/10.1039/d4ta01242a.
[14] A.F. Saber, C.C. Chueh, M. Rashad, S.W. Kuo, A.F.M. EL-Mahdy, Thiazolyl-linked conjugated microporous polymers for enhancement adsorption and photocatalytic degradation of organic dyes from water, Mater. Today Sustain. 23 (2023) 100429, https://doi.org/10.1016/j.mtsust.2023.100429.
[15] A.F. Saber, A.M. Elewa, H.H. Chou, A.F.M. EL-Mahdy, Donor to acceptor charge transfer in Carbazole-based conjugated microporous polymers for enhanced visible-light-driven photocatalytic water splitting, ChemCatChem 15 (2023) e202201287, https://doi.org/10.1002/cctc.202201287.
[16] A.F. Saber, A.F.M. El-Mahdy, (E)-1,2-Diphenylethene-based conjugated nanoporous polymers for a superior adsorptive removal of dyes from water, New J. Chem. 45 (2021) 21834–21843, https://doi.org/10.1039/d1nj04287d.
[17] A.F. Saber, S.U. Sharma, J.T. Lee, A.F.M. EL-Mahdy, S.W. Kuo, Carbazole-conjugated microporous polymers from Suzuki–Miyaura coupling for supercapacitors, Polymer 254 (2022) 125070, https://doi.org/10.1016/j.polymer.2022.125070.
[18] A.F. Saber, K.Y. Chen, A.F.M. EL-Mahdy, S.W. Kuo, Designed azo-linked conjugated microporous polymers for CO_2 uptake and removal applications, J. Polym. Res. 28 (2021) 1–12, https://doi.org/10.1007/s10965-021-02803-8.
[19] A.F. Saber, A.M. Elewa, H.H. Chou, A.F.M. EL-Mahdy, Donor-acceptor carbazole-based conjugated microporous polymers as photocatalysts for visible-light-driven H_2 and O_2 evolution from water splitting, Appl. Catal. B 316 (2022) 121624, https://doi.org/10.1016/j.apcatb.2022.121624.
[20] N. Naz, M.H. Manzoor, S.M.G. Naqvi, U. Ehsan, M. Aslam, F. Verpoort, Porous organic polymers; an emerging material applied in energy, environmental and biomedical applications, Appl. Mater. Today 38 (2024) 102198, https://doi.org/10.1016/j.apmt.2024.102198.
[21] A. Kašpar, B. Bashta, Š. Titlová, J. Brus, A. Vagenknechtová, E. Vrbková, K. Zítová, E. Vyskočilová, J. Sedláček, Ionic hyper-cross-linked porous polymer networks with achiral and chiral pyridinium-type segments, Eur. Polym. J. 210 (2024) 112971, https://doi.org/10.1016/j.eurpolymj.2024.112971.
[22] A. Hayat, M. Sohail, A. El Jery, K.M. Al-Zaydi, S. Raza, H. Ali, Y. Al-Hadeethi, T. A. Taha, I. Ud Din, M. Ali Khan, M.A. Amin, E. Ghasali, Y. Orooji, Z. Ajmal, M. Z. Ansari, Recent advances in ground-breaking conjugated microporous polymers-based materials, their synthesis, modification and potential applications, Mater. Today 64 (2023) 180–208, https://doi.org/10.1016/j.mattod.2023.02.025.
[23] S. Yuan, X. Huang, T. Kong, L. Yan, Y. Wang, Organic electrode materials for energy storage and conversion: Mechanism, characteristics, and applications, Acc. Chem. Res. 57 (2024) 1550–1563, https://doi.org/10.1021/acs.accounts.4c00016.
[24] Y. Cao, Q. Xu, Y. Sun, J. Shi, Y. Xu, Y. Tang, X. Chen, S. Yang, Z. Jiang, H.D. Um, X. Li, Y. Wang, Steering lithium and potassium storage mechanism in covalent organic frameworks by incorporating transition metal single atoms, Proc. Natl. Acad. Sci. USA 121 (2024) e2315407121, https://doi.org/10.1073/pnas.2315407121.
[25] S. Jose, A. Sariga, Varghese, design and structural characteristics of conducting polymer-metal organic framework composites for energy storage devices, Synth. Met. 297 (2023) 117421, https://doi.org/10.1016/j.synthmet.2023.117421.
[26] C. Li, H. Xu, L. Ni, B. Qin, Y. Ma, H. Jiang, G. Xu, J. Zhao, G. Cui, Nonaqueous liquid electrolytes for sodium-ion batteries: Fundamentals, Progress and perspectives, Adv. Energy Mater. 13 (2023) 2301758, https://doi.org/10.1002/aenm.202301758.
[27] J. Fan, Z. Yang, S. Dai, Construction of conjugated scaffolds driven by mechanochemistry towards energy storage applications, GreenChE 5 (2024) 155–172, https://doi.org/10.1016/j.gce.2023.04.001.
[28] P. Novák, K. Müller, K.S.V. Santhanam, O. Haas, Electrochemically active polymers for rechargeable batteries, Chem. Rev. 97 (1997) 207–281, https://doi.org/10.1021/cr941181o.
[29] Y. Xu, S. Jin, H. Xu, A. Nagai, D. Jiang, Conjugated microporous polymers: Design, synthesis and application, Chem. Soc. Rev. 42 (2013) 8012–8031, https://doi.org/10.1039/c3cs60160a.
[30] F. Vilela, K. Zhang, M. Antonietti, Conjugated porous polymers for energy applications, Energy Environ. Sci. 5 (2012) 7819–7832, https://doi.org/10.1039/c2ee22002d.
[31] H.P. Wu, Q. Yang, Q.H. Meng, A. Ahmad, M. Zhang, L.Y. Zhu, Y.G. Liu, Z.X. Wei, A polyimide derivative containing different carbonyl groups for flexible lithium ion batteries, J. Mater. Chem. A 4 (2016) 2115–2121, https://doi.org/10.1039/c5ta07246h.
[32] Y.M. Nabil, S. Abdelnaser, A.A.K. Mohammed, S.W. Kuo, A.F.M. EL-Mahdy, Engineering redox-active benzo[1,2-b:4,5-b']dithiophene-based conjugated polymers: Tuning porosity and linker architecture for high-performance supercapacitors, J. Mater. Chem. A 13 (2025) 26337–26349, https://doi.org/10.1039/d5ta03907j.
[33] L. Zhao, T. Zhang, W. Li, T. Li, L. Zhang, X. Zhang, Z. Wang, Engineering of sodium-ion batteries: Opportunities and challenges, Engineering 24 (2023) 172–183, https://doi.org/10.1016/j.eng.2021.08.032.
[34] P. Poizot, J. Gaubicher, S. Renault, L. Dubois, Y. Liang, Y. Yao, Opportunities and challenges for organic electrodes in electrochemical energy storage, Chem. Rev. 120 (2020) 6490–6557, https://doi.org/10.1021/acs.chemrev.9b00482.
[35] Q. Wang, T. O'Carroll, F. Shi, Y. Huang, G. Chen, X. Yang, A. Nevar, N. Dudko, N. Tarasenko, J. Xie, L. Shi, G. Wu, D. Zhang, Designing organic material electrodes for Lithium-ion batteries: Progress, Challenges, and Perspectives, Electrochem. Energy Rev. 7 (2024) 1–44, https://doi.org/10.1007/s41918-024-00218-9.
[36] Y. Kang, C. Deng, Y. Chen, X. Liu, Z. Liang, T. Li, Q. Hu, Y. Zhao, Binder-free electrodes and their application for Li-ion batteries, Nanoscale Res. Lett. 15 (2020) 1–19, https://doi.org/10.1186/s11671-020-03325-w.
[37] A. Ehsani, F. Soltani, M. Kalhor, A. Andooz, M.D. Najafi, M. Nabatian, Enhanced pseudocapacitance performance of conductive polymer in the presence of synthesized mesoporous MnO_2@zeolite-Y, Electrochim. Acta 491 (2024) 144301, https://doi.org/10.1016/j.electacta.2024.144301.
[38] A. Omidi-Dargahi, M.R. Saadati-Gullojeh, M. Bigdeloo, H.M. Shiri, A. Ehsani, Electrochemical measurement and preparation of $MnCo_2O_4$/g-C_3N_4/POAP nanocomposite and its performance as a supercapacitor electrode, Inorg. Chem. Commun. 180 (2025) 114877, https://doi.org/10.1016/j.inoche.2025.114877.
[39] A. Ehsani, Z. Rezaei, S.M. Atashzar, F. Soltani, Optimized geometric structure of Zn-BTC/POAP and Fe-BTC/POAP systems as electroactive materials in pseudocapacitors, J. Energy Storage 70 (2023) 108058, https://doi.org/10.1016/j.est.2023.108058.
[40] M. Bigdeloo, E. Kowsari, A. Ehsani, S. Ramakrishna, A. Chinnappan, Activated carbon derived from fennel flower waste as high-efficient sustainable materials for improving cycle stability and capacitance performance of electroactive nanocomposite of conductive polymer, J. Energy Storage 55 (2022) 105793, https://doi.org/10.1016/j.est.2022.105793.
[41] X. Zhao, M. Sajjad, Y. Zheng, M. Zhao, Z. Li, Z. Wu, K. Kang, L. Qiu, Covalent organic framework templated ordered nanoporous C60 as stable energy efficient supercapacitor electrode material, Carbon 182 (2021) 144–154, https://doi.org/10.1016/j.carbon.2021.05.061.
[42] M. Sajjad, M. Amin, M.S. Javed, M. Imran, W. Hu, Z. Mao, W. Lu, Recent trends in transition metal diselenides (XSe_2: X = Ni, Mn, co) and their composites for high energy faradic supercapacitors, J. Energy Storage 43 (2021) 103176, https://doi.org/10.1016/j.est.2021.103176.
[43] M. Sajjad, M.I. Khan, F. Cheng, W. Lu, A review on selection criteria of aqueous electrolytes performance evaluation for advanced asymmetric supercapacitors,

J. Energy Storage 40 (2021) 102729, https://doi.org/10.1016/j.est.2021.102729.
[44] M. Sajjad, W. Lu, Covalent organic frameworks based nanomaterials: Design, synthesis, and current status for supercapacitor applications: A review, J. Energy Storage 39 (2021) 102618, https://doi.org/10.1016/j.est.2021.102618.
[45] D. Taylor, S.J. Dalgarno, Z. Xu, F. Vilela, Conjugated porous polymers: Incredibly versatile materials with far-reaching applications, Chem. Soc. Rev. 49 (2020) 3981–4042, https://doi.org/10.1039/c9cs00315k.
[46] N. Singh, V. Singh, N. Bisht, P. Negi, A. Dhyani, R.K. Sharma, B.S. Tewari, A comprehensive review on supercapacitors: Basics to recent advancements, J. Energy Storage 121 (2025) 116498, https://doi.org/10.1016/j.est.2025.116498.
[47] H.R. Khan, A.L. Ahmad, Supercapacitors: Overcoming current limitations and charting the course for next-generation energy storage, J. Ind. Eng. Chem. 141 (2025) 46–66, https://doi.org/10.1016/j.jiec.2024.07.014.
[48] J.S.M. Lee, A.I. Cooper, Advances in conjugated microporous polymers, Chem. Rev. 120 (2020) 2171–2214, https://doi.org/10.1021/acs.chemrev.9b00399.
[49] P. Zhang, Y. Yin, Z. Wang, C. Yu, Y. Zhu, D. Yan, W. Liu, Y. Mai, Porphyrin-based conjugated microporous polymer tubes: Template-free synthesis and a Photocatalyst for visible-light-driven Thiocyanation of anilines, Macromolecules 54 (2021) 3543–3553, https://doi.org/10.1021/acs.macromol.1c00190.
[50] S. Han, Z. Li, S. Ma, Y. Zhi, H. Xia, X. Chen, X. Liu, Bandgap engineering in benzotrithiophene-based conjugated microporous polymers: A strategy for screening metal-free heterogeneous photocatalysts, J. Mater. Chem. A 9 (2021) 3333–3340, https://doi.org/10.1039/d0ta10232f.
[51] M.G. Mohamed, T.C. Chen, S.W. Kuo, Solid-state chemical transformations to enhance gas capture in Benzoxazine-linked conjugated microporous polymers, Macromolecules 54 (2021) 5866–5877, https://doi.org/10.1021/acs.macromol.1c00736.
[52] L. Cui, S. Yu, W. Gao, X. Zhang, S. Deng, C.Y. Zhang, Tetraphenylenthene-based conjugated microporous polymer for aggregation-induced Electrochemiluminescence, ACS Appl. Mater. Interfaces 12 (2020) 7966–7973, https://doi.org/10.1021/acsami.9b21943.
[53] Y. Zhang, Q. Sun, Z. Li, Y. Zhi, H. Li, Z. Li, H. Xia, X. Liu, Light-emitting conjugated microporous polymers based on an excited-state intramolecular proton transfer strategy and selective switch-off sensing of anions, Mater. Chem. Front. 4 (2020) 3040–3046, https://doi.org/10.1039/d0qm00384k.
[54] M.G.M. Bai, H.V. Babu, V. Lakshmi, M.R. Rao, Structure–property–function relationship of fluorescent conjugated microporous polymers, Mater. Chem. Front. 5 (2021) 2506–2551, https://doi.org/10.1039/d0qm00769b.
[55] Z. Zhu, S. Wu, C. Liu, P. Mu, Y. Su, H. Sun, W. Liang, A. Li, Ionic liquid and magnesium hydrate incorporated conjugated microporous polymers nanotubes with superior flame retardancy and thermal insulation, Polymer 194 (2020) 122387, https://doi.org/10.1016/j.polymer.2020.122387.
[56] M.M. Samy, M.G. Mohamed, A.F.M. El-Mahdy, T.H. Mansoure, K.C.W. Wu, S. W. Kuo, High-performance supercapacitor electrodes prepared from dispersions of Tetrabenzonaphthalene-based conjugated microporous polymers and carbon nanotubes, ACS Appl. Mater. Interfaces 13 (2021) 51906–51916, https://doi.org/10.1021/acsami.1c05720.
[57] K. Zhang, W. Liu, Y. Gao, X. Wang, Z. Chen, R. Ning, W. Yu, R. Li, L. Li, X. Li, K. Yuan, L. Ma, N. Li, C. Shen, W. Huang, K. Xie, K.P. Loh, A high-performance Lithium metal battery with ion-selective Nanofluidic transport in a conjugated microporous polymer protective layer, Adv. Mater. 33 (2021) 2006323, https://doi.org/10.1002/adma.202006323.
[58] J.S. Seenath, B.P. Biswal, Construction of MXene-coupled nitrogen-doped porous carbon hybrid from a conjugated microporous polymer for high-performance supercapacitors, Adv. Energy Sustainability Res. 2 (2021) 2000052, https://doi.org/10.1002/aesr.202000052.
[59] J.X. Jiang, F. Su, A. Trewin, C.D. Wood, N.L. Campbell, H. Niu, C. Dickinson, A. Y. Ganin, M.J. Rosseinsky, Y.Z. Khimyak, A.I. Cooper, Conjugated microporous poly(aryleneethynylene) networks, Angew. Chem. Int. Ed. 119 (2007) 8728–8732, https://doi.org/10.1002/ange.200701595.
[60] N. Wan, Q. Chang, F. Hou, S. Zhang, X. Zang, X. Zhao, C. Wang, Z. Wang, Y. Yamauchi, Nanoarchitectured conjugated microporous polymers: State of the art synthetic strategies and opportunities for adsorption science, Chem. Mater. 34 (2022) 7598–7619, https://doi.org/10.1021/acs.chemmater.2c00999.
[61] L. Zhou, Y. Hu, G. Li, Conjugated microporous polymers with built-in magnetic nanoparticles for excellent enrichment of trace hydroxylated polycyclic aromatic hydrocarbons in human urine, Anal. Chem. 88 (2016) 6930–6938, https://doi.org/10.1021/acs.analchem.6b01708.
[62] G. Ji, Z. Yang, Y. Zhao, H. Zhang, B. Yu, J. Xu, H. Xu, Z. Liu, Synthesis of metalloporphyrin-based conjugated microporous polymer spheres directed by bipyridine-type ligands, Chem. Commun. 51 (2015) 7352–7355, https://doi.org/10.1039/c5cc00609k.
[63] P. Kuhn, M. Antonietti, A. Thomas, Microporous polymers porous, covalent Triazine-based frameworks prepared by Ionothermal synthesis, Angew. Chem. Int. Ed. 47 (2008) 3450–3453, https://doi.org/10.1002/anie.200705710.
[64] K. Yuan, C. Liu, L. Zong, G. Yu, S. Cheng, J. Wang, Z. Weng, X. Jian, Promoting and tuning porosity of flexible ether-linked Phthalazinone-based covalent Triazine frameworks utilizing substitution effect for effective CO_2 capture, ACS Appl. Mater. Interfaces 9 (2017) 13201–13212, https://doi.org/10.1021/acsami.7b01783.
[65] E. Troschke, S. Grätz, T. Lübken, L. Borchardt, Mechanochemical Friedel–Crafts Alkylation—A Sustainable Pathway Towards Porous Organic Polymers, Angew. Chem. Int. Ed. 56 (2017) 6859–6863, https://doi.org/10.1002/anie.201702303.
[66] R. Yuan, Z. Yan, A. Shaga, H. He, Solvent-free mechanochemical synthesis of a carbazole-based porous organic polymer with high CO_2 capture and separation, J. Solid State Chem. 287 (2020) 121327, https://doi.org/10.1016/j.jssc.2020.121327.
[67] Y. Peng, M. Huang, Y. Hu, G. Li, L. Xia, Microwave-assisted synthesis of porphyrin conjugated microporous polymers for microextraction of volatile organic acids in tobaccos, J. Chromatogr. A 1594 (2019) 45–53, https://doi.org/10.1016/j.chroma.2019.02.038.
[68] X. Cui, Y. Li, W. Dong, D. Liu, Q. Duan, Microwave-assisted synthesis of novel imine-linked copper porphyrin conjugated microporous polymers as heterogeneous photocatalysts, React. Funct. Polym. 154 (2020) 104633, https://doi.org/10.1016/j.reactfunctpolym.2020.104633.
[69] H. Liu, Y. Wang, W. Mo, H. Tang, Z. Cheng, Y. Chen, S. Zhang, H. Ma, B. Li, X. Li, Dendrimer-based, high-luminescence conjugated microporous polymer films for highly sensitive and selective volatile organic compound sensor arrays, Adv. Funct. Mater. 30 (2020) 1910275, https://doi.org/10.1002/adfm.201910275.
[70] H. Zhang, Y. Zhang, C. Gu, Y. Ma, Electropolymerized conjugated microporous poly(zinc-porphyrin) films as potential electrode materials in supercapacitors, Adv. Energy Mater. 5 (2015) 1402175, https://doi.org/10.1002/aenm.201402175.
[71] W. Zhang, H. Sun, Z. Zhu, R. Jiao, P. Mu, W. Liang, A. Li, N-doped hard carbon nanotubes derived from conjugated microporous polymer for electrocatalytic oxygen reduction reaction, Renew. Energy 146 (2020) 2270–2280, https://doi.org/10.1016/j.renene.2019.08.071.
[72] W. Ma, C. Zhang, X. Gao, C. Shu, C. Yan, F. Wang, Y. Chen, J.H. Zeng, J.X. Jiang, Structure evolution of azo-fused conjugated microporous polymers for high-performance lithium-ion batteries anodes, J. Power Sources 453 (2020) 227868, https://doi.org/10.1016/j.jpowsour.2020.227868.
[73] T. Geng, L. Ma, G. Chen, C. Zhang, W. Zhang, Q. Niu, Fluorescent conjugated microporous polymers containing pyrazine moieties for adsorbing and fluorescent sensing of iodine, Environ. Sci. Pollut. Res. 27 (2020) 20235–20245, https://doi.org/10.1007/s11356-019-06534-8.
[74] T. Geng, Z. Zhu, W. Zhang, Y. Wang, A nitrogen-rich fluorescent conjugated microporous polymer with triazine and triphenylamine units for high iodine capture and nitro aromatic compound detection, J. Mater. Chem. A Mater. 5 (2017) 7612–7617, https://doi.org/10.1039/c7ta00590c.
[75] Y. Liao, H. Wang, M. Zhu, A. Thomas, Efficient supercapacitor energy storage using conjugated microporous polymer networks synthesized from Buchwald–Hartwig coupling, Adv. Mater. 30 (2018) 1705710, https://doi.org/10.1002/adma.201705710.
[76] H. Li, W. Lyu, Y. Liao, Engineering redox activity in conjugated microporous Polytriphenylamine networks using Pyridyl building blocks toward efficient supercapacitors, Macromol. Rapid Commun. 40 (2019) 1900455, https://doi.org/10.1002/marc.201900455.
[77] S. Qiao, Z. Li, B. Zhang, Q. Li, W. Jin, Y. Zhang, W. Wang, Q. Li, X. Liu, Flexible chain & rigid skeleton complementation polycarbazole microporous system for gas storage, Micropor. Mesopor. Mater. 284 (2019) 205–211, https://doi.org/10.1016/j.micromeso.2019.03.042.
[78] H. Zhou, B. Zhao, C. Fu, Z. Wu, C. Wang, Y. Ding, B.H. Han, A. Hu, Synthesis of conjugated microporous polymers through cationic cyclization polymerization, Macromolecules 52 (2019) 3935–3941, https://doi.org/10.1021/acs.macromol.9b00437.
[79] C. Feng, G. Xu, W. Xie, S. Zhang, C. Yao, Y. Xu, Polytriazine porous networks for effective iodine capture, Polym. Chem. 11 (2020) 2786–2790, https://doi.org/10.1039/c9py01948k.
[80] Z. Tan, H. Su, Y. Guo, H. Liu, B. Liao, A.M. Amin, Q. Liu, Ferrocene-based conjugated microporous polymers derived from Yamamoto coupling for gas storage and dye removal, Polymers 12 (2020) 719, https://doi.org/10.3390/polym12030719.
[81] J. Zhu, C. Yang, C. Lu, F. Zhang, Z. Yuan, X. Zhuang, Two-dimensional porous polymers: From Sandwich-like structure to layered skeleton, Acc. Chem. Res. 51 (2018) 3191–3202, https://doi.org/10.1021/acs.accounts.8b00444.
[82] H. Lei, Y. Hu, G. Li, Magnetic poly(phenylene ethynylene) conjugated microporous polymer microspheres for bactericides enrichment and analysis by ultra-high performance liquid chromatography-tandem mass spectrometry, J. Chromatogr. A 1580 (2018) 22–29, https://doi.org/10.1016/j.chroma.2018.10.043.
[83] N. Wan, Q. Chang, F. Hou, J. Li, X. Zang, S. Zhang, C. Wang, Z. Wang, Efficient solid-phase microextraction of twelve halogens-containing environmental hormones from fruits and vegetables by triazine-based conjugated microporous polymer coating, Anal. Chim. Acta 1195 (2022) 339458, https://doi.org/10.1016/j.aca.2022.339458.
[84] K. Zhang, B. Tieke, F. Vilela, P.J. Skabara, Conjugated microporous networks on the basis of 2,3,5,6-tetraarylated diketopyrrolo[3,4-c]pyrrole, Macromol. Rapid Commun. 32 (2011) 825–830, https://doi.org/10.1002/marc.201100045.
[85] J. Kim, C.M. Moisanu, C.N. Gannett, A. Halder, J.J. Fuentes-Rivera, S.H. Majer, K. M. Lancaster, A.C. Forse, H.D. Abruña, P.J. Milner, Conjugated microporous polymers via solvent-free Ionothermal Cyclotrimerization of methyl ketones, Chem. Mater. 33 (2021) 8334–8342, https://doi.org/10.1021/acs.chemmater.1c02622.
[86] Z. Zhou, D. Guo, D.B. Shinde, L. Cao, Z. Li, X. Li, D. Lu, Z. Lai, Precise sub-angstrom ion separation using conjugated microporous polymer membranes, ACS Nano 15 (2021) 11970–11980, https://doi.org/10.1021/acsnano.1c03194.
[87] M. Xu, T. Wang, P. Gao, L. Zhao, L. Zhou, D. Hua, Highly fluorescent conjugated microporous polymers for concurrent adsorption and detection of uranium, J. Mater. Chem. A 7 (2019) 11214–11222, https://doi.org/10.1039/c8ta11764k.

[88] Y. Xu, A. Nagai, D. Jiang, Core–shell conjugated microporous polymers: A new strategy for exploring color-tunable and -controllable light emissions, Chem. Commun. 49 (2013) 1591–1593, https://doi.org/10.1039/c2cc38211c.

[89] M. Xu, X. Han, T. Wang, S. Li, D. Hua, Conjugated microporous polymers bearing phosphonate ligands as an efficient sorbent for potential uranium extraction from high-level liquid wastes, J. Mater. Chem. A 6 (2018) 13894–13900, https://doi.org/10.1039/c8ta02875c.

[90] J. Schmidt, M. Werner, A. Thomas, Conjugated microporous polymer networks via Yamamoto polymerization, Macromolecules 42 (2009) 4426–4429, https://doi.org/10.1021/ma9005473.

[91] K. Yuan, P.G. Wang, T. Hu, L. Shi, R. Zeng, M. Forster, T. Pichler, Y. Chen, U. Scherf, Nanofibrous and graphene-templated conjugated microporous polymer materials for flexible Chemosensors and supercapacitors, Chem. Mater. 27 (2015) 7403–7411, https://doi.org/10.1021/acs.chemmater.5b03290.

[92] L. Sun, Z. Liang, J. Yu, R. Xu, Luminescent microporous organic polymers containing the 1,3,5-tri(4-ethenylphenyl)benzene unit constructed by heck coupling reaction, Polym. Chem. 4 (2013) 1932–1938, https://doi.org/10.1039/c2py21034g.

[93] H. Bohra, P. Li, C. Yang, Y. Zhao, M. Wang, "Greener" and modular synthesis of triazine-based conjugated porous polymers via direct arylation polymerization: Structure–function relationship and photocatalytic application, Polym. Chem. 9 (2018) 1972–1982, https://doi.org/10.1039/c8py00025e.

[94] J.J. Chen, T.L. Zhai, Y.F. Chen, S. Geng, C. Yu, J.M. Liu, L. Wang, B. Tan, C. Zhang, A triptycene-based two-dimensional porous organic polymeric nanosheet, Polym. Chem. 8 (2017) 5533–5538, https://doi.org/10.1039/c7py01122a.

[95] Z. Xie, Y. Wei, X. Zhao, Y. Li, S. Ding, L. Chen, Facile construction of butadiynylene-based conjugated porous polymers by cost-effective Glaser coupling, Mater. Chem. Front. 1 (2017) 867–872, https://doi.org/10.1039/c6qm00190d.

[96] Y. Liu, Z. Liao, X. Ma, Z. Xiang, Ultrastable and efficient visible-light-driven hydrogen production based on donor-acceptor copolymerized covalent organic polymer, ACS Appl. Mater. Interfaces 10 (2018) 30698–30705, https://doi.org/10.1021/acsami.8b10022.

[97] Y. Guo, R. Ma, W. Liu, L. Hao, Q. Wu, Z. Wang, Facile synthesis of conjugated microporous polymer with spherical structure for solid phase extraction of phenyl urea herbicides, J. Chromatogr. A 1622 (2020) 461131, https://doi.org/10.1016/j.chroma.2020.461131.

[98] Y. Liao, Z. Cheng, W. Zuo, A. Thomas, C.F.J. Faul, Nitrogen-rich conjugated microporous polymers: Facile synthesis, efficient gas storage, and heterogeneous catalysis, ACS Appl. Mater. Interfaces 9 (2017) 38390–38400, https://doi.org/10.1021/acsami.7b09553.

[99] X. Ding, B.H. Han, Metallophthalocyanine-based conjugated microporous polymers as highly efficient photosensitizers for singlet oxygen generation, Angew. Chem. Int. Ed. 54 (2015) 6536–6539, https://doi.org/10.1002/anie.201501732.

[100] X. Zhuang, W. Zhao, F. Zhang, Y. Cao, F. Liu, S. Bi, X. Feng, A two-dimensional conjugated polymer framework with fully sp^2-bonded carbon skeleton, Polym. Chem. 7 (2016) 4176–4181, https://doi.org/10.1039/c6py00561f.

[101] H. Lyu, C.S. Diercks, C. Zhu, O.M. Yaghi, Porous crystalline olefin-linked covalent organic frameworks, J. Am. Chem. Soc. 141 (2019) 6848–6852, https://doi.org/10.1021/jacs.9B02848.

[102] J. Chen, W. Yan, E.J. Townsend, J. Feng, L. Pan, V.D.A. Hernandez, C.F.J. Faul, Tunable surface area, porosity, and function in conjugated microporous polymers, Angew. Chem. Int. Ed. 58 (2019) 11715–11719, https://doi.org/10.1002/anie.201905488.

[103] L. Pan, Z. Liu, M. Tian, B.C. Schroeder, A.E. Aliev, C.F.J. Faul, Luminescent and Swellable conjugated microporous polymers for detecting Nitroaromatic explosives and removing harmful organic vapors, ACS Appl. Mater. Interfaces 11 (2019) 48352–48362, https://doi.org/10.1021/acsami.9b16767.

[104] T. Geng, W. Zhang, Z. Zhu, X. Kai, Triazine-based conjugated microporous polymers constructing triphenylamine and its derivatives with nitrogen as core for iodine adsorption and fluorescence sensing I_2, Microporous and Mesoporous Mater. 273 (2019) 163–170, https://doi.org/10.1016/j.micromeso.2018.07.004.

[105] L. Hu, S. Gu, W. Yu, W. Zhang, Q. Xie, C. Pan, J. Tang, G. Yu, Facile preparation of CoO nanoparticles embedded N-doped porous carbon from conjugated microporous polymer for oxygen reduction reaction, J. Colloid Interface Sci. 562 (2020) 550–557, https://doi.org/10.1016/j.jcis.2019.11.079.

[106] R. Dawson, F. Su, H. Niu, C.D. Wood, J.T.A. Jones, Y.Z. Khimyak, A.I. Cooper, Mesoporous poly(phenylenevinylene) networks, Macromolecules 41 (2008) 1591–1593, https://doi.org/10.1021/ma702411b.

[107] A.B. Marco, D.C. Lacalle, I.P. Miqueo, G. Valenti, A. Boni, J. Plas, K. Strutyński, S. D. Feyter, F. Paolucci, M. Montes, A.N. Khlobystov, M.M. Franco, A.M. Alonso, Twisted aromatic frameworks: Readily Exfoliable and solution-Processable two-dimensional conjugated microporous polymers, Angew. Chem. Int. Ed. 129 (2017) 7050–7055, https://doi.org/10.1002/ange.201700271.

[108] Y. He, Z. Cheng, H. Zuo, C. Yan, Y. Liao, Green synthesis of Pyridyl conjugated microporous polymers as precursors for porous carbon microspheres for efficient electrochemical energy storage, ChemElectroChem 7 (2020) 959–966, https://doi.org/10.1002/celc.201901975.

[109] N. Baig, S. Shetty, S. Al-Mousawi, B. Alameddine, Conjugated microporous polymers using a copper-catalyzed [4+2] cyclobenzannulation reaction: Promising materials for iodine and dye adsorption, Polym. Chem. 12 (2021) 2282–2292, https://doi.org/10.1039/d1py00193k.

[110] B.F. Hoskins, R. Robson, Design and construction of a new class of scaffolding-like materials comprising infinite polymeric frameworks of 3D-linked molecular rods. A reappraisal of the $Zn(CN)_2$ and $cd(CN)_2$ structures and the synthesis and structure of the diamond-related frameworks $[N(CH_3)_4][CuIZnII(CN)_4]$ and CuI [4,4',4'',4'''-tetracyanotetraphenylmethane]$BF_4{\cdot}xC_6H_5NO_2$, J. Am. Chem. Soc. 112 (1990) 1546–1554, https://doi.org/10.1021/ja00160a038.

[111] Z. Wang, S.M. Cohen, Postsynthetic covalent modification of a neutral metal-organic framework, J. Am. Chem. Soc. 129 (2007) 12368–12369, https://doi.org/10.1021/ja074366o.

[112] Y.Y. Cui, C.X. Yang, X.P. Yan, Thiol-yne click post-modification for the synthesis of chiral microporous organic networks for chiral gas chromatography, ACS Appl. Mater. Interfaces 12 (2020) 4954–4961, https://doi.org/10.1021/acsami.9b22023.

[113] Y. Zhang, S.N. Riduan, Functional porous organic polymers for heterogeneous catalysis, Chem. Soc. Rev. 41 (2012) 2083–2094, https://doi.org/10.1039/c1cs15227k.

[114] J.L. Segura, S. Royuela, M.M. Ramos, Post-synthetic modification of covalent organic frameworks, Chem. Soc. Rev. 48 (2019) 3903–3945, https://doi.org/10.1039/c8cs00978c.

[115] L. Chen, Y. Yang, D. Jiang, CMPs as scaffolds for constructing porous catalytic frameworks: A built-in heterogeneous catalyst with high activity and selectivity based on nanoporous metalloporphyrin polymers, J. Am. Chem. Soc. 132 (2010) 9138–9143, https://doi.org/10.1021/ja1028556.

[116] J.X. Jiang, C. Wang, A. Laybourn, T. Hasell, R. Clowes, Y.Z. Khimyak, J. Xiao, S. J. Higgins, D.J. Adams, A.I. Cooper, Metal-organic conjugated microporous polymers, Angew. Chem. Int. Ed. 123 (2011) 1104–1107, https://doi.org/10.1002/ange.201005864.

[117] Y. Song, P.C. Lan, K. Martin, S. Ma, Rational design of bifunctional conjugated microporous polymers, Nanoscale Adv. 3 (2021) 4891–4906, https://doi.org/10.1039/d1na00479d.

[118] A. Nagai, Z. Guo, X. Feng, S. Jin, X. Chen, X. Ding, D. Jiang, Pore surface engineering in covalent organic frameworks, Nat. Commun. 2 (2011) 1–8, https://doi.org/10.1038/ncomms1542.

[119] H. Xu, J. Gao, D. Jiang, Stable, crystalline, porous, covalent organic frameworks as a platform for chiral organocatalysts, Nat. Chem. 7 (2015) 905–912, https://doi.org/10.1038/nchem.2352.

[120] Q. Sun, B. Aguila, J. Perman, L.D. Earl, C.W. Abney, Y. Cheng, H. Wei, N. Nguyen, L. Wojtas, S. Ma, Postsynthetically modified covalent organic frameworks for efficient and effective mercury removal, J. Am. Chem. Soc. 139 (2017) 2786–2793, https://doi.org/10.1021/jacs.6b12885.

[121] B. Kiskan, J. Weber, Versatile postmodification of conjugated microporous polymers using thiol-yne chemistry, ACS Macro Lett. 1 (2012) 37–40, https://doi.org/10.1021/mz200060z.

[122] X. Wang, X. Zhao, W. Dong, X. Zhang, Y. Xiang, Q. Huang, H. Chen, Integrating amino groups within conjugated microporous polymers by versatile thiol–yne coupling for light-driven hydrogen evolution, J. Mater. Chem. A 7 (2019) 16277–16284, https://doi.org/10.1039/c9ta04018h.

[123] T. Ratvijitvech, R. Dawson, A. Laybourn, Y.Z. Khimyak, D.J. Adams, A.I. Cooper, Post-synthetic modification of conjugated microporous polymers, Polymer 55 (2014) 321–325, https://doi.org/10.1016/j.polymer.2013.06.004.

[124] D. Cui, C. Yao, Y. Xu, R. Li, Conjugated microporous polymers with azide groups: A new strategy for postsynthetic fluoride functionalization and effectively enhanced CO_2 adsorption properties, Chem. Commun. 53 (2017) 11422–11425, https://doi.org/10.1039/c7cc06528k.

[125] L. Zhang, N. Pu, B. Yu, G. Ye, J. Chen, S. Xu, S. Ma, Skeleton engineering of Homocoupled conjugated microporous polymers for highly efficient uranium capture via synergistic coordination, ACS Appl. Mater. Interfaces 12 (2020) 3688–3696, https://doi.org/10.1021/acsami.9b20944.

[126] S.P.S. Badwal, S.S. Giddey, C. Munnings, A.I. Bhatt, A.F. Hollenkamp, Emerging electrochemical energy conversion and storage technologies, Front. Chem. 2 (2014) 97517, https://doi.org/10.3389/fchem.2014.00079.

[127] R. Kumar, S. Sahoo, E. Joanni, R.K. Singh, A review on the current research on microwave processing techniques applied to graphene-based supercapacitor electrodes: An emerging approach beyond conventional heating, J. Energy Chem. 74 (2022) 252–282, https://doi.org/10.1016/j.jechem.2022.06.051.

[128] F. Bonaccorso, L. Colombo, G. Yu, M. Stoller, V. Tozzini, A.C. Ferrari, R.S. Ruoff, V. Pellegrini, Graphene, related two-dimensional crystals, and hybrid systems for energy conversion and storage, Science 347 (2015), https://doi.org/10.1126/science.1246501.

[129] V.D. Nithya, A review on holey graphene electrode for supercapacitor, J. Energy Storage 44 (2021) 103380, https://doi.org/10.1016/j.est.2021.103380.

[130] R. Kumar, S. Sahoo, E. Joanni, R.K. Singh, K.K. Kar, Microwave as a tool for synthesis of carbon-based electrodes for energy storage, ACS Appl. Mater. Interfaces 14 (2022) 20306–20325, https://doi.org/10.1021/acsami.1c15934.

[131] R. Kumar, S. Sahoo, E. Joanni, R.K. Singh, K. Maegawa, W.K. Tan, G. Kawamura, K.K. Kar, A. Matsuda, Heteroatom doped graphene engineering for energy storage and conversion, Mater. Today 39 (2020) 47–65, https://doi.org/10.1016/j.mattod.2020.04.010.

[132] R. Kumar, S. Sahoo, E. Joanni, R.K. Singh, W.K. Tan, K.K. Kar, A. Matsuda, Recent progress in the synthesis of graphene and derived materials for next generation electrodes of high-performance lithium ion batteries, Prog. Energy Combust. Sci. 75 (2019) 100786, https://doi.org/10.1016/j.pecs.2019.100786.

[133] R. Kumar, S. Sahoo, E. Joanni, R.K. Singh, R.M. Yadav, Graphene-metal oxide hybrid materials with 2D and 3D morphologies for advanced supercapacitor electrodes: Status, challenges and prospects, Mater. Today Nano 24 (2023) 100399, https://doi.org/10.1016/j.mtnano.2023.100399.

[134] R. Kumar, S. Sahoo, E. Joanni, R.K. Singh, R.M. Yadav, R.K. Verma, D.P. Singh, W. K. Tan, A. Pérez del Pino, S.A. Moshkalev, A. Matsuda, A review on synthesis of

graphene, h-BN and MoS_2 for energy storage applications: Recent progress and perspectives, Nano Res. 12 (2019) 2655–2694, https://doi.org/10.1007/s12274-019-2467-8.
[135] J. Xu, K. Wang, S.Z. Zu, B.H. Han, Z. Wei, Hierarchical nanocomposites of polyaniline nanowire arrays on graphene oxide sheets with synergistic effect for energy storage, ACS Nano 4 (2010) 5019–5026, https://doi.org/10.1021/nn1006539.
[136] C. Xiong, B. Li, X. Lin, H. Liu, Y. Xu, J. Mao, C. Duan, T. Li, Y. Ni, The recent progress on three-dimensional porous graphene-based hybrid structure for supercapacitor, Compos. Part B Eng. 165 (2019) 10–46, https://doi.org/10.1016/j.compositesb.2018.11.085.
[137] C. Zhang, J. Zeng, C. Xu, T. Gao, X. Wang, Electric double layer capacitors based on porous three-dimensional graphene materials for energy storage, J. Electron. Mater. 50 (2021) 3043, https://doi.org/10.1007/s11664-021-08812-z.
[138] D.P. Chatterjee, A.K. Nandi, A review on the recent advances in hybrid supercapacitors, J. Mater. Chem. A 9 (2021) 15880–15918, https://doi.org/10.1039/d1ta02505h.
[139] N.H.N. Azman, M.S. Mamat @ Mat Nazir, L.H. Ngee, Y. Sulaiman, Graphene-based ternary composites for supercapacitors, Int. J. Energy Res. 42 (2018) 2104–2116, https://doi.org/10.1002/er.4001.
[140] K. Ramadass, K.S. Lakhi, C.I. Sathish, A.M. Ruban, R. Bahadur, G. Singh, H. S. Gujral, M. Al-Abri, A.H. Al-Muhtaseb, E. Tavakkoli, J. Yi, A. Karakoti, A. Vinu, Copper nanoparticles decorated N-doped mesoporous carbon with bimodal pores for selective gas separation and energy storage applications, Chem. Eng. J. 431 (2022) 134056, https://doi.org/10.1016/j.cej.2021.134056.
[141] R. Lakra, R. Kumar, P.K. Sahoo, D. Thatoi, A. Soam, A mini-review: Graphen based composites for supercapacitor application, Inorg. Chem. Commun. 133 (2021) 108929, https://doi.org/10.1016/j.inoche.2021.108929.
[142] R. Kumar, R.K. Singh, A.R. Vaz, S.A. Moshkalev, Microwave-assisted synthesis and deposition of a thin ZnO layer on microwave-exfoliated graphene: Optical and electrochemical evaluations, RSC Adv. 5 (2015) 67988–67995, https://doi.org/10.1039/c5ra09936f.
[143] R. Kumar, R.K. Singh, P. Kumar Dubey, D.P. Singh, R.M. Yadav, R.S. Tiwari, Hydrothermal synthesis of a uniformly dispersed hybrid graphene–TiO_2 nanostructure for optical and enhanced electrochemical applications, RSC Adv. 5 (2014) 7112–7120, https://doi.org/10.1039/c4ra06852a.
[144] K. Ramadass, C.I. Sathish, G. Singh, S.M. Ruban, A.M. Ruban, R. Bahadur, G. Kothandam, T. Belperio, J. Marsh, A. Karakoti, J. Yi, A. Vinu, Morphologically tunable nanoarchitectonics of mixed kaolin-halloysite derived nitrogen-doped activated nanoporous carbons for supercapacitor and CO_2 capture applications, Carbon 192 (2022) 133–144, https://doi.org/10.1016/j.carbon.2022.02.047.
[145] R. Kumar, S.M. Youssry, M.M. Abdel-Galeil, A. Matsuda, One-pot synthesis of reduced graphene oxide nanosheets anchored ZnO nanoparticles via microwave approach for electrochemical performance as supercapacitor electrode, J. Mater. Sci. Mater. Electron. 31 (2020) 15456–15465, https://doi.org/10.1007/s10854-020-04108-w.
[146] R. Kumar, S.M. Youssry, E. Joanni, S. Sahoo, G. Kawamura, A. Matsuda, Microwave-assisted synthesis of iron oxide homogeneously dispersed on reduced graphene oxide for high-performance supercapacitor electrodes, J. Energy Storage 56 (2022) 105896, https://doi.org/10.1016/j.est.2022.105896.
[147] L.L. Zhang, R. Zhou, X.S. Zhao, Graphene-based materials as supercapacitor electrodes, J. Mater. Chem. 20 (2010) 5983–5992, https://doi.org/10.1039/c000417k.
[148] S. Vadahanambi, J.H. Jung, R. Kumar, H.J. Kim, I.K. Oh, An ionic liquid-assisted method for splitting carbon nanotubes to produce graphene nano-ribbons by microwave radiation, Carbon 53 (2013) 391–398, https://doi.org/10.1016/j.carbon.2012.11.029.
[149] S.K. Tiwari, S. Sahoo, N. Wang, A. Huczko, Graphene research and their outputs: Status and prospect, J. Sci. Adv. Mater. Device 5 (2020) 10–29, https://doi.org/10.1016/j.jsamd.2020.01.006.
[150] Y. Ma, J. Liu, Y. Lin, Y. Jia, Recent advances in hierarchical MoS_2/graphene-based materials for supercapacitor applications, Phys. Chem. Chem. Phys. 25 (2023) 8263–8280, https://doi.org/10.1039/d2cp05685b.
[151] V. Babaahmadi, S.E.M. Pourhosseini, O. Norouzi, H.R. Naderi, Designing 3D ternary hybrid composites composed of graphene, Biochar and Manganese Dioxide as High-Performance Supercapacitor Electrodes, Nanomaterials 13 (2023) 1866, https://doi.org/10.3390/nano13121866.
[152] G. Kothandam, G. Singh, X. Guan, J.M. Lee, K. Ramadass, S. Joseph, M. Benzigar, A. Karakoti, J. Yi, P. Kumar, A. Vinu, Recent advances in carbon-based electrodes for energy storage and conversion, Adv. Sci. 10 (2023) 2301045, https://doi.org/10.1002/advs.202301045.
[153] O.S. Adedoja, E.R. Sadiku, Y. Hamam, An overview of the emerging technologies and composite materials for supercapacitors in energy storage applications, Polymers 15 (2023) 2272, https://doi.org/10.3390/polym15102272.
[154] M.G. Kotp, M. Gamal Mohamed, S.W. Kuo, M.G. Mohamed, Conjugated microporous polymer electrodes for supercapacitors: Recent progress, key challenges, and future directions, Chem. Sci. 16 (2025) 20718–20754, https://doi.org/10.1039/d5sc05384f.
[155] C. Largeot, C. Portet, J. Chmiola, P.L. Taberna, Y. Gogotsi, P. Simon, Relation between the ion size and pore size for an electric double-layer capacitor, J. Am. Chem. Soc. 130 (2008) 2730–2731, https://doi.org/10.1021/ja7106178.
[156] T.A. Gaber, L.R. Ahmed, A.F.M. EL-Mahdy, Efficient faradaic supercapacitor energy storage using redox-active pyrene- and benzodithiophene-4,8-dione-tethered conjugated microporous polymers, J. Mater. Chem. A 11 (2023) 19408–19417, https://doi.org/10.1039/d3ta03198e.
[157] S.X. Liao, A.F.M. EL-Mahdy, Redox-active conjugated microporous polymers featuring a precise pore size for high-performance supercapacitor energy storage, ACS Appl. Energy Mater. 8 (2025) 3074–3086, https://doi.org/10.1021/acsaem.4c03232.
[158] S.K. Yadav, R. Kumar, A.K. Sundramoorthy, R.K. Singh, C.M. Koo, Simultaneous reduction and covalent grafting of polythiophene on graphene oxide sheets for excellent capacitance retention, RSC Adv. 6 (2016) 52945–52949, https://doi.org/10.1039/c6ra07904k.
[159] X. Yang, A.L. Rogach, X. Yang, A.L. Rogach, Electrochemical techniques in battery research: A tutorial for nonelectrochemists, Adv. Energy Mater. 9 (2019) 1900747, https://doi.org/10.1002/aenm.201900747.
[160] B. Hsia, Materials Synthesis and Characterization for Micro-supercapacitor Applications, (2013) 3616556.
[161] N. Elgrishi, K.J. Rountree, B.D. McCarthy, E.S. Rountree, T.T. Eisenhart, J. L. Dempsey, A practical beginner's guide to cyclic voltammetry, J. Chem. Educ. 95 (2018) 197–206, https://doi.org/10.1021/acs.jchemed.7b00361.
[162] M.D. Stoller, R.S. Ruoff, Best practice methods for determining an electrode material's performance for ultracapacitors, Energy Environ. Sci. 3 (2010) 1294–1301, https://doi.org/10.1039/c0ee00074d.
[163] E. Frackowiak, F. Béguin, Carbon materials for the electrochemical storage of energy in capacitors, Carbon 39 (2001) 937–950, https://doi.org/10.1016/s0008-6223(00)00183-4.
[164] E. Frackowiak, K. Metenier, V. Bertagna, F. Beguin, Supercapacitor electrodes from multiwalled carbon nanotubes, Appl. Phys. Lett. 77 (2000) 2421–2423, https://doi.org/10.1063/1.1290146.
[165] Y. Gogotsi, P. Simon, True performance metrics in electrochemical energy storage, Science 334 (2011) 917–918, https://doi.org/10.1126/science.1213003.
[166] Y. Zhai, Y. Dou, D. Zhao, P.F. Fulvio, R.T. Mayes, S. Dai, Carbon materials for chemical capacitive energy storage, Adv. Mater. 23 (2011) 4828–4850, https://doi.org/10.1002/adma.201100984.
[167] G. Wang, L. Zhang, J. Zhang, A review of electrode materials for electrochemical supercapacitors, Chem. Soc. Rev. 41 (2012) 797–828, https://doi.org/10.1039/c1cs15060j.
[168] P. Simon, Y. Gogotsi, Materials for electrochemical capacitors, Nat. Mater. 7 (2008) 845–854, https://doi.org/10.1038/nmat2297.
[169] A. Patra, K. Namsheer, J.R. Jose, S. Sahoo, B. Chakraborty, C.S. Rout, Understanding the charge storage mechanism of supercapacitors: In situ/operando spectroscopic approaches and theoretical investigations, J. Mater. Chem. A 9 (2021) 25852–25891, https://doi.org/10.1039/d1ta07401f.
[170] B. Dunn, H. Kamath, J.M. Tarascon, Electrical energy storage for the grid: A battery of choices, Science 334 (2011) 928–935, https://doi.org/10.1126/science.1212741.
[171] V. Augustyn, P. Simon, B. Dunn, Pseudocapacitive oxide materials for high-rate electrochemical energy storage, Energy Environ. Sci. 7 (2014) 1597–1614, https://doi.org/10.1039/c3ee44164d.
[172] X.C. Li, Y. Zhang, C.Y. Wang, Y. Wan, W.Y. Lai, H. Pang, W. Huang, Redox-active triazatruxene-based conjugated microporous polymers for high-performance supercapacitors, Chem. Sci. 8 (2017) 2959–2965, https://doi.org/10.1039/c6sc05532j.
[173] K. Yuan, T. Hu, Y. Xu, R. Graf, L. Shi, M. Forster, T. Pichler, T. Riedl, Y. Chen, U. Scherf, Nitrogen-doped porous carbon/graphene nanosheets derived from two-dimensional conjugated microporous polymer sandwiches with promising capacitive performance, Mater. Chem. Front. 1 (2017) 278–285, https://doi.org/10.1039/c6qm00012f.
[174] N.M.T. Tran, V. Lazeran, J.S. Pena, N. Berton, Cross-linked electrodeposited conjugated polymers based on bis-thiophene-carbazole bis-adducts with an aromatic core for high performance supercapacitor electrodes, J. Mater. Chem. A 13 (2025) 24933–24947, https://doi.org/10.1039/d5ta01820j.
[175] Y. Li, S. Zheng, X. Liu, P. Li, L. Sun, R. Yang, S. Wang, Z.S. Wu, X. Bao, W.Q. Deng, Conductive microporous covalent Triazine-based framework for high-performance electrochemical capacitive energy storage, Angew. Chem. Int. Ed. 130 (2018) 8124–8128, https://doi.org/10.1002/ange.201711169.
[176] M. Zhang, T. Zhao, J. Dou, Z. Xu, W. Zhang, X. Chen, X. Wang, B. Zhou, Bottom-up construction of conjugated microporous Polyporphyrin-coated graphene hydrogel composites with hierarchical pores for high-performance capacitors, ChemElectroChem 6 (2019) 5946–5950, https://doi.org/10.1002/celc.201901586.
[177] M.G. Kotp, J. Luder, S.W. Kuo, A.F.M. El-Mahdy, Phenazine-integrated conjugated microporous polymers for modulating the mechanics of supercapacitor electrodes, Mater. Adv. 5 (2024) 4142–4150, https://doi.org/10.1039/d3ma00979c.
[178] M.M. Samy, M.G. Mohamed, S.U. Sharma, S.V. Chaganti, J.T. Lee, S.W. Kuo, An Ultrastable Tetrabenzonaphthalene-linked conjugated microporous polymer functioning as a high-performance electrode for supercapacitors, J. Taiwan Inst. Chem. Eng. 158 (2024) 104750, https://doi.org/10.1016/j.jtice.2023.104750.
[179] M.G. Mohamed, B. Halder, P.N. Singh, A.A.K. Mohammed, P. Elumalai, S.W. Kuo, Molecular engineering and synergistic redox-active hexaazatrinaphthalene and pyrene-based conjugated microporous polymers for superior faradaic supercapacitor energy storage, Chem. Eng. J. 520 (2025) 165892, https://doi.org/10.1016/j.cej.2025.165892.
[180] S. Bandyopadhyay, C. Singh, P. Jash, M.W. Hussain, A. Paul, A. Patra, Redox-active, pyrene-based pristine porous organic polymers for efficient energy storage with exceptional cyclic stability, Chem. Commun. 54 (2018) 6796–6799, https://doi.org/10.1039/c8cc02477d.
[181] S. Abdelnaser, S.W. Kuo, A.F.M. EL-Mahdy, Conjugated microporous polymers incorporating pyridine moieties for efficient faradaic supercapacitor energy

storage, J. Power Sources 635 (2025) 236535, https://doi.org/10.1016/j.jpowsour.2025.236535.
[182] J. Zhan, A.F.M. EL-Mahdy, Redox-active Benzodithiophene-4,8-dione-based conjugated microporous polymers for high-performance faradaic supercapacitor energy storage, Chem. Eng. J. 473 (2023) 145124, https://doi.org/10.1016/j.cej.2023.145124.
[183] A.C. Lim, H.S. Jadhav, J.G. Seo, Electron transport shuttle mechanism via an Fe–N–C bond derived from a conjugated microporous polymer for a supercapacitor, Dalton Trans. 47 (2018) 852–858, https://doi.org/10.1039/c7dt04094f.
[184] L. Mei, J.C. Wei, Q. Duan, Construction of copper porphyrin-linked conjugated microporous polymer/carbon nanotube composite as flexible electrodes for supercapacitors, J. Mater. Sci. Mater. Electron. 32 (2021) 24953–24963, https://doi.org/10.1007/s10854-021-06952-w.
[185] M. Jang, Y. Cho, Y. Kim, M. Hahn, D. Jung, S.Y. Park, W. Lee, Y. Piao, Redox-active conjugated microporous anthraquinonylamine-based polymer network grafted with activated graphene toward high-performance flexible asymmetric supercapacitor electrodes, Electrochim. Acta 434 (2022) 141315, https://doi.org/10.1016/j.electacta.2022.141315.
[186] L. Peng, Q. Guo, Z. Ai, Y. Zhao, Y. Liu, D. Wei, Nitrogen doped carbons derived from graphene aerogel templated triazine-based conjugated microporous polymers for high-performance supercapacitors, Front. Chem. 7 (2019) 438792, https://doi.org/10.3389/fchem.2019.00142.
[187] H. Wang, L. Liang, L. Duan, S. Sun, X. Cheng, Fabrication of MWNT@CMPs and carbonized MWNT@CMPs for supercapacitors, Mater. Chem. Phys. 226 (2019) 309–317, https://doi.org/10.1016/j.matchemphys.2019.01.036.
[188] X. Zhang, L. Teng, J. Chen, X. Gong, H. Liu, J. Duan, L. Jiang, X. Hou, W. Lyu, Y. Liao, Conjugated microporous polymers via a one-pot Buchwald-Hartwig/Suzuki-Miyaura double-coupling for high-performance flexible supercapacitors, J. Colloid Interface Sci. 701 (2026) 138671, https://doi.org/10.1016/j.jcis.2025.138671.
[189] B. Luo, Y. Chen, Y. Zhang, J. Huo, Nitrogen-rich anthraquinone–triazine conjugated microporous polymer networks as high-performance supercapacitor, New J. Chem. 45 (2021) 17278–17286, https://doi.org/10.1039/d1nj03180e.
[190] A.F. Saber, A.F.M. EL-Mahdy, S.W. Kuo, Development of heteroatom-rich fluorene-based benzoxazine-linked porous organic polymers as potential candidates for energy storage, J. Taiwan Inst. Chem. Eng. 168 (2025) 105935, https://doi.org/10.1016/j.jtice.2024.105935.
[191] J. Choi, J.H. Ko, C.W. Kang, S.M. Lee, H.J. Kim, Y.J. Ko, M. Yang, S.U. Son, Enhanced redox activity of a hollow conjugated microporous polymer through the generation of carbonyl groups by carbonylative Sonogashira coupling, J. Mater. Chem. A 6 (2018) 6233–6237, https://doi.org/10.1039/c8ta01379a.
[192] A.M. Khattak, H. Sin, Z.A. Ghazi, X. He, B. Liang, N.A. Khan, H.R. Alanagh, A. Iqbal, L. Li, Z. Tang, Controllable fabrication of redox-active conjugated microporous polymers on reduced graphene oxide for high performance faradaic energy storage, J. Mater. Chem. A 6 (2018) 18827–18832, https://doi.org/10.1039/c8ta07913g.
[193] W. Liu, M. Ulaganathan, I. Abdelwahab, X. Luo, Z. Chen, S.J.R. Tan, X. Wang, Y. Liu, D. Geng, Y. Bao, J. Chen, K.P. Loh, Two-dimensional polymer synthesized via solid-state polymerization for high-performance supercapacitors, ACS Nano 12 (2018) 852–860, https://doi.org/10.1021/acsnano.7b08354.
[194] Y. Chen, H. Li, M. Tang, S. Zhuo, Y. Wu, E. Wang, S. Wang, C. Wang, W. Hu, Capacitive conjugated ladder polymers for fast-charge and -discharge sodium-ion batteries and hybrid supercapacitors, J. Mater. Chem. A 7 (2019) 20891–20898, https://doi.org/10.1039/c9ta07546a.
[195] Y. Kou, Y. Xu, Z. Guo, D. Jiang, Supercapacitive energy storage and electric power supply using an Aza-fused π-conjugated microporous framework, Angew. Chem. Int. Ed. 50 (2011) 8753–8757, https://doi.org/10.1002/anie.201103493.
[196] S. Chandra, D. Roy Chowdhury, M. Addicoat, T. Heine, A. Paul, R. Banerjee, Molecular level control of the capacitance of two-dimensional covalent organic frameworks: Role of hydrogen bonding in energy storage materials, Chem. Mater. 29 (2017) 2074–2080, https://doi.org/10.1021/acs.chemmater.6b04178.
[197] P. Bhanja, S.K. Das, K. Bhunia, D. Pradhan, T. Hayashi, Y. Hijikata, S. Irle, A. Bhaumik, A new porous polymer for highly efficient capacitive energy storage, ACS Sustain. Chem. Eng. 6 (2018) 202–209, https://doi.org/10.1021/acssuschemeng.7b02234.
[198] D.P. Dubal, N.R. Chodankar, D.H. Kim, P. Gomez-Romero, Towards flexible solid-state supercapacitors for smart and wearable electronics, Chem. Soc. Rev. 47 (2018) 2065–2129, https://doi.org/10.1039/c7cs00505a.
[199] L. Wang, X. Fu, J. He, X. Shi, T. Chen, P. Chen, B. Wang, H. Peng, Application challenges in Fiber and textile electronics, Adv. Mater. 32 (2020) 1901971, https://doi.org/10.1002/adma.201901971.
[200] Y. Li, X. Yan, X. Zheng, H. Si, M. Li, Y. Liu, Y. Sun, Y. Jiang, Y. Zhang, Fiber-shaped asymmetric supercapacitors with ultrahigh energy density for flexible/wearable energy storage, J. Mater. Chem. A 4 (2016) 17704–17710, https://doi.org/10.1039/c6ta07163e.
[201] Z. Pan, J. Yang, Q. Zhang, M. Liu, Y. Hu, Z. Kou, N. Liu, X. Yang, X. Ding, H. Chen, J. Li, K. Zhang, Y. Qiu, Q. Li, J. Wang, Y. Zhang, All-solid-state Fiber supercapacitors with ultrahigh volumetric energy density and outstanding flexibility, Adv. Energy Mater. 9 (2019) 1802753, https://doi.org/10.1002/aenm.201802753.
[202] Y. Zhou, Q. Wei, L. Xiao, C. Meng, Q. Yin, S. Song, Y. He, R. Qiang, Y. Yang, Z. Li, Z. Hu, Quinone-enriched polymer with a large π-conjugated structure for high-energy supercapacitors: Synthesis and electrochemical assessment, Energy Fuel 38 (2024) 7399–7411, https://doi.org/10.1021/acs.energyfuels.4c00778.
[203] X. Liu, G. Sun, Y. Gong, C.F. Liu, S. Wang, S. Xu, X. Yang, L. Yang, W.Y. Lai, Redox-active conjugated microporous polymers as electron-accepting organic pseudocapacitor electrode materials for flexible energy storage, Sci. China Chem. 65 (2022) 1767–1774, https://doi.org/10.1007/s11426-022-1320-3.
[204] Y. Dai, Y. Wang, H. Xu, X. Li, X. Yan, X. Xu, Structure, morphology and energy storage properties of imide conjugated microporous polymers with different cores and the corresponding composites with CNT, Electrochim. Acta 441 (2023) 141820, https://doi.org/10.1016/j.electacta.2023.141820.
[205] W. Lyu, W. Zhang, H. Liu, Y. Liu, H. Zuo, C. Yan, C.F.J. Faul, A. Thomas, M. Zhu, Y. Liao, Conjugated microporous polymer network grafted carbon nanotube fibers with tunable redox activity for efficient flexible wearable energy storage, Chem. Mater. 32 (2020) 8276–8285, https://doi.org/10.1021/acs.chemmater.0c02089.
[206] M. Khalid, H. Varela, A general potentiodynamic approach for red phosphorus and sulfur nanodot incorporation on reduced graphene oxide sheets: Metal-free and binder-free electrodes for supercapacitor and hydrogen evolution activities, J. Mater. Chem. A 6 (2018) 3141–3150, https://doi.org/10.1039/c7ta11342k.
[207] J. Cao, Y. Zhao, Y. Xu, Y. Zhang, B. Zhang, H. Peng, Sticky-note supercapacitors, J. Mater. Chem. A 6 (2018) 3355–3360, https://doi.org/10.1039/c7ta10756k.
[208] X. Zhuang, F. Zhang, D. Wu, X. Feng, Graphene coupled schiff-base porous polymers: Towards nitrogen-enriched porous carbon nanosheets with ultrahigh electrochemical capacity, Adv. Mater. 26 (2014) 3081–3086, https://doi.org/10.1002/adma.201305040.
[209] Z.S. Wu, Y. Zheng, S. Zheng, S. Wang, C. Sun, K. Parvez, T. Ikeda, X. Bao, K. Mullen, X. Feng, Stacked-layer Heterostructure films of 2D Thiophene Nanosheets and graphene for high-rate all-solid-state Pseudocapacitors with enhanced volumetric capacitance, Adv. Mater. 29 (2017) 1602960, https://doi.org/10.1002/adma.201602960.
[210] L. Mei, X. Cui, J. Wei, Q. Duan, Y. Li, Metal phthalocyanine-based conjugated microporous polymer/carbon nanotube composites as flexible electrodes for supercapacitors, Dyes Pigments 190 (2021) 109299, https://doi.org/10.1016/j.dyepig.2021.109299.
[211] P.A. Troshin, R. Koeppe, A.S. Peregudov, S.M. Peregudova, M. Egginger, R. N. Lyubovskaya, N.S. Sariciftci, Supramolecular association of pyrrolidinofullerenes bearing chelating pyridyl groups and zinc phthalocyanine for organic solar cells, Chem. Mater. 19 (2007) 5363–5372, https://doi.org/10.1021/cm071243u.
[212] J. Mu, C. Shao, Z. Guo, M. Zhang, Z. Zhang, P. Zhang, B. Chen, Y. Liu, Solvothermal synthesis and electrochemical properties of 3D flower-like iron phthalocyanine hierarchical nanostructure, Nanoscale 3 (2011) 5126–5131, https://doi.org/10.1039/c1nr10627a.
[213] Z. Cabrane, M. Ouassaid, M. Maaroufi, Analysis and evaluation of battery-supercapacitor hybrid energy storage system for photovoltaic installation, Int. J. Hydrog. Energy 41 (2016) 20897–20907, https://doi.org/10.1016/j.ijhydene.2016.06.141.
[214] H. Ahn, Y.C. Huang, C.W. Lin, Y.L. Chiu, E.C. Lin, Y.Y. Lai, Y.H. Lee, Efficient defect healing of transition metal Dichalcogenides by Metallophthalocyanine, ACS Appl. Mater. Interfaces 10 (2018) 29145–29152, https://doi.org/10.1021/acsami.8b09378.
[215] A.T. Chidembo, K.I. Ozoemena, Electrochemical capacitive behaviour of multiwalled carbon nanotubes modified with Electropolymeric films of nickel Tetraaminophthalocyanine, Electroanalysis 22 (2010) 2529–2535, https://doi.org/10.1002/elan.201000290.
[216] L. Mei, X. Cui, Q. Duan, Y. Li, X. Lv, H.G. Wang, Metal phthalocyanine-linked conjugated microporous polymer hybridized with carbon nanotubes as a high-performance flexible electrode for supercapacitors, Int. J. Hydrog. Energy 45 (2020) 22950–22958, https://doi.org/10.1016/j.ijhydene.2020.06.208.
[217] A. Modak, M. Nandi, J. Mondal, A. Bhaumik, Porphyrin based porous organic polymers: Novel synthetic strategy and exceptionally high CO_2 adsorption capacity, Chem. Commun. 48 (2011) 248–250, https://doi.org/10.1039/c1cc14275e.
[218] E.L. Spitler, J.W. Colson, F.J. Uribe-Romo, A.R. Woll, M.R. Giovino, A. Saldivar, W.R. Dichtel, Lattice expansion of highly oriented 2D Phthalocyanine covalent organic framework films, Angew. Chem. Int. Ed. 124 (2012) 2677–2681, https://doi.org/10.1002/ange.201107070.
[219] M.G. Mohamed, M.M. Samy, T.H. Mansoure, S.U. Sharma, M.S. Tsai, J.H. Chen, J. T. Lee, S.W. Kuo, Dispersions of 1,3,4-Oxadiazole-linked conjugated microporous polymers with carbon nanotubes as a high-performance electrode for supercapacitors, ACS Appl. Energy Mater. 5 (2022) 3677–3688, https://doi.org/10.1021/acsaem.2c00100.
[220] H. Zuo, J. Duan, B. Lyu, W. Lyu, Y. Li, X. Mei, Y. Liao, Carbon nanotube template-assisted synthesis of conjugated microporous Polytriphenylamine with high porosity for efficient Supercapacitive energy storage, Macromol. Rapid Commun. 45 (2024) 2300238, https://doi.org/10.1002/marc.202300238.
[221] C. Gu, N. Huang, J. Gao, F. Xu, Y. Xu, D. Jiang, Controlled synthesis of conjugated microporous polymer films: Versatile platforms for highly sensitive and label-free chemo- and biosensing, Angew. Chem. Int. Ed. 53 (2014) 4850–4855, https://doi.org/10.1002/anie.201402141.
[222] X. Wang, C. Drew, S.H. Lee, K.J. Senecal, J. Kumar, L.A. Samuelson, Electrospun Nanofibrous membranes for highly sensitive optical sensors, Nano Lett. 2 (2002) 1273–1275, https://doi.org/10.1021/nl020216u.
[223] Y. Wang, A. La, Y. Ding, Y. Liu, Y. Lei, Novel signal-amplifying fluorescent nanofibers for naked-eye-based ultrasensitive detection of buried explosives and explosive vapors, Adv. Funct. Mater. 22 (2012) 3547–3555, https://doi.org/10.1002/adfm.201200047.
[224] L. Teng, J. Duan, H. Liu, X. Zhang, J. Li, Y. Li, J. Hong, W. Lyu, Y. Liao, A conjugated microporous polymer–graphene composite porous sandwich-like

film for highly efficient flexible supercapacitors, J. Mater. Chem. A 12 (2024) 12423–12434, https://doi.org/10.1039/d4ta01603c.
[225] A. Basit, Y.C. Kao, Y.A. El-Ossaily, S.W. Kuo, M.G. Mohamed, Rational engineering and synthesis of pyrene and thiazolo[5,4-d]thiazole-functionalized conjugated microporous polymers for efficient supercapacitor energy storage, J. Mater. Chem. A 12 (2024) 30508–30521, https://doi.org/10.1039/d4ta05908e.
[226] G.K. Silori, P.Y. Lee, S.C. Chien, L.C. Lin, K.C. Ho, Two-dimensional conjugated microporous polymer unveiling three-state electrochromism and faradaic energy-storage, Electrochim. Acta 540 (2025) 147265, https://doi.org/10.1016/j.electacta.2025.147265.
[227] A.A. Saddik, H.N. Abdelhamid, Conjugated tetraphenylethene-based polymers for supercapacitor, Polymer 315 (2024) 127778, https://doi.org/10.1016/j.polymer.2024.127778.
[228] J. Chmiola, G. Yushin, Y. Gogotsi, C. Portet, P. Simon, P.L. Taberna, Anomalous increase in carbon at pore sizes less than 1 nanometer, Science 313 (2006) 1760–1763, https://doi.org/10.1126/science.1132195.
[229] Y. Zhu, S. Murali, M.D. Stoller, K.J. Ganesh, W. Cai, P.J. Ferreira, A. Pirkle, R. M. Wallace, K.A. Cychosz, M. Thommes, D. Su, E.A. Stach, R.S. Ruoff, Carbon-based supercapacitors produced by activation of graphene, Science 332 (2011) 1537–1541, https://doi.org/10.1126/science.1200770.
[230] F. Béguin, E. Frackowiak, Supercapacitors: Materials, systems, and applications, supercapacitors: Materials, systems, and applications, copyright © 2013 Wiley-VCH Verlag GmbH & co, KGaA (2013), https://doi.org/10.1002/9783527646661.
[231] M. Sajjad, R. Tao, L. Qiu, Phosphine based covalent organic framework as an advanced electrode material for electrochemical energy storage, J. Mater. Sci. Mater. Electron. 32 (2021) 1602–1615, https://doi.org/10.1007/s10854-020-04929-9.
[232] M. Sajjad, K. Kang, Z. Wu, Y. Ma, R. Tao, L. Qiu, Phosphine-based porous organic polymer/rGO composite anode and α-MnO_2 nanowire cathode cooperatively enabling high-voltage aqueous asymmetric supercapacitors, J. Energy Storage 40 (2021) 102772, https://doi.org/10.1016/j.est.2021.102772.
[233] M. Sajjad, R. Tao, K. Kang, S. Luo, L. Qiu, Phosphine-based porous organic polymer/rGO aerogel composites for high-performance asymmetric supercapacitor, ACS Appl. Energy Mater. 4 (2021) 828–838, https://doi.org/10.1021/acsaem.0c02725.
[234] X. Li, H. Wang, H. Chen, Q. Zheng, Q. Zhang, H. Mao, Y. Liu, S. Cai, B. Sun, C. Dun, M.P. Gordon, H. Zheng, J.A. Reimer, J.J. Urban, J. Ciston, T. Tan, E. M. Chan, J. Zhang, Y. Liu, Dynamic covalent synthesis of crystalline porous graphitic frameworks, Chem 6 (2020) 933–944, https://doi.org/10.1016/j.chempr.2020.01.011.
[235] M. Wu, Y. Zhao, B. Sun, Z. Sun, C. Li, Y. Han, L. Xu, Z. Ge, Y. Ren, M. Zhang, Q. Zhang, Y. Lu, W. Wang, Y. Ma, Y. Chen, A 2D covalent organic framework as a high-performance cathode material for lithium-ion batteries, Nano Energy 70 (2020) 104498, https://doi.org/10.1016/j.nanoen.2020.104498.
[236] R. Shi, L. Liu, Y. Lu, C. Wang, Y. Li, L. Li, Z. Yan, J. Chen, Nitrogen-rich covalent organic frameworks with multiple carbonyls for high-performance sodium batteries, Nat. Commun. 11 (2020) 1–10, https://doi.org/10.1038/s41467-019-13739-5.
[237] Y. Fan, F. Fu, D. Yang, W. Liu, Z. Li, X. Qiu, Balancing the gravimetric and volumetric capacitance of nitrogen-enriched lignin porous carbon for high performance supercapacitors, J. Energy Storage 63 (2023) 106947, https://doi.org/10.1016/j.est.2023.106947.
[238] E. Vitaku, C.N. Gannett, K.L. Carpenter, L. Shen, H.D. Abruña, W.R. Dichtel, Phenazine-based covalent organic framework cathode materials with high energy and power densities, J. Am. Chem. Soc. 142 (2020) 16–20, https://doi.org/10.1021/jacs.9b08147.
[239] C. Zhang, X. Yang, W. Ren, Y. Wang, F. Su, J.X. Jiang, Microporous organic polymer-based lithium ion batteries with improved rate performance and energy density, J. Power Sources 317 (2016) 49–56, https://doi.org/10.1016/j.jpowsour.2016.03.080.
[240] Z. Lei, Q. Yang, Y. Xu, S. Guo, W. Sun, H. Liu, L.P. Lv, Y. Zhang, Y. Wang, Boosting lithium storage in covalent organic framework via activation of 14-electron redox chemistry, Nat. Commun. 9 (2018) 1–13, https://doi.org/10.1038/s41467-018-02889-7.
[241] L. Meng, S. Ren, C. Ma, Y. Yu, Y. Lou, D. Zhang, Z. Shi, Synthesis of a 2D nitrogen-rich π-conjugated microporous polymer for high performance lithium-ion batteries, Chem. Commun. 55 (2019) 9491–9494, https://doi.org/10.1039/c9cc04036f.
[242] C. Peng, G.H. Ning, J. Su, G. Zhong, W. Tang, B. Tian, C. Su, Yu Di, L. Zu, J. Yang, M.F. Ng, Y.S. Hu, Y. Yang, M. Armand, K.P. Loh, Reversible multi-electron redox chemistry of π-conjugated N-containing heteroaromatic molecule-based organic cathodes, Nat. Energy 2 (2017) 1–9, https://doi.org/10.1038/nenergy.2017.74.
[243] C. Huang, J. Mahmood, Z. Wei, D. Wang, S. Liu, Y. Zhao, H.J. Noh, J. Ma, J. Xu, J. B. Baek, Metal (M = Ru, Pd and co) embedded in C2N with enhanced lithium storage properties, Mater. Today Energy 14 (2019) 100359, https://doi.org/10.1016/j.mtener.2019.100359.
[244] I. Ahmed, H.J. Lee, S.H. Jhung, Porous carbon derived from covalent organic frameworks and relevant porous polymers: Preparation and application in adsorption and catalysis, Chem. Eng. J. 499 (2024) 156148, https://doi.org/10.1016/j.cej.2024.156148.
[245] S. Wang, Q. Wang, P. Shao, Y. Han, X. Gao, L. Ma, S. Yuan, X. Ma, J. Zhou, X. Feng, B. Wang, Exfoliation of covalent organic frameworks into few-layer redox-active Nanosheets as cathode materials for Lithium-ion batteries, J. Am. Chem. Soc. 139 (2017) 4258–4261, https://doi.org/10.1021/jacs.7b02648.
[246] Y. Zhu, X. Chen, Y. Cao, W. Peng, Y. Li, G. Zhang, F. Zhang, X. Fan, Reversible intercalation and exfoliation of layered covalent triazine frameworks for enhanced lithium ion storage, Chem. Commun. 55 (2019) 1434–1437, https://doi.org/10.1039/c8cc10262g.
[247] K. Amin, J. Zhang, H.Y. Zhou, R. Lu, M. Zhang, N. Ashraf, C. Yueli, L. Mao, C.F. J. Faul, Z. Wei, Surface controlled pseudo-capacitive reactions enabling ultra-fast charging and long-life organic lithium-ion batteries, sustain, Energy Fuel 4 (2020) 4179–4185, https://doi.org/10.1039/d0se00610f.
[248] A.I. Cooper, Conjugated microporous polymers, Adv. Mater. 21 (2009) 1291–1295, https://doi.org/10.1002/adma.200801971.
[249] F. Ren, F. Wang, Y. Pan, H. Sun, Z. Zhu, C. Ma, C. Xiao, W. Liang, L. Chen, A. Li, Flexible and UV resistant films based on Thiophene-substituted conjugated microporous polymers bearing alkyl chains: Tuning of rigidity into soft, Macromol. Mater. Eng. 303 (2018) 1700619, https://doi.org/10.1002/mame.201700619.
[250] G. Cheng, T. Hasell, A. Trewin, D.J. Adams, A.I. Cooper, Soluble conjugated microporous polymers, Angew. Chem. Int. Ed. 51 (2012) 12727–12731, https://doi.org/10.1002/anie.201205521.
[251] B. Huang, P. Zhao, Y. Dai, S. Deng, A. Hu, Size-controlled synthesis of soluble-conjugated microporous polymer nanoparticles through sonogashira polycondensation in confined nanoreactors, J. Polym. Sci. A Polym. Chem. 54 (2016) 2285–2290, https://doi.org/10.1002/pola.28108.
[252] A. Molina, N. Patil, E. Ventosa, M. Liras, J. Palma, R. Marcilla, New Anthraquinone-based conjugated microporous polymer cathode with ultrahigh specific surface area for high-performance Lithium-ion batteries, Adv. Funct. Mater. 30 (2020) 1908074, https://doi.org/10.1002/adfm.201908074.
[253] J.H. Lee, Y.M. Kang, K.C. Roh, Enhancing gravimetric and volumetric capacitance in supercapacitors with nanostructured partially graphitic activated carbon, Electrochem. Commun. 154 (2023) 107560, https://doi.org/10.1016/j.elecom.2023.107560.
[254] D. Tang, Z. Xiong, J.D. Worth, T. Qiu, C.F.J. Faul, J. Chen, One-pot scalable production of conjugated microporous polymers with exceptional functionality, J. Mater. Chem. A 13 (2025) 19007–19014, https://doi.org/10.1039/d5ta01740h.
[255] D. Zhou, K. Zhang, S. Zou, X. Li, H. Ma, Conjugated microporous polymers: Their synthesis and potential applications in flexible electrodes, J. Mater. Chem. A 12 (2024) 17021–17053, https://doi.org/10.1039/d4ta02085e.
[256] Y. Jia, D. Yang, L. Zhang, Y. Shi, J. Xie, F. Lei, L. Fan, Ionic conductivity enhancement achieved by binder in electrodes and its influence in supercapacitor, ChemElectroChem 9 (2022) e202200662, https://doi.org/10.1002/celc.202200662.
[257] N.H. Hatsey, M. Oh, A. Kim, J.Y. Lee, H.M. So, S. Hyun, Binder effect on electrochemical and mechanical properties of flexible electrodes, ACS Appl. Electron. Mater. 7 (2025) 322–330, https://doi.org/10.1021/acsaelm.4c01796.